

ABSTRACT

Title of Thesis: **RF TO DC POWER GENERATION**

Juventino Delfino Rosas Espejel, Master of Science, 2003

Thesis directed by: Professor Robert Wayne Newcomb
Department of Electrical & Computer Engineering

This work considers the reception of radio frequency signals as a way to power wirelessly a passive strain sensor circuit, possibly on or embedded in the body of a concrete bridge. The received signal, sent by an interrogator device, generates a sinusoidal voltage in the terminals of the sensor circuit antenna. This voltage is then rectified, filtered and multiplied to generate a DC voltage that can be used to supply and activate the circuitry of the strain-sensor. Throughout, theoretical formulation and simulation are used as tools to prove the feasibility of different voltage multiplier circuits as charge pumps and transformers.

The design and fabrication theory of a novel threshold-voltage free RF-to DC-Voltage circuit is presented in chapter IV. The circuit is designed with MOSFET transistors. Chapter V reviews some of the potential open problems and opportunities in an interrogator-strain-sensor system based in totally different technologies.

RF TO DC POWER GENERATION

by

Juventino Delfino Rosas Espejel

Thesis submitted to the Faculty of the Graduate School of the
University of Maryland, College Park in partial fulfillment
of the requirements for the degree of
Master of Science
2003

Advisory Committee:

Professor Robert W. Newcomb, Chair/Advisor
Professor Ankur Srivastava
Professor C. Martin Peckerar

ACKNOWLEDGEMENTS

I want to show my appreciation to my professors and the institutions that have shaped my life and work. Besides, I would like to express my gratitude to the Fulbright Program for the support and supervision to my program during my stay in the United States. I have been also fortunate to have the support of my home institution the Tecnológico de Monterrey, Campus Estado de México and Dr. Juan López Díaz, Director de la División de Profesional y Graduados.

There is a special person that I must acknowledge due to their importance in my work, support, his belief in me and the encouragement to the next step in my future: my advisor Professor Robert Wayne Newcomb. I know this is one more step in the never-ending learning process in life. Thank you!

The University of Maryland at College Park is an incredible learning place. At the same time that I was taking the courses in my program, I could enrich my acknowledgement with many graduate courses in other three fields I was interested on. To all those professors who asked themselves “what is that guy doing here”, thanks.

“Creative leadership and liberal education ... are the first requirements for a hopeful future for humankind. Fostering these – leadership, earning, and empathy between cultures – was and remains the purpose of the international scholarship program.”

Senator J. William Fulbright

TABLE OF CONTENTS

ABSTRACT	ii
AKNOWLEDGEMENT	iii
Chapter 1. INTRODUCTION	1
a. Basic Wireless Sensor System	1
b. Power Transfer	2
c. Applications	7
d. Important Results in this Research	13
Chapter 2. STATE OF TECHNOLOGY	14
a. History: Wireless Sensors and Previous Power Transfer Technologies	14
i. RF Identification Tags	17
ii. Wireless Sensor Systems	18
b. Physics of the Components in the Magnetic Coupled RF System	19
i. Radio Frequency Magnetic Waves	19
ii. Inductance of the Antenna	22
iii. Mutual Inductance Between Antennas	24
iv. Resonance	28
Chapter 3. RADIO FREQUENCY TO DC CIRCUITS	36
a. Regulator Circuit	37
b. Charge Pump Circuits	39
c. Charge Pump Circuit Simulations	47
Chapter 4. DESIGNS AND TEST RESULTS	55
a. Design of a Sensor Circuit Based on an Up-Transformer	55
i. Design of the basic sensor circuit with an up-transformer in resonance	55
ii. Reader-Sensor system circuit with an up-transformer in resonance	58
iii. Reader-Sensor system circuit with an up-transformer in resonance and output doubler charge pump	61
b. Design of an RF-to-DC-Voltage Circuit for VLSI Implementation	72
i. MOSFET Antenna-Rectifier Circuit	73
ii. MOSFET Antenna-Rectifier-Charge-Pump Circuit	78
c. Test results to the Commercial RFID MCRF355 Tag Chip	81
d. Construction Material Issues in the Design of Embedded Magnetic Coupled Circuits	84

Chapter 5. CONCLUSIONS AND OPEN PROBLEMS	87
a. Open Problems and Opportunities	89
i. Surface Acoustic Wave Sensors	90
ii. Out of the Box Reader-Sensor System Implementation	94
Appendix A: RF Power Transfer in Free Space	99
Appendix B: Antenna Near Field Region	101
Appendix C: Interrogator-Sensor Communication Issues	105
a. Modulation	105
b. Encoding – Decoding	106
c. Bandwidth, DC Component and Collision Detection	110
d. Error Correcting Codes and Security	114
Appendix D: Wiring and Matching in the Strain-Sensor System Design	116
Appendix E: Standards	120
REFERENCES	121

Chapter I. INTRODUCTION

a. Basic Wireless Sensor System

This research deals with the use of radio frequency signals to transfer and feed power to some target circuit. However, it is important to remark that the main application envisaged of this research will be applied to sense strain of a bridge. Therefore, research and implementation must consider issues regarding the attenuation and distortion of the signal by the material used in the construction of the bridge. The sensor circuit will be embedded in the concrete of the bridge. Besides, the sensor is a passive circuit, i.e., there are no batteries in the sensor circuit to power it, through the lifetime of the bridge, usually more than fifty years.

Through out history, there have been many attempts to eliminate wiring from a reader system to a sensor circuit, commonly known as a transponder. The cost associated with installation and maintenance of a network prevented wide use of sensors in multiple applications. A cable network has poor reliability due to failing connections and contacts, especially in corrosive environments.

Given these circumstances, there have been multiple efforts to look for alternatives. Wireless circuit sensors in a chip were the logical step. By adding radio telemetry capacity to a circuit sensor, it was possible to overcome the problems associated with wiring. Wireless sensor networks allow companies to benefit from machine monitoring, to perform preventive maintenance, and as consequence to increase productivity. It is also possible to embed the sensor in products for logistic real time information to reduce costs. See Figure 1.

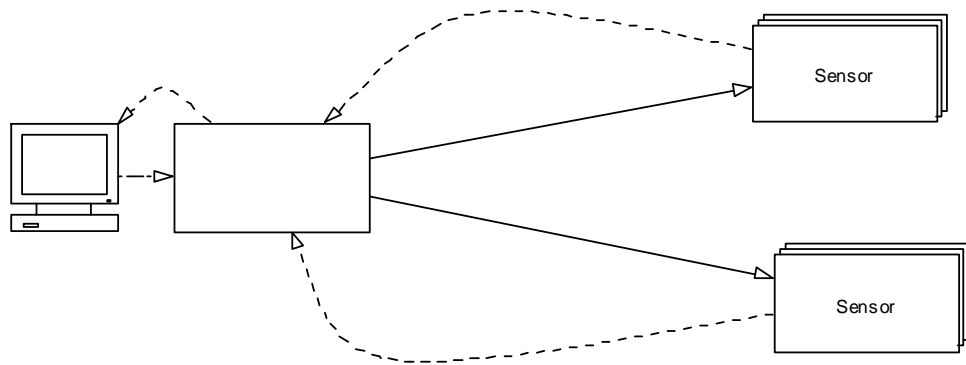


Figure 1. Basic Wireless Sensor Network

In this model, it is possible to deploy sensors stuck on or embedded in machines, products, structures or systems that can be remotely accessed via the Internet. There are some basic limitations for success of sensor networks: cost, robustness on industrial environments and power.

Cost can be addressed through mass production. Sensor systems fit economies of scale up to some minimal production cost given by the sensor application and application market. Robustness on industrial environments could require relatively expensive sensor circuits, however, they will be able to protect expensive capital assets. Moreover, it is known that deployment of this technology can improve production efficiency and reduce emissions, helping industries to cope with intense competition and improving relations with their communities.

b. Power Transfer

Power is not a problem when it is possible to feed sensor circuits through wires or batteries. However, wireless passive sensors must be considered for applications where no accesses to power sources are available. Consider the researchers at DARPA, who

propose to sprinkle thousands of very small sensors in a battlefield [45, pp 357-360]. Sensors would self-organize in a network and send data on foes movements without alerting them to their presence. The information would be collected, filtered and sent to the central command. The lifetime of the “intelligent dust” network would be limited mainly by the time that batteries could deliver power to the sensors. Ideally, sensors would be passive, and they would be able to get power through RF signals, or any other means.

An important question is: how to power passive devices in an efficient way? There have been some methods proposed and implemented: microwave power transmission [2, pp 87-89], bio-batteries [51, pp 25-28], RFID [46 pp 1-5], surface acoustic wave devices [47, pp 69-72], piezoelectric generators [48, pp 897-904], differential-heat generators [49, pp 5/1-5/6], solar cells [50, pp 1199-1206], and so on.

Given the development of high power microwave tubes, in the 1950s DARPA supported the design of a system to wirelessly power aircrafts. Later in 1964 William C. Brown [2, pp 87-89] of Raytheon Co. showed a 2.45 GHz wireless-powered chopper with assembled tether (conducting cable) to collect the power. These kinds of systems are able to transmit power on the order of kilowatts, more than 30KW, but they are expensive.

Figure 2 shows a typical rectenna, acronym for “RECTifier_anTENNA. The elements of the antenna collect the power sent by a microwave antenna, rectify and filter it to deliver a DC voltage. Actual implementations include arrays of many of these rectennas, and use of a back reflector at $\lambda/4$ to improve efficiency by 6 dB. The most common operation frequency is 2.45 GHz [2, pp 87-89] because of the negligible atmospheric losses at that

frequency. The efficiency reached by this system is about 97% @ 19 GW, for Gaussian shaped beams.

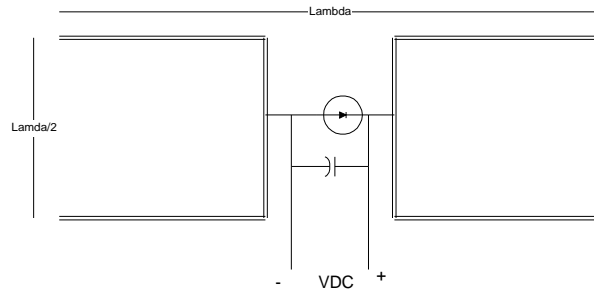


Figure 2. Rectenna

A rectenna circuit with full-wave rectifier is shown in Figure 3. The dipoles, at $\lambda/2$ lengths, collect the RF signal. The signal is rectified and filtered by the bridge-capacitor combination and to yield a constant voltage at the output terminals.

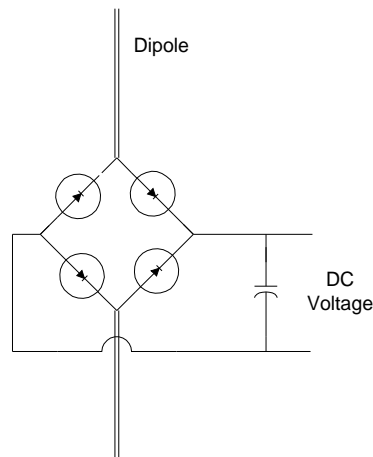


Figure 3. Rectenna Circuit

However, rectenna circuits can deliver more power if they work in arrays as shown in Figure 4 [5, pp 1234-1236]. Separation between bridges is about $\lambda/2$. Theoretically, the full-wave rectifier is more efficient to deliver DC voltage, however, because the simplicity of construction and cost, half-wave rectifiers are more popular in rectenna implementations.

Given their importance they are a good alternative for transmission of power in the future. Nowadays, to power chips or small systems wirelessly, though, the system is expensive.

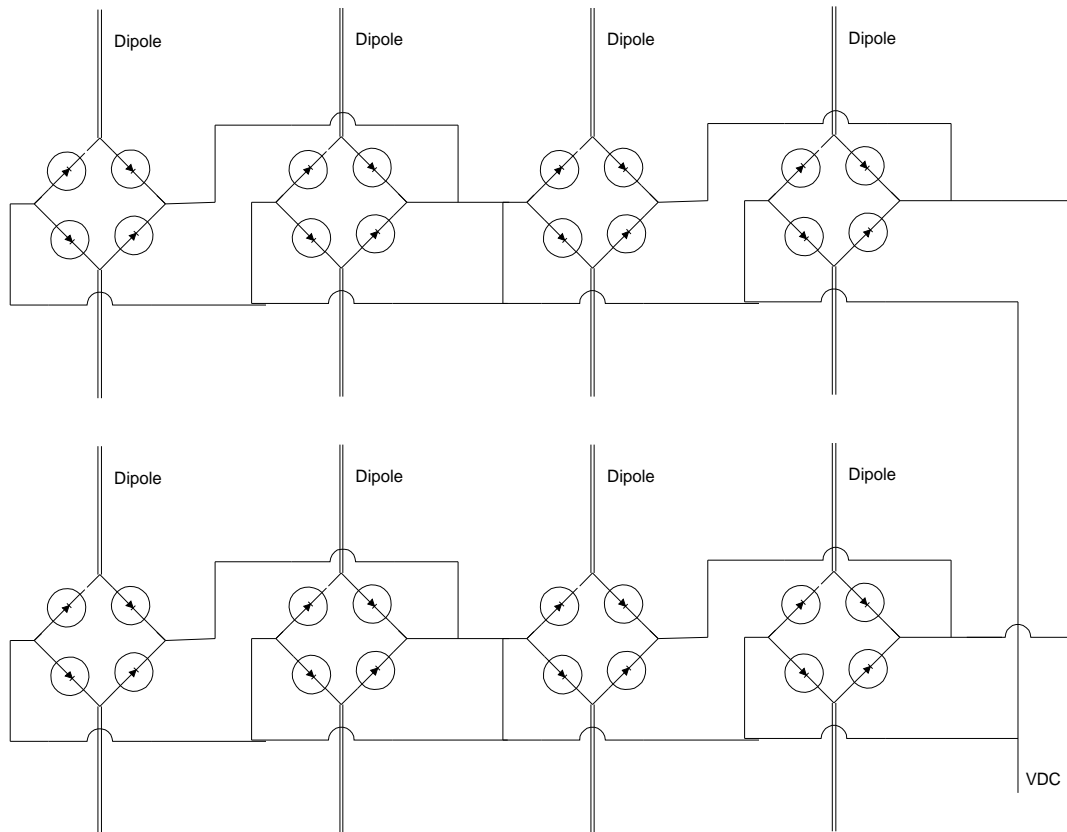


Figure 4. Rectenna Array [Brown, W.C., Patent 3,434,678, 1984, page 1]

Bio-fuel cells use a colony of bacteria to break down sugar without the use of oxygen, depositing electrons as a byproduct. If the colony is placed in an electrode and this electrode is wired to another electrode exposed to air, a flow of current is observed [53, pp 172-177]. Efficiency has been very low, as low as 1%. There has been some research showing potential by using *Rhodospirillum rubrum* bacteria to do the job [52, pp 1229-1232], with those bio-fuel cells said to have reached an efficiency of 80%. In

practice, an electrode with the colony should be placed at the bottom of a pile of waste to generate electricity. The power could be used to operate sensors, or any other device, in remote areas where no other source of power is available. Theoretically, a cup of sugar would be enough to power a 60 watts light bulb for 17 hours. No more data is presently available; researchers just argue that voltage is still small and conversion from sugar to current is slow for some practical applications [52, pp 1229-1232].

Thermoelectric generators work based on the thermocouple principle, i.e., two different metals are connected together, and each one is exposed to a different temperature. The resultant effect is an electric potential between the wires, which can be translated into a current flow. Different temperatures can be obtained from different sources. In space, this condition is reached by exposing one of the metals to the sunlight and the other to the darkness. In geothermal areas, like Iceland, hot water is used to heat one metal and ice to cool the other metal. The higher the difference of temperatures, the higher the power that is delivered by the thermoelectric generator. Nowadays thermoelectric generators have efficiencies in the order of 3%.

This work will be focused on passive wireless sensors applied to monitoring strain in steady structures as bridges, buildings, etc. Therefore power transfer through a wall is one important challenge. An option is to place an exterior antenna to collect the power and deliver to the sensor circuit via cable to the embedded sensor circuit, however periodic maintenance must be carried out to check for corrosion or any other defect that may interfere with the correct performance of the system. A better option could be to embed the whole sensor circuit in the bridge concrete so that no maintenance is necessary in the lifetime of the bridge, usually more than 50 years, because the sensor circuit is

protected from the exterior environment. The sensor circuit design must be highly reliable and, in order to increase the reader distance, attenuation of the bridge structure concrete must be maintained at a minimum for the signal and frequency used. Some research [3, pp 674-682] indicates that attenuation of the electrical field inside the concrete is high. As expected, this attenuation is increased as thickness of concrete increases. Tests run in the microelectronics laboratory showed that this attenuation is small for magnetic fields if thickness of the construction material is less than 2 inches.

c. Applications

The first fatigue test on steel chains, at ten cycles per second, was performed, in 1829. The material fatigue behavior is important for safety on structures, as bridges. The structural response to loading is important to monitor structure condition and for reliability analysis.

In order to monitor the structure condition remote wireless sensors can be used in the field of material damage and health assessment. Remotely powered, possibly embedded, wireless sensors could allow for the building of a remote sensing network that could monitor in real time the condition on a bridge. By saving data on fatigue, it could be possible to analyze the health of the bridge avoiding collapsing in serious events.

After occurrence of an earthquake, it could be possible to monitor the state of the bridge without risk to human lives, and allow for traffic as the health of the bridge, monitored in real time, allows.

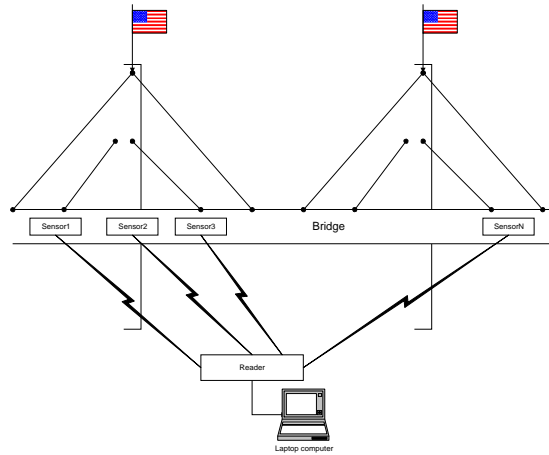


Figure 5. Basic Bridge Sensor System

The basic bridge system is shown in Figure 5 where the reader interrogates the sensor network. It sends a radio frequency signal to wake up the sensor communication circuits. Then, every sensor circuit sends its last strain measurement to the reader. The reader collects and sends them to the database for analysis.

Ideally, all sensors should have gotten their power from external sources. This thesis work considers an electrical power source from a vibration-bending generator to feed the internal sensor circuit and read a strain measurement. Then a radio frequency signal is sent to the communication circuit, to turn it on and send the measurement data back to the reader. In general, transponders will be embedded in the bridge structure with no access for maintenance on the bridge lifespan.

Therefore, the sensor circuit must be reliable and dependable through many years.

Another important application for wireless sensors is to identification tags. In recent years, there has been a trend to take RFID (Radio Frequency Identification) technology from labs to commercial applications. In this application, the system must maximize reading distance and robustness to collisions with cheap tag fabrication. Tags

can be used to keep track on some retail products for inventory control, automatic selling systems, intelligent systems at home, and so on.

The following list shows some milestones on the life of some representative wireless identification systems:

1949 -- the first barcode is invented

1959 -- first wildlife radio tags

1967 -- first retail barcode scanning system

1975 --anti-theft material tags appear in libraries and stores

1980 -- RFID is invented

1990 -- Automobile toll-collection tags appear

1997 -- first all-polymer IC tag demonstrated

Bernard Silver invented the barcode in the Drexel Institute of Technology in Philadelphia. A local food chain president requested an automatic product read system for checkout. At the beginning, a code of four white lines in a black background was made, allowing classification of seven different products. Encoding was done based on the presence or absence of lines a binary system with $2^3 - 1$ combinations because the first combination was useless. The system progressed to 10 lines with potential to recognize up to 1023 tags. (US Patent 2,612,994)

The system started gaining recognition in 1966 when the National Association of Food Chains called for a system to speed up the checkout process. In 1969, the process to develop a standard started and finally in 1974 NCR Corp. installed the first system in Troy, Ohio.

Nowadays, the most popular barcode is the EAN (European Article Number) with structure shown in Figure 6. The CD acronym stands for company identifier.

Country Identifier		Company Identifier					Item Number					CD
4	4	0	8	7	4	3	1	7	7	2	5	4
FRG		JR Technology Systems University Boulevard 1025					Intelligent Sensor 1032					

Figure 6. Barcode Structure

Researchers use different systems to get remote information on wildlife. They use transmitters to monitor behavior on animals. In this case, transmitters must be adequate to species under study. Transmitters must be robust but at the same time must not disturb normal behavior on the animal under study. If the animal spends an important amount of time under water, the transmitter must be designed to survive frequent immersions; implants should be considered. Therefore, monitor systems must be chosen on basis of size, lifestyle and body type. For some species, radio tags could be a good and cheap option to collect data.

Automatic fare collection is a reality. There are some commercial systems available. As an example, people living along the eastern seaboard can enjoy E – Zpass, which uses radio frequency identification cards to collect fares. See Figure 7.

Toll collecting tags can be used to improve today’s fare collecting systems, which rely on paper tickets in an ample variety of services. By using a prepaid card costumers could get access to different services without staying on line; fares could automatically be discounted from their prepaid card.

Nowadays, these systems are relatively expensive but as technology improves, it could be possible to extend automatic fare discount to more and more services, from shopping to product tracking on manufacturing companies. The idea could be to move tags at least to mass production, or ideally, to economies of scope, permeating automatic tracking to all products, cheap ones included.

A detailed description of the electronic collecting system is shown in Figure 8. The driver must buy a transponder, size of a credit card, and deposit money in the account of it. The transponder must be placed inside the windshield, behind the rear mirror. When the car drives through the toll lane there is a detector sensor to know that a car is arriving. At the same time an array of two antennas aim a RF signal to power the transponder chip, the transponder wakes up and sends its identification number back. A computer system automatically charges the account based on the number of axes detected by the sensor strips embedded in the road.

With E-ZPass, paying tolls is convenient. Just use the E-ZPass Lanes. As you pass through the toll plaza, an antenna electronically reads account information on your E-ZPass tag. Your toll is electronically deducted from your prepaid account.

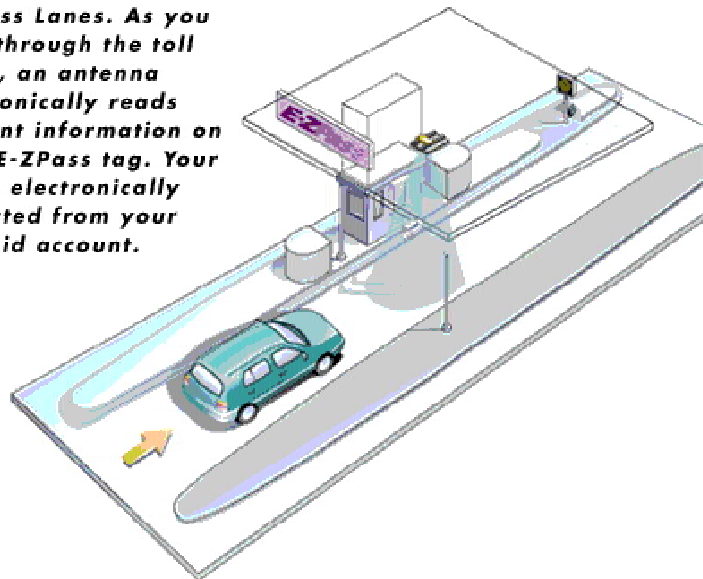


Figure 7. Automatic Toll System [1]

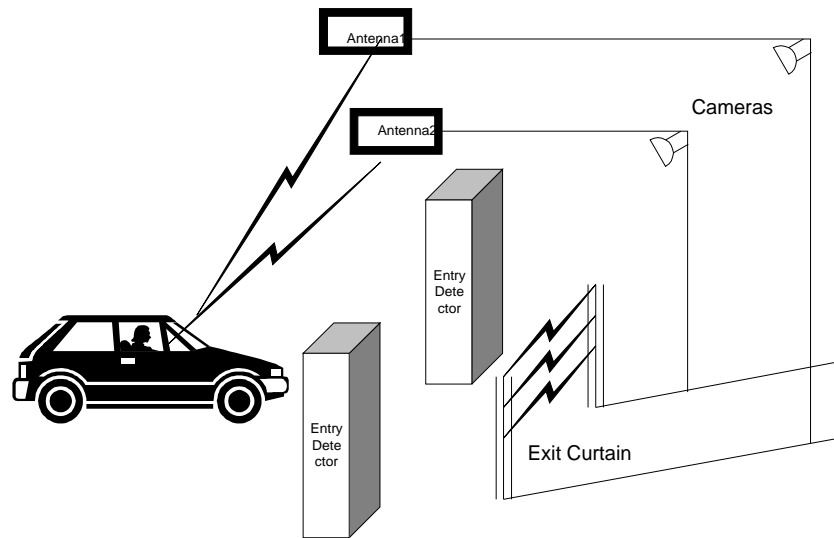


Figure 8. Detailed Automatic Toll System

If the prepaid account has not enough money or no transponder is in the car, a monitoring camera takes a picture of the car tag and a fine is mailed to the violator owner. The range of the antennas is about 3 meters, working at 900 MHz. The velocity drivers can drive through the setup is in the range from 8 to 85 Km/hr. Sometimes special transponders are issued to drivers when their car windows use some metallic tint that impedes the RF reach of the transponder. In those cases, transponders must be stacked outside the car.

It is known that companies today lose approximately 10% of some popular products because somebody stole them on their way to the consumer. With this technology in place, it could be possible to track every product, from production to consumer purchase.

Some public concerns, regarding privacy, must be addressed. People don't like "big brother" looking on their shoulder. I believe that for most commercial applications, benefits clearly overcome any possible disruption on public privacy.

d. Important Results in this research

As mentioned before, this work is focused on the efficient power transmission through radio frequency signals, given the application of the project to strain passive sensors embedded in a concrete bridge. Some of the important results produced in this work are:

1. Simulation and comparison in the performance of combination of magnetic coupled rectifiers with up-transformers and charge pumps working in resonance as RF to DC generators. Chapters III and IV.
2. Analytical setup to analyze the severe voltage drop on the circuits mentioned in bullet one, and working in resonance. Chapter IV.
3. Design of an MOSFET RF-to-DC-Voltage circuit free of threshold voltage. Chapter IV.
4. In the search for bigger reading distance range: analysis and theoretical design of a RF powered strain sensor circuit based on a surface acoustic wave device operating in the far field, i.e., powered by the electrical field instead of the magnetic field. Chapter V.

These results will be presented through this thesis in the chapters mentioned and with strong theoretical support of chapter II and the appendices.

2. STATE OF TECHNOLOGY

a. History: Wireless Sensors and Previous Power Transfer Technologies

This section will review wireless sensors powered by radio frequency signals and their previous technologies. Some of the previous technologies seems not to be directly related to the transfer of power through RF, however, when there is more than one wireless sensor in the area of the reader coverage, some kind of identification code and communication protocol must be implemented to identify the sensor that is transmitting measured data and when the sensors must transmit. The effects of these elements must be considered to minimize the use of the limited power. If two or more sensors try to send information at the same time a collision will occur, and one algorithm must be added to make sure data is read successfully. Intrinsicly, it implies the use of additional power. When there is only one sensor circuit the design target is usually to maximize distance between sensor and reader circuits with accurate reception of data measured. If the system grows to a network of passive sensor circuits, there is an additional burden of processing to identify the sensor that is transmitting the data. Processing uses power, therefore, the circuit design must be power efficient, and the processing program must be performed as fast as possible.

Therefore, the first part of this chapter will review the history of some of the systems used to automatically identify products, persons, etc. They focus on processes, but some ideas can be translated to sensor network power efficiency, verification and safety.

Traditionally, most data collection is done by writing on paper or typing to enter data in a computer system. If, for example, somebody wants to know the condition of a bridge, usually, it will involve running tests in the field or lab, collection of data to the computer

system and writing reports. This process is repetitive, costly, outdated and sometimes inaccurate.

Another example involves production and service activities. As diversification and activities of companies increase there is a need to collect larger amounts of data, doing this by hand is inappropriate given the amount of personnel required to keep the information system updated. There is big pressure on companies to keep them competitive; therefore, they try to add optimal operating schemes such as “just in time” or “project management” to daily operations. To operate efficiently the flow of information must be sufficient to synchronize process and personnel work.

The solution to this kind of problem involves adding some kind of automatic collection information system. Consider a bridge after an earthquake; depending on the earthquake magnitude there is a need to know if the bridge is safe to traffic. Nowadays, transportation personnel must perform tests to verify bridge safety; in the mean time, as the bridge is closed, economic loss piles up unnecessarily.

In an ideal situation, the state of the bridge must be known in real time, so transportation officers can make decisions in short time. A real time information system also can be helpful in the maintenance program and annual budgeting.

The real time information system of the bridge should have a network of sensors that send information to a central database, and then, information could be preprocessed before being presented to the personnel in charge of the bridge. This information could

be delivered to a state or national safety organization or as many stakeholders as necessary.

The project, that includes research in this thesis, involves sensing of strain as a way to check the bridge condition, as mentioned in the introduction.

A possible sensor network should have a sensor with a passive circuit so that it only turns active when some external source of power feeds it. A further improvement could include the use of more than one external source of power to secure continuous operation. One of the power sources could feed the circuit when acquisition is carried out, and could get power through compression/decompression of a piezoelectric element embedded on the bridge. The piezoelectric element generates power from the compression produced by the car wheels as cars circulate on the bridge. The advantage of the piezoelectric generator is its ability to generate relatively high voltages. The disadvantage of piezoelectric generators is that they need a relatively long time to accumulate the charge in a capacitor, before charge can feed the sensor circuit.

Reading of the sensor data must be done as fast as possible. If it is done with a handset, the operator wants to read one sensor and move to the next one. Therefore, the operator would be happy if his/her handset interrogation device wakes up the sensor circuit rapidly, instantaneously in her/his perception, by sending a radio frequency signal.

Ideally, collection of data should be done in real time, however, given power constraints imposed on the RF power delivered by any device, the interrogator device must operate relatively close to the sensor circuit to turn it into its active state. Next Section will explain these technologies.

i. RF Identification Tags (RFID)

RFID is considered a wireless automatic product identification. They use an RF signal to power a tag-circuit. RFID systems are more expensive than bar code systems, but their cost is expected to decrease as products move to economy of scale. There are important advantages of RFID tags over other identification systems. First, they can be attached to almost anything. Secondly, they do not need any battery to operate; the power is taken from the RF signal sent by the reader device. Third, the chips embedded in the tags can be as small as 0.4 mm^2 . Usually they operate around 134 KHz but there are systems working up to 5.8 GHz. To read the tag information it is not necessary to be in the line of sight for low and middle frequencies, as long as the tag is in the range of the reader device.

Commercial applications for this technology go from inventory control to automatic payment at shopping stores.

There are some disadvantages, first, tag activation is done by a magnetic field, and because of that, they must operate in the near field given the strong attenuation of magnetic signals in the far field.

Secondly, the cost per tag is at present around \$0.50. This is expensive for reaching vast number of products. However, there is some research that suggests \$0.05 per tag as the threshold cost per tag to get them attached to almost everything.

Third, there are concerns regarding privacy. In a good use, tags can be used to pay shopping automatically. Later, in your home, your refrigerator can automatically sense if you are running out of your favorite ice cream, or any other product by reading the

information on the tags. Then, if you instruct your system to do that, it can send the information to the store, and the shopping store can deliver your ice cream to home at some predetermined time when they know you are there to receive it. This will allow getting closer to an intelligent house. On the bad side, it could be possible for anybody to track your products, so they could collect information about your preferences. That information could be then saved in a database, with the information of other people, and sold to the companies that later will bother you with “new promotions”. In addition to this problem, from the database it is possible to get unintended information that could be used, for example, increasing your health insurance given your consumption pattern, etc.

ii. Wireless Sensor Systems

As sensors become smaller and more reliable, their applications increase. By adding a wireless feature into the sensor, it could be possible to array them into a network.

Microsensors could be ultimately embedded into any physical system, the human body included, to get measures of unprecedented detail. The research in this thesis is an example for this technology. To operate correctly, networks must be scalable and robust with small power consumption circuits.

Sensor networks must operate under limited power, with self-configuration ability as sensors are taken into and out of the network. Finally, sensor localization is important in order to know what part of the system is being monitored.

The theory and implementation of an RF sensor system will be further explored in this thesis.

b. Physics of the Components in the Magnetic Coupled RF System

i. Radio Frequency Magnetic Waves

From Figure 5, the strong attenuation suffered by electromagnetic signals through lossy media [10, pp 1-5], and the encouraging results obtained in the laboratory for magnetic fields when the receiving antenna is embedded in concrete, a sensor system operating under inductive coupling is recommended.

As it is known, a flux with strength H is generated around a current carrying conductor. This phenomenon can be described by [11, equation (16-9-3), pp 439]

$$I = \vec{H} \cdot d\vec{s} \quad (2.1)$$

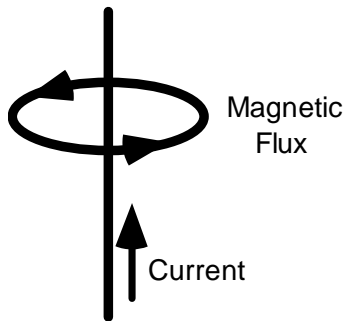


Figure 9. Magnetic Flux Around a Wire

It is known that for a straight conductor the field strength is given by [11, equation (14-3-6), pp 372]

$$H = \frac{1}{2\pi r} \quad (2.2)$$

In the basic sensor system, described in Figure 1, a loop conductor is used as an antenna to generate a magnetic alternating field. The alternating field is coupled to the receiver antenna, another loop conductor, to generate power in order to turn on the sensor circuit

and send back to the reader the strain sensor measurement. When the antennas were tested, it was noticed, as expected, that H decreases with distance.

Consider the inductor, with radius r, shown in Figure 10.a. Note that the flux line density is stronger in the x direction as shown in Figure 10.b. Therefore, when the strain sensor system is operating, in order to optimize the reading distance, transmission and reception antennas should be aligned on the same “x” axis.

The strength of the magnetic field along the x direction is calculated from [11, equation 14-5-3, pp 375]

$$H = \frac{I N \mu_o r^2}{2\sqrt{(r^2 + x^2)^3}} \quad (2.3)$$

Where r is the coil radius, N is the number of windings, and x is the distance from the center of the inductor along the x axe.

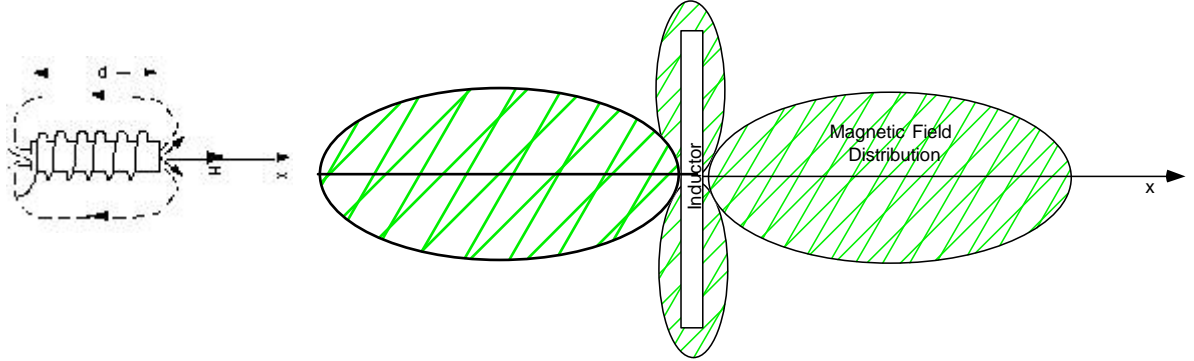


Figure 10. (a) Magnetic flux around the interrogator/sensor antenna. (b) Magnetic Field distribution on the neighborhood of a short inductor antenna

We want to work in the near field to generate adequate voltage level, therefore x must be smaller than $2\pi/\lambda$. We recommend the design of the antenna to be made on a printed circuit board to make it less disruptive to the bridge structure. From equation 2.3 it is

clear that increasing N or I increase H , on the contrary an increase in r decreases H . A typical coil antenna described by (2.3) exhibits the behavior shown on Figure 11. Note that the magnetic field strength holds constant up to some distance and after that, it decreases at an approximate 60 dB per decade. The inflexion point will be at a bigger distance as the radius decreases but simultaneously the constant magnetic field, before the inflexion point, will be smaller as the radius decreases for some fixed N and I .

Considering (2.3) again, assume N and I constant; fix x to some value and compute H for an interval that includes x . The optimal radius results to be $x = 2^{1/2} r$ as shown in Figure 12. It means that the optimal radius between the reader and sensor as distance increases also increases in the same proportion. This effect can be obtained by taking the derivative with respect to r in (2.3).

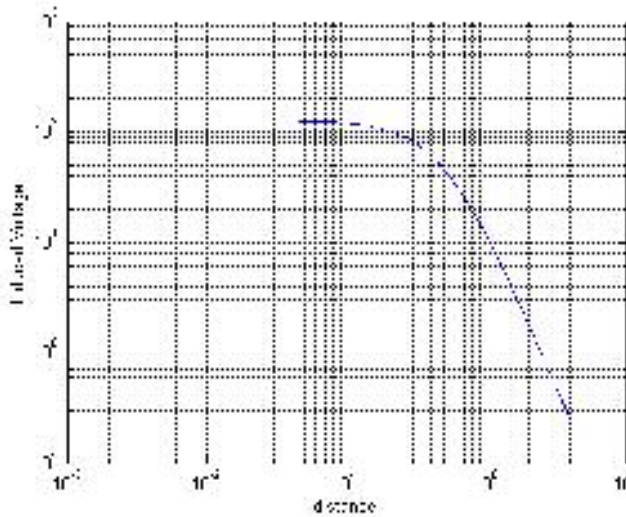


Figure 11. Typical induced voltage as distance between transmitter and receiver coil antennas increases

It is important to remark that these graphs result by considering operation on the near field.

When the distance between the interrogator and strain-sensor is increased to work in the closer far field, the antenna radius must be bigger to generate a stronger magnetic field in the sensor circuit and as a consequence to generate an adequate voltage to feed the sensor circuit.

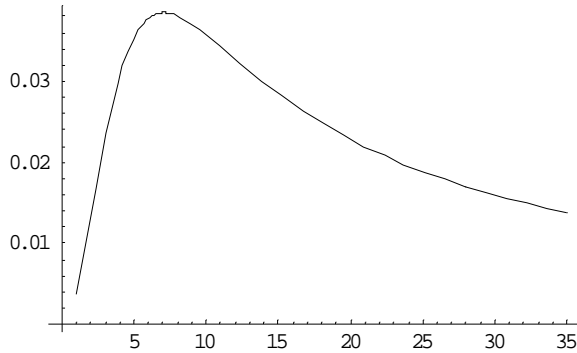


Figure 12. Optimal radius for reader antenna when the distance x , between the reader and sensor is 5 centimeters

If the strain sensor circuit, with the antenna, is embedded in some construction material, an additional attenuation is expected, given the higher absorption produced by materials different from a vacuum. This effect must be considered because it results in reduction of the interrogation range for some fixed power transmitted. Theoretically, it can be considered by changing the permeability $\mu = \mu_o \mu_r$ in (2.3), and assuming it constant through the concrete material, i.e., take the average permeability. However, in practice, the shielding effect produced by reinforced concrete or the structure of the bridge is not captured in (2.3), and it changes for different bridges.

Therefore, reading distances will vary along a bridge, and for different bridges as metallic rods and beams are distributed on the structure.

ii. Inductance of the Antenna

It is desirable to compute the inductance L associated with the designed antenna because, later, we will learn that the antenna circuit must operate in an LC resonant circuit in order

to maximize reading range. By using the Biot-Savart Law, and (2.3), the flux density is given by [11, 14-2-3, pp 369]

$$B(x) = \mu H = \mu_0 \mu_r H = \frac{\mu I N r^2}{2(r^2 + x^2)^{\frac{3}{2}}} \quad (2.4)$$

And magnetic flux is $\Phi = B A = L I / N$. In general the inductance is computed for a closed loop antenna with the diameter of the loop much bigger than the diameter of the conductor used in winding, see Figure 13.

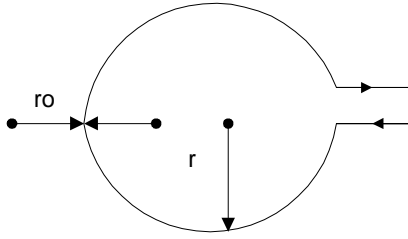


Figure 13. Loop used to compute inductance

The inductance, using (2.3), at some distance x will be

$$L = \frac{N\Phi}{I} = \frac{NBA}{I} = \frac{N\mu HA}{I} = \frac{N\mu A}{I} \left(\frac{I N \mu r^2}{2\sqrt{(r^2 + x^2)^3}} \right) = \frac{N^2 \mu^2 r^4 \pi}{2\sqrt{(r^2 + x^2)^3}} \quad (2.5)$$

with $\mu = \mu_0 = 4\pi 10^7$ (V / A) for free space coupling. Some adjustment will be required because it is easier for the software used in the antenna printed circuit board to design an antenna with a square shape. However, a closed inductance approximation results with the equation (2.5).

iii. Mutual Inductance Between Antennas

In the interrogator-sensor system, the coupling factor is influenced by the distance between both circuits and the relative position of the antennas with respect to their axis of optimal coupling.

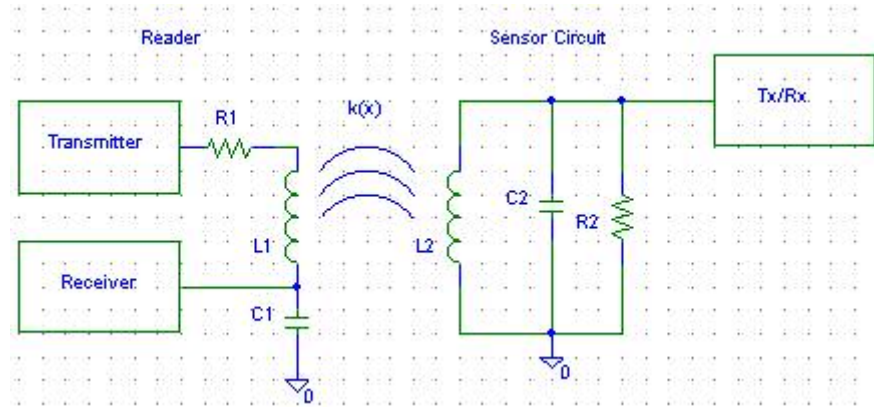


Figure 14. Interrogator – Strain Sensor System

In order to analyze this effect a transformer circuit model will be used, see Figure 15.

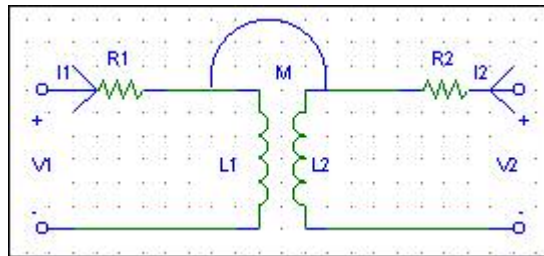


Figure 15. Transformer Model

It is important to remark that the transformer model for magnetic fields is only valid in the near field.

The equations describing this model are:

$$\begin{aligned} V_1 &= I_1(R_1 + sL_1) + I_2sM \quad (V) \\ V_2 &= I_2(R_2 + sL_2) + I_1sM \quad (V) \end{aligned} \quad (2.6)$$

Where M , the mutual inductance, is given as a function of the magnetic coupling factor

$M = k\sqrt{L_1L_2}$. And $0 < k < 1$, with $k = 0$ for large distance or a strong shielding

condition, and $k = 1$ when both coils closely wound on the same high permeability core.

Recall that the induced voltage in the antenna coil when in a sinusoidal magnetic field

$\Phi = B A \cos(\omega t)$ is given by

$$V = N \frac{d\Phi}{dt} = -N B A \omega \sin(\omega t) \quad (2.7)$$

then from (2.4), μ_0 , (2.6) and inductance with a core different from air [12, pp 401]

$$L = \frac{\mu_0 \mu_r N^2 A}{l} = \frac{\mu_0 \mu_r \pi N^2 d^2}{4l} \quad (2.8)$$

the coupling coefficient will be given by

$$k(x) = \frac{r_{Tx}^2 r_{Rx}^2 \cos(\theta)}{\sqrt{r_{Tx} r_{Rx}} (x^2 + r_{Rx}^2)^{\frac{3}{2}}} \quad (2.9)$$

Figure 16 describes the general arrangement of interrogator/sensor antennas in order to

describe how the angle θ affects the coupling coefficient.

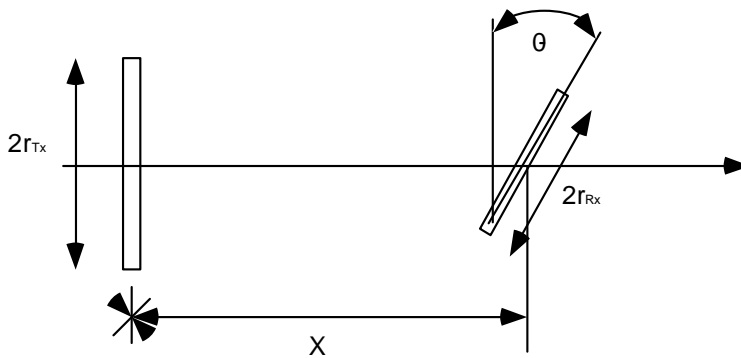


Figure 16. Antenna arrangement to compute the coupling coefficient

Clearly, in order to maximize coupling between antennas ϕ must be given by $n\pi$, $n = 0, 1, 2, \dots$. The size of the antennas should be the same and the distance X must be as small as possible.

From Figure 17, the coupling coefficient decreases as distance X between antennas increases. And as the diameter of the interrogator antenna is increased more energy reaches the sensor antenna at farther distances.

In practice, there is a limit to the antenna size because of cost constraints, and it is a good idea to make $r_{\text{reader}} \approx r_{\text{transponder}}$, because the sensor circuit, antenna included, should be as small as possible in order to avoid disturbing the bridge structure where the sensor should be embedded.

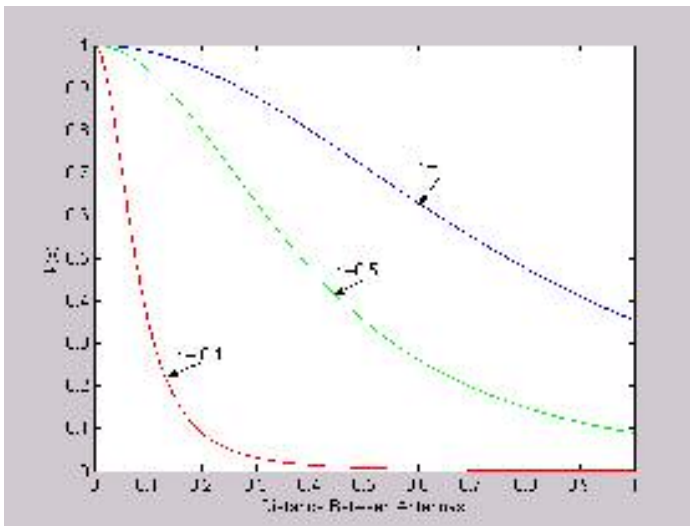


Figure 17. Coupling Coefficient behavior for different $r = r_{\text{transponder}} = r_{\text{reader}}$

It is possible to integrate the antenna on-chip as a square-type planar spiral as shown in Figure 18.

A zero-order estimate of the inductance in this kind of antenna is: $L \approx \mu_0 n^2 r$ [Henries], where n is the number of turns and r is half of the maximum length of a side of the square

spiral, as described in Figure 18 [9, equation (17), pp 48]. Exactitude of the formula is in the 30% range.

As an example in [9, pp 47-52], a 120 – nH inductor needs 27 turns and a half of the maximum length of a side of the square spiral $r = 140 \mu\text{m}$. That is the equivalent area taken by the bond pads. Therefore, the integration on-chip of an inductor is “area” expensive.

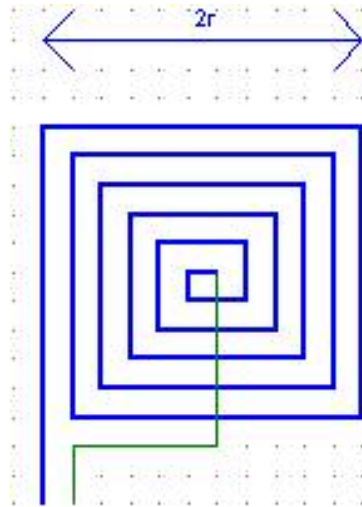


Figure 18. Square Planar Spiral Inductor [9, pp 48]

Additionally the skin effect reduces the effective cross-sectional area increasing the series resistance. Finally, the inner area is too small to work as an antenna, and such an approach is not worth additional consideration in present CMOS IC technology.

iv. Resonance

A voltage is induced in the sensor antenna. In order to maximize it, the antenna circuit must operate in resonance as an LC circuit. A capacitor is placed in parallel with L_2 of Figure 15, to set a resonance condition. Figure 19 shows a typical resonance curve. Note, voltage is maximized at the resonance frequency; therefore, in order to increase readout distance, it is best that the interrogator and strain sensor circuits work in resonance.

In practice, instead of one capacitor, two capacitors exist on the sensor circuit one of them is the parasitic capacitance C_L mainly associated with the coil antenna and the other is C_2 , see Figure 22.

The resonant frequency of an LC circuits is given by

$$f = 1/2\pi\sqrt{L_2C_2} \quad (2.10.a)$$

$C_2 = C_2 + C_L$, and C_L is the parasitic capacitance on the circuit.

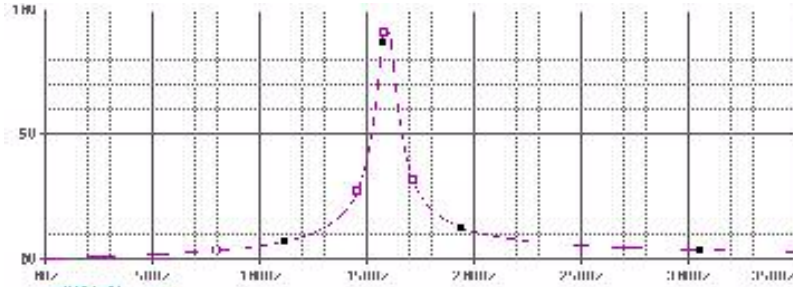


Figure 19. Typical Resonance Curve

The definition in (2.10.a) does not include the effect of the coupling between antennas or the interaction with the rest of the components of the circuit, because (2.10.a) is for simple serie or parallel LC circuits. A complete analysis is shown in (4.4), the resultant equation is reproduced here for convenience.

$$V_2 = \frac{j\omega k \sqrt{L_1 L_2} I_1}{(j\omega L_2 + R_2)(j\omega C_2 + \frac{1}{R_L}) + 1} \quad (2.10.b)$$

To compute the real resonant frequency we need to solve for the frequency when

$$(j\omega L_2 + R_2)(j\omega C_2 + \frac{1}{R_L}) = -1 \quad (2.10.c)$$

given

$$f_{1,2} = \frac{1}{8\pi^2 C_2 L_2 R_L} \left(2\pi \pi L_2 + 2\pi \pi C_2 R_2 R_L \pm \sqrt{-16\pi^2 C_2 L_2 (-R_2 - R_L) R_L + (-2\pi \pi L_2 - 2\pi \pi C_2 R_2 R_L)^2} \right) \quad (2.10.d)$$

For sake of completeness, let's fix: $L_1 = 200 \mu\text{H}$, $L_2 = 3.5 \mu\text{H}$, $C_2 = 16.61 \text{ nF}$, $R_L = 10\text{K}$, $R_2 = 0.1$, $k = 0.01$, and solve for the resonant frequency.

Solving for 2.10.c gives $f_1 = -668151. + 2764.52 \text{ } \ddot{\alpha}$, and $f_2 = 668151. + 2764.52 \text{ } \ddot{\alpha}$, resulting in an absolute value in both cases of: $f_{\text{resonance}} = 668,156 \text{ Hz}$. Now we want check last result against the simulation of (4.4) in Figure 20.

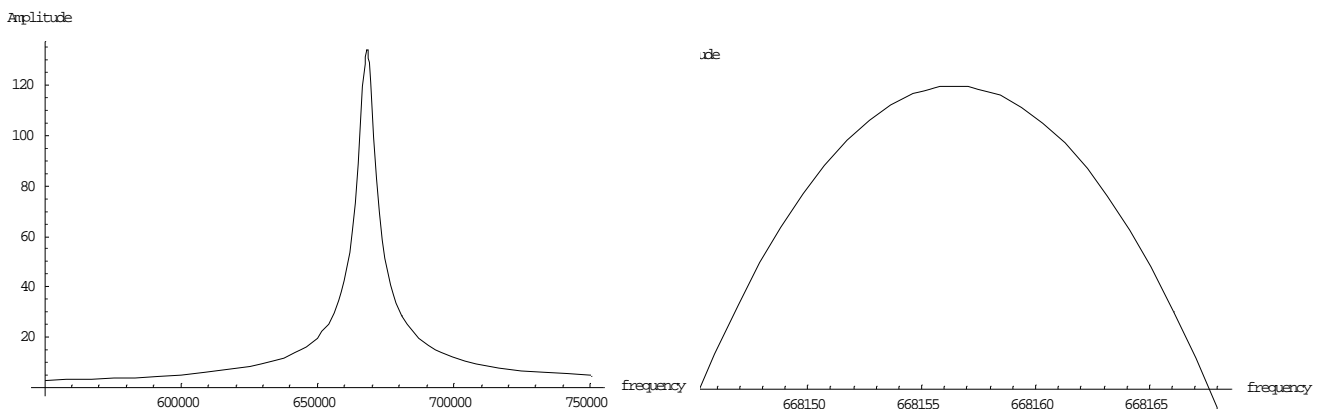


Figure 20. Resonant Frequency in Example

From Figure 20 clearly the resonant frequency matches our calculations. Let's go a step further and allow the coupling coefficient k vary from zero to one, to observe the effect of the variation k on the resonant frequency. The resultant plot is described in Figure 21, observe that the resonant frequency in the sensor circuit is practically independent from the coupling coefficient k .

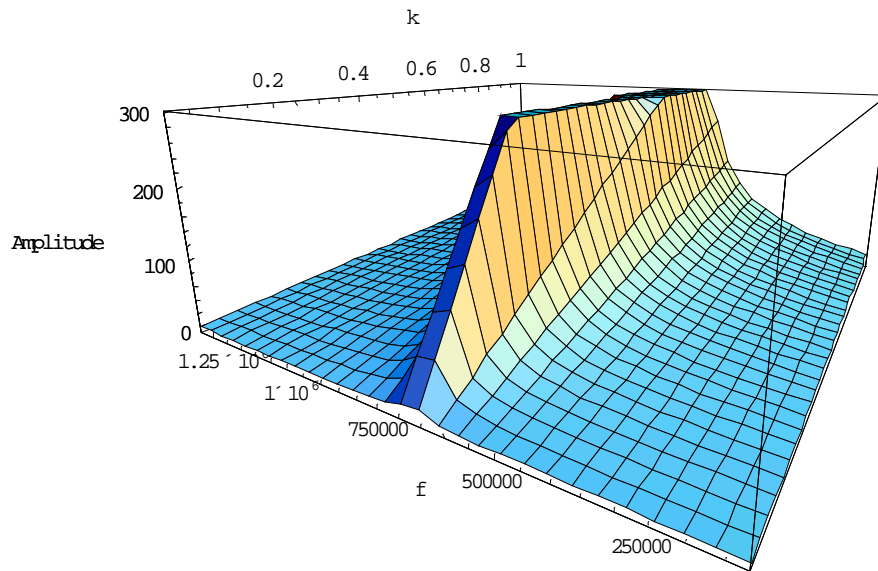


Figure 21. Resonant Frequency Versus Coupling Coefficient

A high quality factor in the reader antenna is important to increase reading distance. It is defined as: $Q \equiv 2\pi$ (maximum instantaneous energy stored/energy dissipated in a single cycle) = $f_0 / \Delta f$ where f_0 is the resonance frequency and Δf is the bandwidth 3 dB below the maximum voltage peak. In a final design, the quality factor is also important to fix the system bandwidth, the lower the quality factor, the wider the bandwidth, and vice versa.

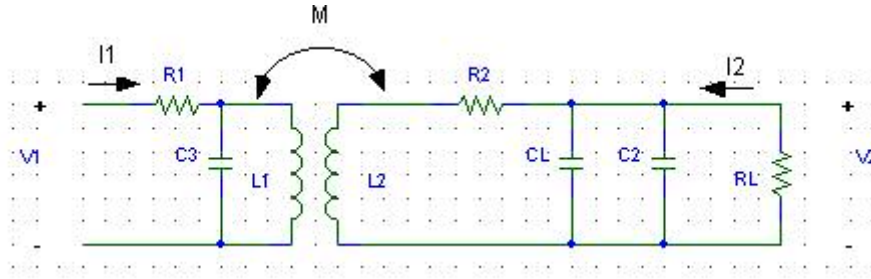


Figure 22. Circuit with Parasitic Capacitor Included

Lets express the quality factor as function of the reader components [9, pp 89]:

$$Q = \frac{2\pi f_0 L_1}{R_1} \quad (2.11)$$

And then the resonance voltage in the reader becomes:

$$V_{L_1} = \frac{2QV_1}{\pi} \quad (2.12)$$

Therefore, as quality factor increases so does the voltage in the reader antenna, reaching voltages in the order of hundred volts. The high voltage induces high currents [9, pp 89]:

$$|I_{L_1}| = Q |I_{in}| \quad (2.13)$$

Therefore, when the antenna is designed this effect must be considered. As an example, if $Q = 1500$ and $I_{in} = 2/3$ Amperes, then the current in the resistor will be 0.67 ampere but the current in the inductor will be 1000 amperes. It seems that high voltages could be dangerous to people, however, when somebody touches the antenna the additional capacitance of his body, or more specifically his hand, rapidly detunes the circuit, and as a consequence the voltage decreases rapidly.

When the reader – transponder circuit operates, both circuits must be tuned to the same resonant frequency. It is possible to have a series LC circuit in the reader and a parallel circuit LC in the transponder. In practice, there is not exactly the same resonant frequency, even when circuits are carefully designed because of temperature effects and

component tolerances. If frequencies in the reader and transponder are different, it could happen that no signal can be detected. To analyze this case, consider a real interrogator-sensor circuit, as described in the Figure 23. We want to compute the impedance of the sensor circuit as seen by the interrogator, Z_0 , as described in Figure 23.

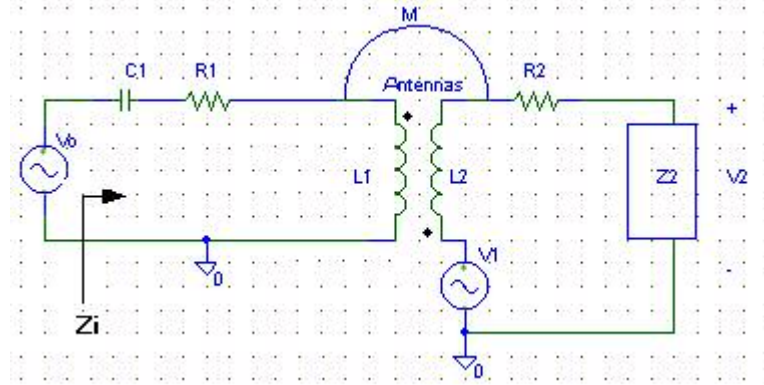


Figure 23. Equivalent Reader – Transponder Circuit

In the last Figure the voltage source V_1 represents the induced voltage in inductor L_2 , R_2 is the intrinsic resistance of the inductor L_2 , and Z_2 is the impedance of the rest of the sensor circuit; generally represented as a resistor in parallel with a capacitor. Note the sensor antenna was separated in its inductance, resistance and induced voltage effects to make analysis easier. The mutual inductance M is defined as

$$M = M_{12} = M_{21} = \oint_{\text{Sensor Antenna Area}} \frac{B_{\text{Reaching Sensor Antenna}} d(\text{area sensor antenna})}{I_{\text{ReaderCircuit}}} = \frac{\mu_0 NH(x, I_{\text{Reader}}) A_{\text{Sensor}}}{I_{\text{Reader}}} \quad (2.14)$$

Where A_{Sensor} is the area of the sensor antenna, and x is the distance between antennas.

However it is customary to work with the coupling coefficient, $k = M / \sqrt{L_1 L_2}$, instead of the mutual inductance.

$$\begin{aligned}
V_0 &= sL_1 I_1 + \frac{1}{sC_1} I_1 + R_1 I_1 - sM I_2 = sL_1 I_1 + \frac{1}{sC_1} I_1 + R_1 I_1 - sM \frac{V_1}{R_2 + sL_2 + Z_2} = \\
& sL_1 I_1 + \frac{1}{sC_1} I_1 + R_1 I_1 - sM \frac{sM I_1}{R_2 + sL_2 + Z_2} = sL_1 I_1 + \frac{1}{sC_1} I_1 + R_1 I_1 - \frac{s^2 k^2 L_1 L_2 I_1}{R_2 + sL_2 + Z_2}
\end{aligned} \tag{2.15}$$

Therefore, the impedance of the sensor seen by the reader circuit becomes:

$$Z_i(s) = sL_1 + \frac{1}{sC_1} + R_1 - \frac{s^2 k^2 L_1 L_2}{R_2 + sL_2 + Z_2} \tag{2.16.a}$$

and at resonance

$$Z_i(j\omega_0) = R_1 - \frac{(j\omega_0)^2 k^2 L_1 L_2}{R_2 + j\omega_0 L_2 + Z_2} \tag{2.16.b}$$

In (2.16.b), it was assumed that the resonance frequencies in the interrogator and sensor circuits were equal. However, when the interrogator and sensor circuits are not well tuned, some drift will occur between the transmitted signal and the signal sends back by the sensor circuit. Its effect can be described by the formula [13, pp 33-41]:

$$\theta = - \left(\arctan \left(Q_{Reader} \left(\frac{f_s}{f_R} - \frac{1}{\frac{f_s}{f_R}} \right) \right) \right) \frac{180}{\pi} \tag{2.17}$$

Where f_s is the sensor circuit resonant frequency, f_R is the reader resonant frequency and θ is the phase shift. Figure 24 shows a typical behavior of phase drift between the send and received signals as effect of the difference between resonant frequencies.

When $f_s/f_R = 1$, phase shift is zero, any other value results in phase shift.

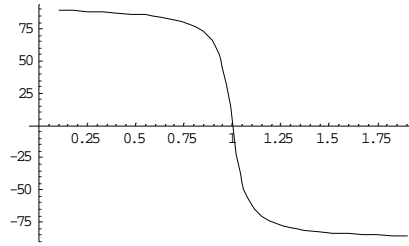


Figure 24. Phase Shift

The phase drift could be 90° as a result of the different resonant frequencies in the interrogator and sensor circuits, but could be more phase shift because of the distance between interrogator and sensor. However, this effect does not affect the demodulation of the data send by the strain sensor, unless it is modulated in phase and there is need to add a reference phase. Nevertheless, to mitigate the frequency shift it is recommended to use components with small tolerances and low sensitivity to temperature in the range where the system will be operating.

This Chapter established the theory necessary to efficiently transfer the power through RF signals in interrogator-sensor systems based on magnetic coupling. For maximum readout distances these systems must operate at resonance along the same axis, as described in Figure 10. However, readout distance will change depending on the cement mix of the bridge where the sensor circuit is embedded, as the relative permeability μ_r changes, equation (2.4). The readout distance can be increased by using antennas with ferromagnetic cores. By the contrary, if the sensor is embedded in a cement mix with high permittivity, as steel, it creates a shield effect that makes the embedded sensor circuit unreadable. Note that “maximum readout distance” is equivalent to “highest power transfer”.

The information of this chapter will be used in chapter V to design the RF-to-DC power circuit for the strain sensor circuit. The next chapter will address how to take the RF

signal generated in the sensor antenna and get an adequate DC voltage to power the rest of the sensor circuit.

Chapter 3. RADIO FREQUENCY TO DC CIRCUITS

The previous chapter analyzed how to transfer in an optimal way an RF signal. The antenna allows collecting a sinusoidal signal, then this signal is converted to a DC voltage and used to power the sensor circuit, see Figure 25.

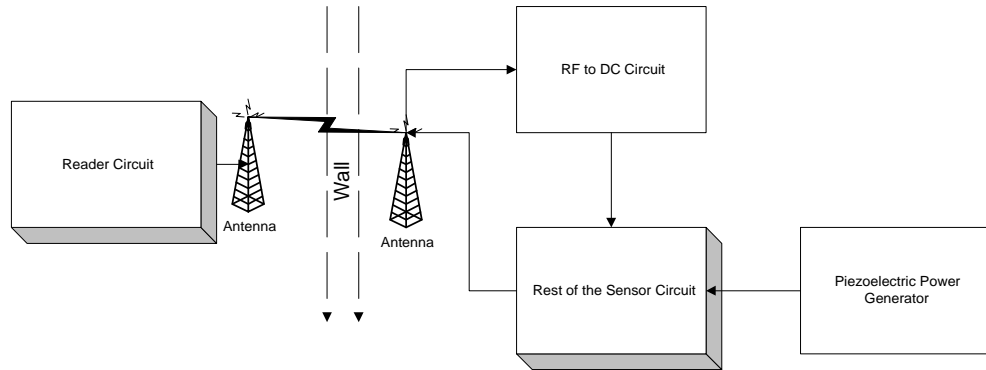


Figure 25. Sensor Circuit Power Configuration

Observe that there is an additional piezoelectric power generator, this approach is considered in the implementation of a sensor circuit in this thesis, but it is optional. The RF to DC circuit can be as simple as a half-wave rectifier or as complex as a multistage pump-charge circuit. An inherent trade-off exists between reading distance and the complexity of the circuit, given the threshold voltage, the voltage at which a PN junction begins to pass a current, of the discrete components used in the implementation of the RF to DC circuits. As more discrete components are used, the reading distance is decreased because the input signal must provide not just power to the sensor circuit but voltage to overcome the accumulated threshold voltage of all discrete components. The threshold voltage is taken off the rest of the circuit.

The rest of the chapter will present different circuit approaches on RF to DC conversion, some of them can be implemented in an electric circuit board, but most of

them are suitable for VLSI fabrication. Comments in their advantages and disadvantages will be provided.

a. Regulator Circuit

In order to power the sensor circuit the input signal must be converted from AC to DC with the smallest ripple. To accomplish this task, half or full-wave bridges using diodes can be used. However, diodes need peak input voltages bigger than their added threshold voltage to operate, reducing in this way the amount of power the regulator circuit can deliver to the rest of the sensor circuit.

In order to mitigate this problem Germanium diodes would be more conveniently used in a half-bridge rectifier configuration, as shown in Figure 26.

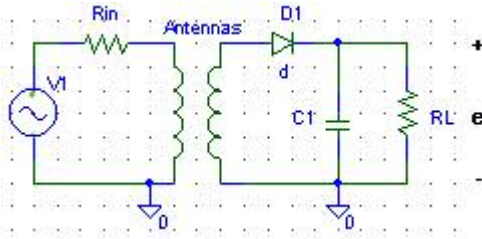


Figure 26. Regulation Circuit in Sensor Circuit

The output voltage for this circuit, as the load changes, can be considered constant for the voltage range on the sensor circuit. It is known that $B = \mu H$ and from (2.3) the output voltage in the sensor circuit, for sinusoidal RF signal, results [11, (3-6-1), pp 50]:

$$e = BA\omega \text{Sin}(\omega t) = (H\mu)(\pi r^2)(2\pi f)\text{Sin}(\omega t) = \frac{IN\mu^2 r^4 \pi^2 f}{(r^2 + x^2)^{3/2}} \text{Sin}(\omega t) \quad (3.1)$$

In practice the area, frequency and permeability keep constant, therefore $e \approx k_1 H \text{sin}(\omega t)$, and Figure 11 results. Note, how the induced voltage, e , rapidly decreases as distance

between reader and transponder increases after some point defined by the radius of the antenna, as explained in chapter 2.

Some circuit configurations are used to eliminate diode threshold voltage. However, all of them rely on additional voltage sources, not available in a passive circuit.

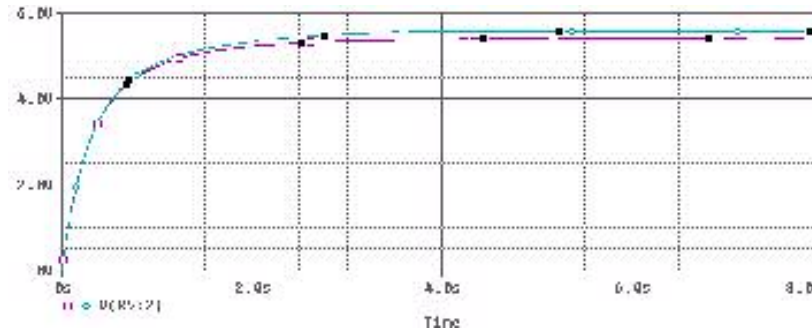


Figure 27. Output of the Regulator Circuit in Figure 26

In order to keep V_{out} constant it will be necessary to change R_L over some range that could consume too much scarce power. A better circuit solution could be the shunt circuit in Figure 28. This circuit can reduce its internal resistance when some threshold voltage is reached, and therefore keep the output voltage constant over a large range. The shunt circuit consumes almost no power up to some threshold voltage, when transistor Q_1

turns on.

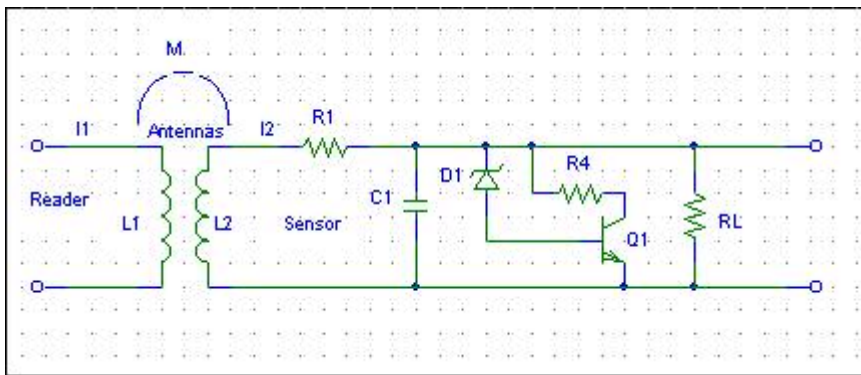


Figure 28. Shunt regulator

Another potential approach considered and tested, in this thesis was the use of low-voltage charge pumps to multiply the RF input voltage “n” times before delivering to the load as DC voltage.

b. Charge Pump Circuits

An approach widely explored and tested in this work is the use of charge pumps. Ideally, these circuits are able not only to rectify the input signal but they can deliver a DC output signal that is a multiple of the input signal amplitude. Theoretically, by increasing the number of stages on the charge pump circuit it is possible to deliver whatever DC voltage is needed at the output.

The basic circuit for a voltage doubler is shown in Figure 29. The circuit operates as follows:

1. Assuming a sinusoidal input signal, $V_{in} = A \sin(\omega t)$, with peak amplitude larger than the threshold voltage, V_{th} , of two similar diodes, and with load resistance that goes to infinity. If the first semi cycle is positive, and after $V_{in} \geq V_{th}$ the capacitor C_1 start to charge, and keeps charging up to the peak voltage ($A - V_{th}$), at that moment $V_{C1} = A - V_{th}$. This behavior can be observed in the first 4 ms of Figure 31.
2. When the sinusoidal semi cycle starts decreasing in magnitude, the capacitor retains its voltage because it has not available discharge path, $V_{C1} \geq V_{L2} = V_{secondary}$ and both diodes behave as open circuits. See Figure 31 in the 4 to 8 ms range.

3. In the sinusoidal negative semi cycle D1 behaves as an open circuit, and D2 as a short-circuit, after $|V_{in}| \leq |V_{th}|$, see Figure 30.b. Now C2 charges up to $(A - V_{th})$. Note polarity of V_{C2} , and $V_{C2} = A - V_{th}$. The output voltage is given by $V_{out} = V_{C1} + V_{C2} = (A - V_{th}) + V_{C2}$. Notice how VC2 is incrementing in the 8 to 12 ms range of Figure 31.
4. Similarly, as explained in bullet 2, $V_{C2} \leq V_{L2}$ and both diodes behave as open circuits with no trajectory to discharge.
5. Because both the capacitors have charged, and behave as DC voltage sources in series, the output voltage is: $V_{out} = V_{C1} + V_{C2} = 2(A - V_{th})$, and it represents roughly twice the peak voltage of the input signal. See the 12 to 15 ms range in Figure 31.
6. Actually, the load current should be different from zero and, therefore, some current will be applied to the load resistance. The current load will discharge the capacitors and $V_{out} = V_{C1} + V_{C2} < 2(A - V_{th})$. To mitigate, to some extent, the voltage reduction; capacitors of larger values should be used. In order to operate correctly, the input signal amplitude must be considerably larger than the diode threshold voltage (V_{th}), i.e., $V_{th} = 0.7$ volts if we use Silicon diodes or $V_{th} = 0.3$ volts if Germanium diodes are used.

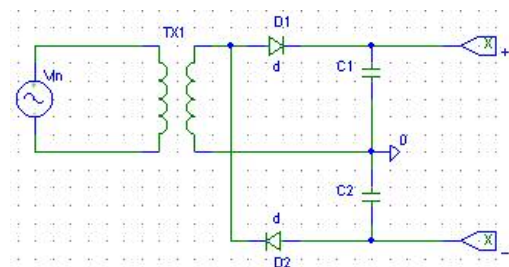


Figure 29. Doubler Circuit

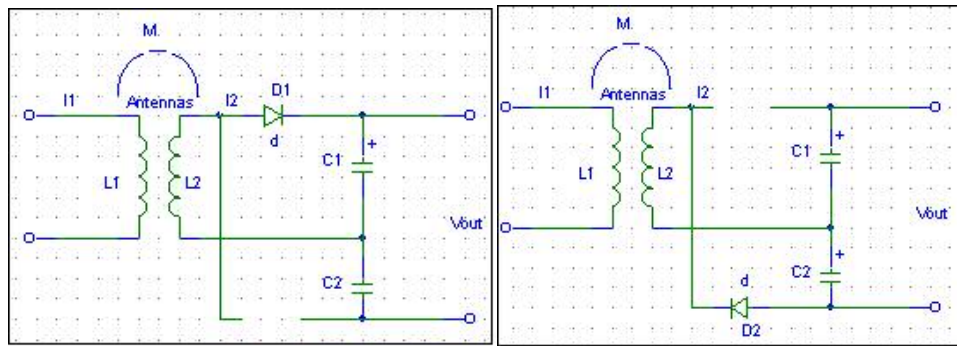


Figure 30. Doubler Circuit Operation

a) Positive Semi Cycle b) Negative Semi Cycle

Figure 31 shows the output signal of the doubler circuit. As expected, the output voltage is twice the input peak voltage of 10 V, minus twice the diode threshold voltage, 1.4 V. The output voltage is taken in the output terminals of the circuit, with the lower terminal used as ground reference. If ground is in the middle then we have a positive and negative output voltage.

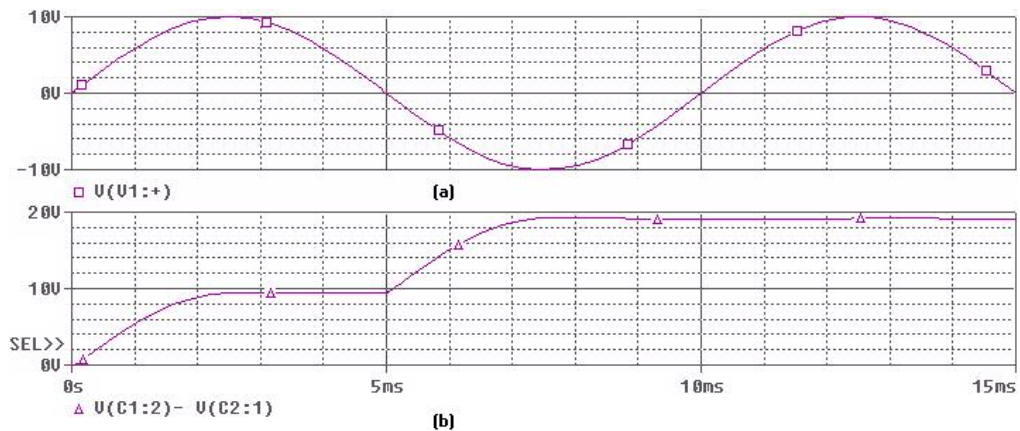


Figure 31. Doubler Output Signal. (a) Input Signal. (b) Output Signal

The circuit concept in Figure 29 can be extended to “n” stages. Theoretically, this circuit produces $2nV_{in}$ as output voltage in the terminals of the output capacitor, C_{2n} in Figure 32.

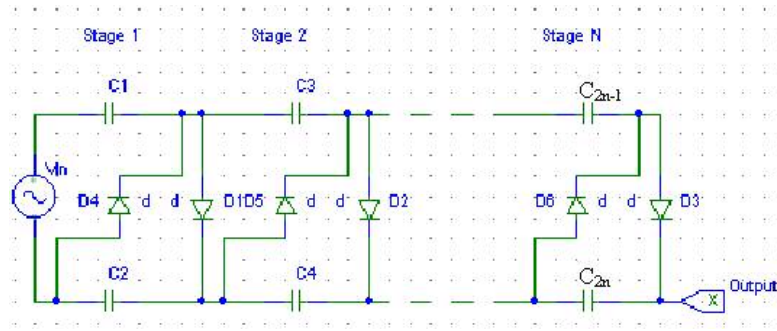


Figure 32. Cascade of Doubler Circuits as Voltage Multiplier

However, this ideal output voltage is valid only when the load of the circuit is negligible. When the circuit is loaded, there is a charge drained from the capacitors that results in a drop of the output voltage. The charge drained by the load per period is [17, (24), pp 526]

$$\Delta q = I_{load} T = I_{load} / f \quad (3.2)$$

A complete analysis on the causes of the voltage drop using charge variations in charge pumps is given in [17 (50)-(51), pp528]. The output voltage of an n-stage charge pump as described in Figure 32 results in:

$$V_o = nV_{in} - \frac{n-1}{fC} I_{load} \quad (3.3)$$

Where C is the stage capacitance, I_{load} is the load current, f is the frequency of the input signal and n is the number of stages. From (3.3), the voltage drop increases as the load current or the number of stages increases. To compensate for this drop, the frequency or the capacitance must increase.

There are some important assumptions used to derive (3.3) in [17]: the multiplier network consists of n ideal capacitors, ideal diodes and one sinusoidal voltage source. The analysis is done in the steady state, the capacitance of the last capacitor goes to infinity,

and the rest of the capacitors have the same value. The topology of the charge pump used to derive (3.3) is described in Figure 32.

Effort was done to summarize derivation in [17] in a few pages, but it was not possible to do that without losing the essence of the major results in that paper. Please, refer to [17] for the derivation of (3.3). For graph theory and notation, not explained in [17], refer to [18, pp 104-112]. As an example, if we assume $I_{load} = 3.25 \text{ mA}$, $f = 125 \text{ KHz}$, $C = 1 \mu\text{F}$ and $n = 4$ in (3.3), the voltage drop results to be 78 mV. The result is not a considerable voltage drop. However, there are also non-linear and charge- storage effects of the diodes that cause additional voltage drop. To analyze the additional voltage drop, consider a non-ideal model for the diode as shown in Figure 33, where C_1 is given by the summation of the junction capacitance C_j and the storage capacitance C_s . V_D is the threshold voltage, 0.7 for Silicon and 0.3 for Germanium respectively.

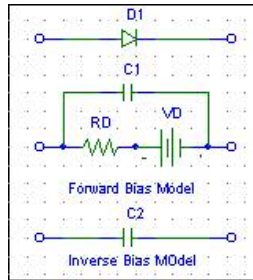


Figure 33. Silicon Diode Large Signal Model

a) Diode b) Forward Bias Model c) Inverse Bias Model

Note: $C_1 = C_j \parallel C_s$ [13, pp 33-41], where C_j is the junction capacitance due to the depletion region and C_s is the storage capacitance due to diffused charges.

$$C_j = \frac{C_{j0}}{\left(1 - \frac{V_D}{\phi_0}\right)^m} \quad (3.4)$$

Where C_{j0} is the zero-bias capacitance, V_D is the diode voltage, m is the grading coefficient and φ_0 is the built-in potential

$$\varphi_0 = V_T \ln \left(\frac{N_A N_D}{n_i^2} \right) \quad (3.5)$$

N_A and N_D are the acceptor and donor dopings, $V_T = \frac{kT}{q}$, the thermal equivalent voltage

and n_i is the intrinsic Silicon carrier concentration. A typical behavior of C_j in (3.4) is sketched on Figure 34.

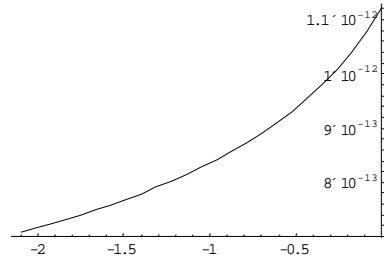


Figure 34. Depletion Capacitance vs. V_D , with $m = 1/2$ and $\varphi_0 = 0.75V$

In this model, there is power dissipation in R_D , a drop voltage V_D and a current leakage through C_1 . C_j is the dominant capacitance in the model, and m depends on doping geometry. For uniform abrupt junction $m = 1/2$, and for linear variation doping $m = 1/3$.

The storage capacitance is given by:

$$C_S = \frac{I_D \tau_R}{n V_T} \quad (3.6)$$

Where I_D is the diode current, τ_R is the carrier lifetime, i.e., time to recombine an electron with a hole, n is the non-ideality factor in the typical range between one and two.

When the diode is reverse biased the depletion region is widened as the majority carriers are pulled away from the PN junction. The model for this condition is described in Figure 33.c, and C_2 is given by [19, (4.3.8), 190]

$$C_2 = \left[\frac{q\epsilon_s}{2 \left(\frac{1}{N_a} + \frac{1}{N_d} \right) (\phi_0 - V_{in})} \right]^{\frac{1}{2}} \quad (3.7)$$

$\epsilon = \epsilon_0 \epsilon_r$ is the permittivity, ϵ_0 is the permittivity of vacuum

($\epsilon_0 = 8.854 \times 10^{-14} \text{ F cm}^{-1}$), ϵ_r is the relative permittivity of the semiconductor material

($\epsilon_r = 11.7$ Silicon, 16 Germanium) and q is the electronic charge ($q = 1.602 \times 10^{-19} \text{ C}$). If

a Silicon PN junction with $N_d = 10^{15} \text{ cm}^{-3}$, $N_a = 10^{18} \text{ cm}^{-3}$, and $n_i = 1.45 \times 10^{10} \text{ cm}^{-3}$ is

fabricated, then from (3.5) and (3.7) the C_2 capacitance results

$$\phi_0 = \frac{kT}{q} \ln \left(\frac{N_A N_D}{n_i^2} \right) = 0.75 \text{ V}$$

and

$$C_2 = \left[\frac{q\epsilon_s}{2 \left(\frac{1}{N_a} + \frac{1}{N_d} \right) (\phi_0 - V_{in})} \right]^{\frac{1}{2}} = \left[\frac{(1.6 \times 10^{-19})(8.854 \times 10^{-14})(11.7)}{2 \left(\frac{1}{10^{-18}} + \frac{1}{10^{-15}} \right) (0.75 - V_{in})} \right]^{\frac{1}{2}} = 2.877 \times 10^{-25} \frac{1}{(0.75 - V_{in})^{\frac{1}{2}}} \text{ F}$$

Plotting C_2 versus the bias voltage on previous example shows how the capacitance

decreases as the inverse voltage increases.

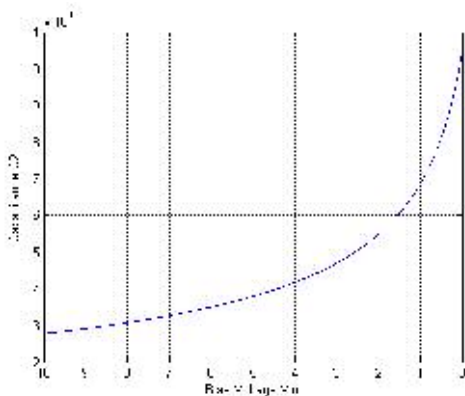


Figure 35. Capacitance Versus Inverse Bias Voltage in a PN Junction

The capacitance effect is more evident as the charge pump operation frequency is increased because the impedance of the capacitor decreases with frequency,

$$|Z_c| = \left| \frac{1}{j\omega C} \right| = \frac{1}{2\pi f C}. \text{ To complete the potential causes of the voltage drop in a charge}$$

pump it is necessary to review the currents in a PN junction. For forward bias, the most important limitation of the diodes in a charge pump is the threshold voltage associated to all PN junctions, because the threshold voltage sets an inferior limit to the amplitude of the input RF signal to generate voltage to the rest of the sensor circuit.

For reverse bias the current associated with the minority carriers, i.e., holes in the “n” region and electrons in the “p” region, leaks the charge stored in the capacitors of the charge pump circuit decreasing the voltage in the capacitors in that process. The total minority current can be calculated as [19, (5.3.15) and (5.3.19), pp 237 and 239]

$$J_t = J_0 \left(e^{\frac{qV_a}{kT}} - 1 \right) \quad (3.8)$$

J_0 is the saturation current density when a negative bias is equal to kT/q volts and V_a is the applied voltage, negative or positive as described in Figure 36. J_0 is determined by the less doped region in a PN junction [19, p239]. Equation (3.8) describes the current flow in a PN junction for both forward and reverse bias. The diode threshold voltage is given by the built-in potential at the PN junction [19, (4.2.10), pp181] as described by

$$V_{th} = \frac{kT}{q} \ln \frac{N_d N_a}{n_i^2} \quad (3.9)$$

Those capacitances, their associated leakage currents and the diode threshold voltage result in an ineffective power driven multiplier. The effect becomes more evident as the input voltage becomes smaller.

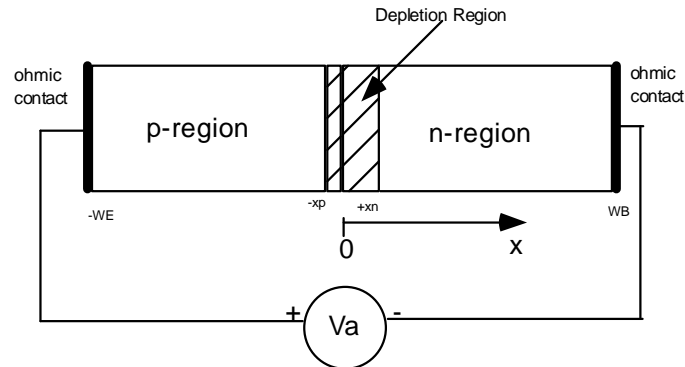


Figure 36. PN Junction Diode Structure Used to Derive Inverse Current [19, Figure 5.5, pp 233]

c. Charge Pump Circuit Simulations

Next, simulations will show how internal capacitances and leaky current affect the performance of charge pumps. Figure 37 shows a potential quintupler circuit. For an input signal of $0.75 \sin(\omega t)$ the ideal expected output voltage is five times 0.75 V , or 3.75 volts. However, from Figure 38 and R_7 in 37, the output is 3.25 volts at 3.25 mA load, i.e., a loss of 0.5 volts. Now lets consider (3.3)

$$V_{o2} = nV_{in} - V_{th} - \frac{n-1}{fC} I_{load} = 5 \times 0.75 - 0.3 - \frac{4}{125,000 \times 5 \times 10^{-6}} \times 0.0035 = 3.4276 \text{ Volts}$$

where $V_{th} = 0.33$ volts is the threshold voltage of the Schottky diodes in Figure 37.

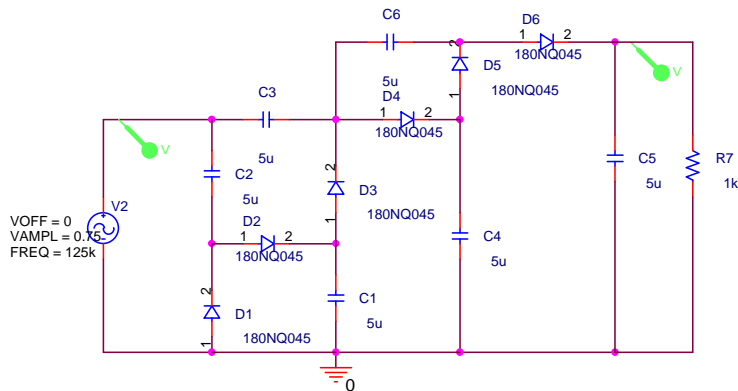


Figure 37. Quintupler Charge Pump Circuit

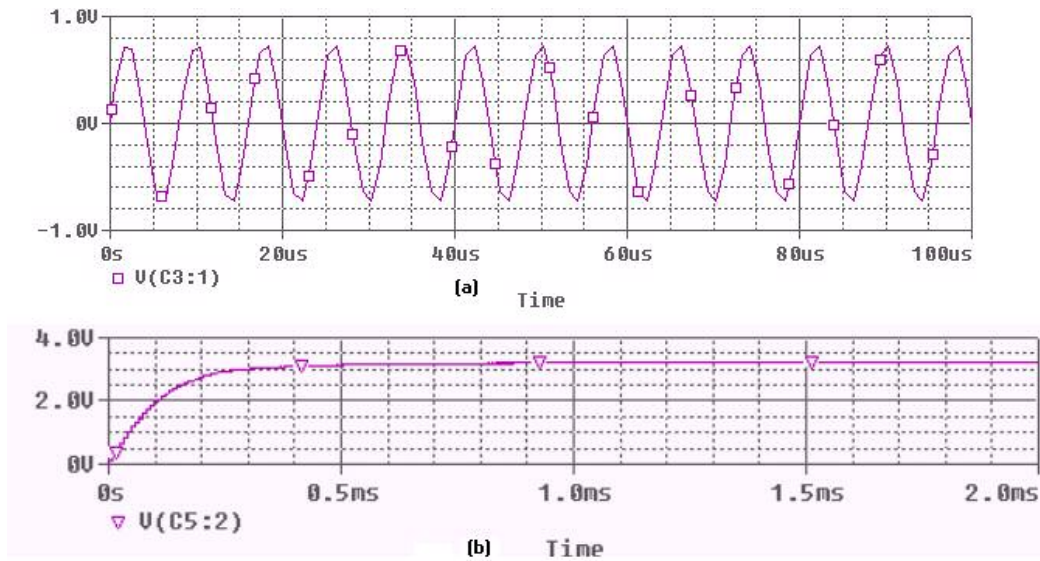


Figure 38. (a) Quintupler Input Signal. (b) Quintupler Output Signal (Plots not at scale)
 Therefore, the diode parasitic capacitances and inverse current saturation are responsible for an additional voltage drop of

$$\Delta V = V_{o2} - V_o_{measured_in_simulation} = 3.4276 - 3.25 = 0.1776 \text{Volts} .$$

Given the limitations on the input voltage, it seems that this circuit works acceptably well, the additional losses are mainly due to the threshold voltage of the Schottky diode: 0.33 volts compared to 0.1776 of the other undesirable effects.

However, the front-end of this circuit will be used to send measurement data. Data will produce a dynamic variation on the input power supply resistance because the sidebands of the modulated signal are not at the resonant frequency. To simulate this effect a variable resistance in the input circuit is added. Besides, it is desirable to consider the effect of the intrinsic resistance of the nodes in the breadboard on which the charge pump will be assembled. Small resistors throughout the charge pump circuit simulate this influence as shown in Figure 39.

Fifthtupler with Resistance
Effect Added . This Circuit
Varies Input Resistance.

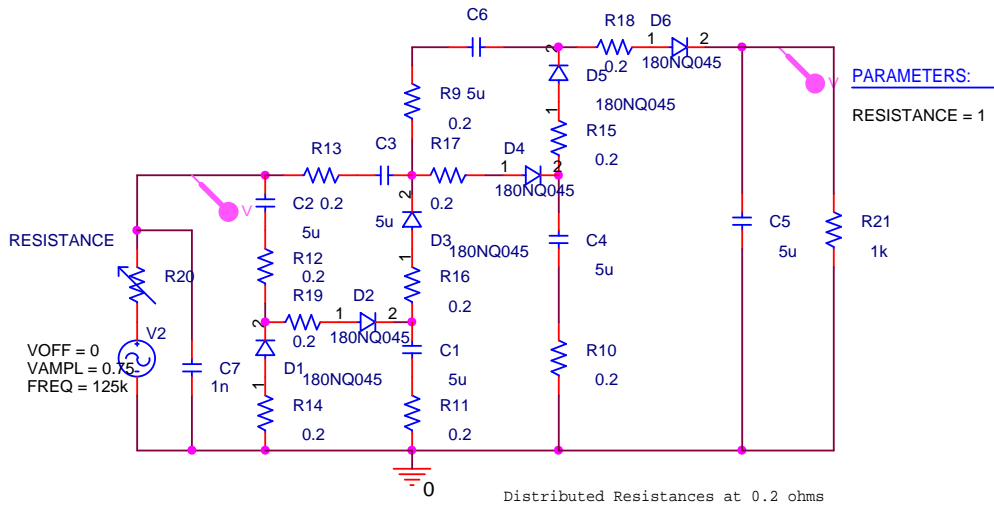


Figure 39. Charge Pump Circuit with Variable Input Resistance

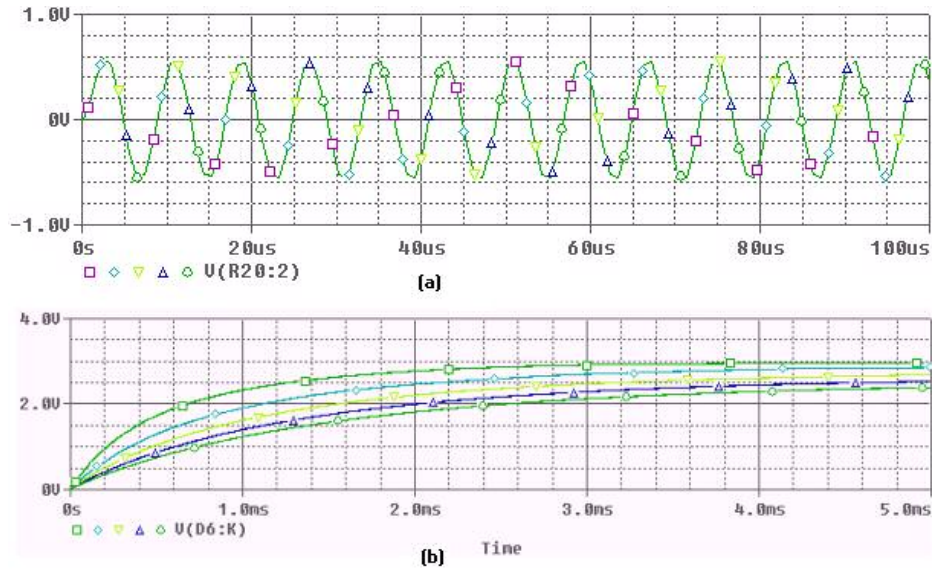


Figure 40. (a) Input Signal. (b) Output Signals for Variable Resistance (Not to Scale)

The resistance is increases from the top to the bottom curves. As expected, the output voltage decreases as the input resistance increases. The output voltage is as low as 2.4 volts with a voltage loss of 1.35 volts. In the reader–sensor system of Figure 25, it means that a smaller reader-sensor distance is allowed.

A popular charge pump, due to Dickson [20, pp 378], has the configuration shown in Figure 41. This circuit uses two complementary phase clocks to multiply the input voltage. Note the stray capacitance, C_{s1} - C_{s4} , has been added on the top of the circuit of Figure 41 to get a simulation closer to the real implementation of the circuit.

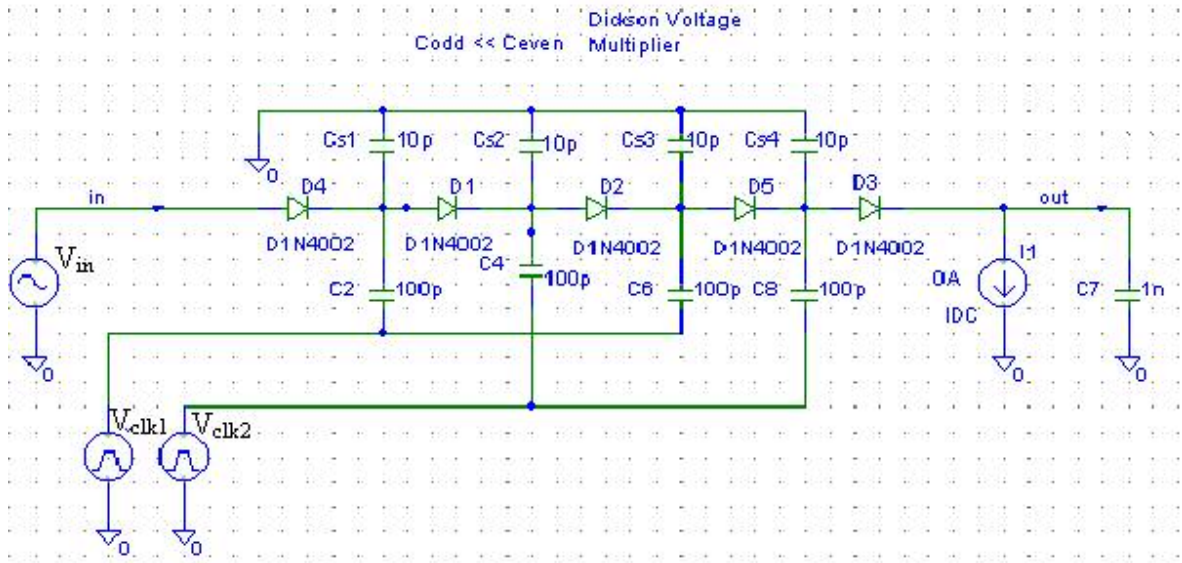


Figure 41. Dickson Charge Pump

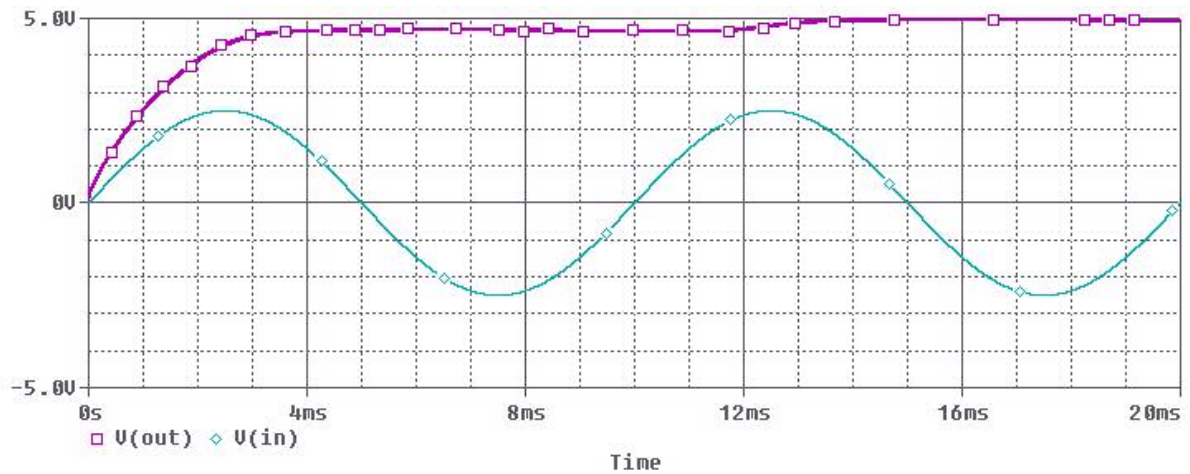


Figure 42. Dickson Charge Pump Input and Output Signals

The analysis of the circuit [20, pp 376] shows that the output voltage is given by

$$V_{out} = V_{in} + N(V_{\phi} - V_D) - V_D \quad (3.10)$$

where V_ϕ is the voltage amplitude of the two anti-phase clock signals and V_D is the built-in voltage of the diodes. However, the stray capacitance reduces the transferred voltage by $C/(C + C_s)$, where C is any of the capacitances in the circuit. The output voltage will be

$$V_{out} = V_{in} + N \left(\frac{C}{C + C_s} V_\phi - V_D \right) - V_D \quad (3.11)$$

Observe in Figure 41 that the load current is zero. If the effect of the load current is considered, then the output voltage will be additionally reduced by the factor [20, (2), pp 376]

$$\frac{NI_{out}}{(C + C_s)f_{osc}} \quad (3.12)$$

and the output voltage will be

$$V_{out} = V_{in} + N \left(\frac{C}{C + C_s} V_\phi - V_D - \frac{I_{out}}{(C + C_s)f_{osc}} \right) - V_D \quad (3.13)$$

with multiplication effect if and only if

$$\frac{C}{C + C_s} V_\phi - V_D - \frac{I_{out}}{(C + C_s)f_{osc}} > 0 \quad (3.14)$$

In practice, the diodes are substituted by NMOS transistors connected as diodes, and V_D becomes the threshold voltage V_{th} of the diodes. If the Dickson charge-pump circuit is cascaded to the strain-sensor circuit of Figure 28, the anti-phase clock signals can be obtained from the terminals of the antenna as described in Figure 69 in the role of the terminals of the inductor L_{sen} . More elaborated circuits have been designed [21, 22, 23], some of them to work on input voltages as low as one volt, however, all of them require an external power supply to provide a voltage bigger than one volt. Another drawback of

those circuits, if operated as part of a passive wireless sensor, is the relatively large power dissipation. There are some other papers that consider ultra low voltage operation [27, 28], but they try to overcome the threshold voltage by a floating-well or by using cell arrays. The last approach considers the use of a cell that can be driven by input voltages as low as $0.3\sin(\omega t)$. However, to make the cell active, it requires an external voltage supply of at least 1.2 v, making the circuit useless when there is no access to the 1.2 voltage supply, as in the sensor circuit of interest here. Anyway, it is possible to reduce the threshold voltage on the charge pump circuit just by using Germanium transistors in a diode connection. It produced a modest gain on the reading distance.

Another approach considered to increase reading distance, by overcoming the diode threshold voltage, was the use of an up-transformer. In theory it is a sound idea because given a small sinusoidal input voltage, the output voltage can be made as big as necessary just by increasing the number of winding turns on the transformer secondary as indicated in (3.15). See Figure 43.

$$V_{out} = V_{in} \frac{N_s}{N_p} \tag{3.15}$$

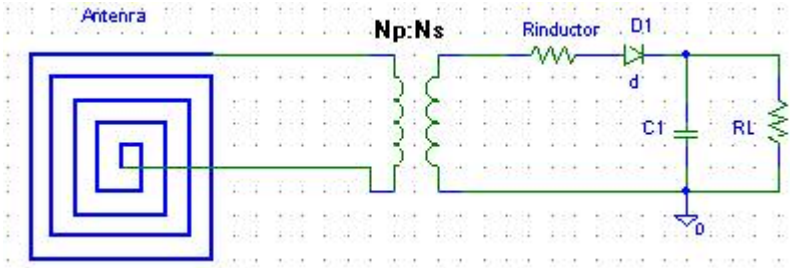


Figure 43. Sensor Circuit with Transformer

A run simulation in Figures 44 and 45 show the validity of the approach.

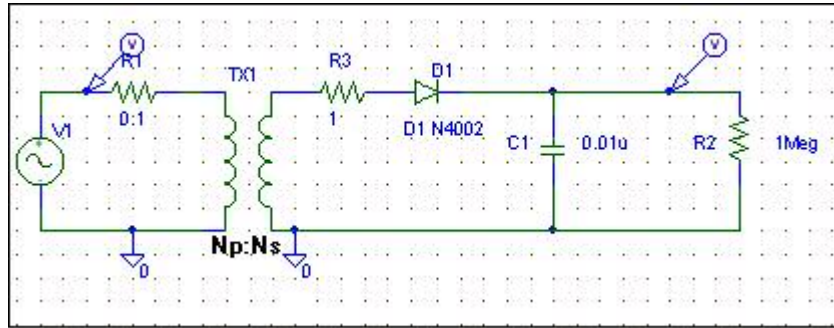


Figure 44. Sensor Circuit with Transformer

Observe in Figure 45 the peak amplitude of the sinusoidal input signal is just 20 mV, and the output is slightly more than 2.5 volts, i.e., a voltage multiplication of 125. It is not possible to display clearly the sinusoidal input signal given the long time took by the capacitor C_1 to charge. The input inductance was set to $3.5 \mu\text{H}$ and the output to $100,000 \mu\text{H}$, working at 125KHz .

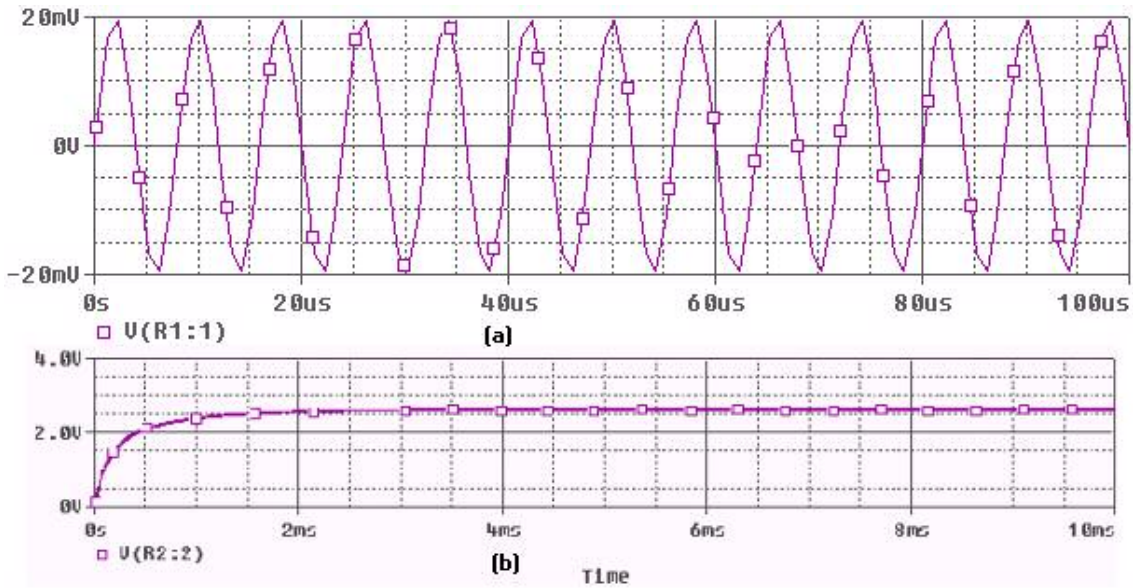


Figure 45. (a) Input Signal. (b) Output Signal (Plot (a) not at Scale)

However, the expected output voltage, from (3.15) and circuit in Figure 44, is:

$$V_{out} \approx V_{in} \frac{N_s}{N_p} - V_{th} = V_{in} \frac{L_s}{L_p} - V_{th} = 20 \times 10^{-3} \left(\frac{100,000 \times 10^{-6}}{3.5 \times 10^{-6}} \right) - 0.7 = 570.73 \text{ volts}$$

The output voltage on the simulation is small compared to the expected output voltage. The reason of this huge difference is based in the transformer behavior at relatively high frequencies. There is a tendency for high frequency currents in the wiring to move to the wire surface, reducing the transversal area of the wire, then, increasing the resistance associated to the cable, $R = \rho L / A$, resulting in a substantial increasing of the winding loss. Also, as frequency increases, the impedance of the stray capacitance between winding turns, $|Z_c| = |1 / j \omega C|$, decreases limiting the amplitude of the transformer-generated signal.

These, effects can be mitigated at some level, by interleaving coil windings, and a good transformer design can produce the desired output voltage, especially at medium frequencies like 125 KHz.

The last discussion shows the feasibility of the transformer approach to increase the reading distance as desired. However there is an insolvable characteristic in all transformers: they are bulky, and they become bulkier as the desired reading distance, between reader and sensor circuits, is increased, and proportionally the number of turns in the secondary of the transformer need to increase.

If the design of the structure of the bridge allows embedding sensor circuits the size of a HP calculator, this is a good approach to consider. In the next chapter, the design of a complete sensor circuit based on an up-transformer will be presented.

Finally, it is important to remember that the reading distance of the up-transformer sensor circuit is limited to operate in the near field, see appendix B.

Chapter 4. DESIGNS AND TEST RESULTS

a. Design of a Sensor Circuit Based on an Up-Transformer

Consider the design of the transformer for the circuit simulated in Figure 44, and implemented as in Figure 43, reproduced in Figure 46.

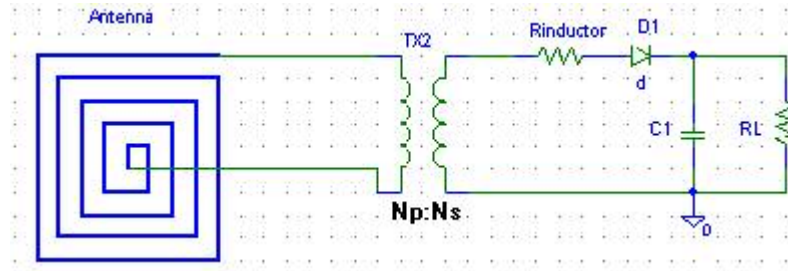


Figure 46. Sensor Circuit with Transformer

The design will be explored in three steps:

- i. Design of the basic sensor circuit with an up-transformer in resonance
- ii. Reader-Sensor system circuit with an up-transformer in resonance
- iii. Reader-Sensor system circuit with an up-transformer in resonance and output doubler charge pump

i. Design of the basic sensor circuit with an up-transformer in resonance

For the first design, Figure 47, it is necessary to compute the self-inductances of the primary and secondary windings, from [24, (8.19), pp 190]:

$$L = \frac{\mu N^2 A}{l} \text{ Henrys} \quad (4.1)$$

where A is the transversal area of the core in square meters, l is the length of the winding in meters and μ is the permeability.

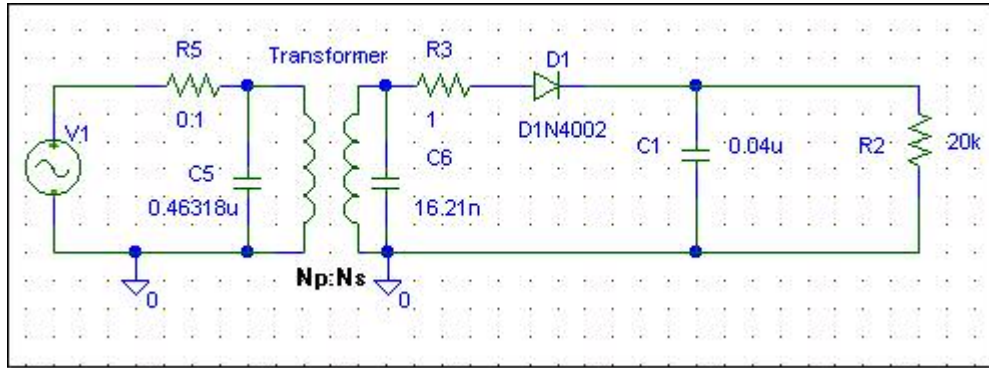


Figure 47. Sensor Circuit with Up-Transformer in Resonance

A natural design approach is first to try to design the smallest possible transformer by using a ferromagnetic core with high permeability. However, a high permeability core does not allow the design of the primary winding of the transformer to be $3.5 \mu\text{H}$, with at least one turn in the primary winding. Therefore, it is necessary to solve for the relative permeability, with one turn and $L_{\text{primary}} = 3.5 \mu\text{H}$, thus the circuit is at 13.56 MHz resonance.

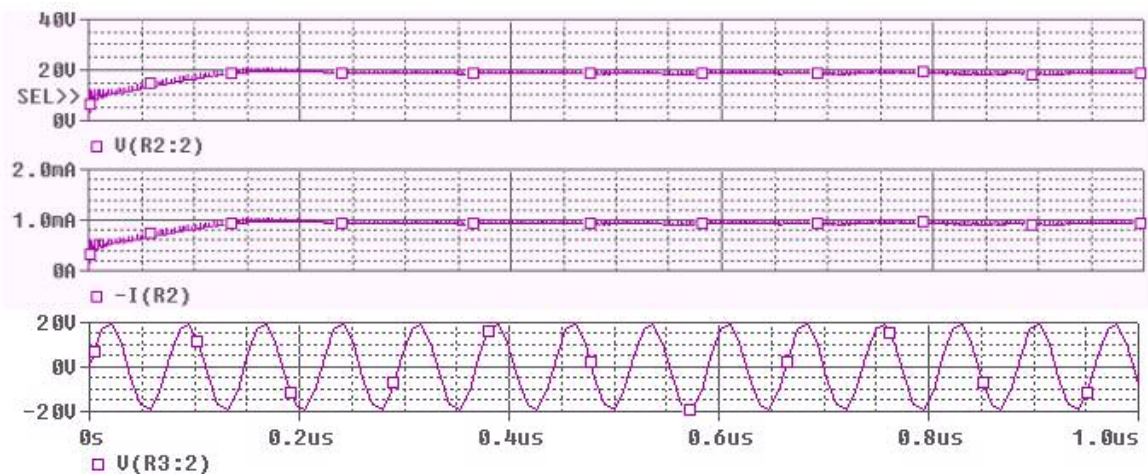


Figure 48. Sensor Circuit with Up-Transformer in Resonance. From top to bottom:
Output DC voltage, Output Current, Sinusoidal Voltage Signal in the Transformer

Secondary

Let us use a commercial iron toroidal core with dimensions: 36/25/7 mm, (external_perimeter/internal_perimeter/wide), and cross sectional area $A = 7 \times 11 \text{ mm} = 0.000077 \text{ m}^2$. We want to keep the transformer primary turns to a minimum, $N = 1$, so, that the relative permeability of the core is so large that saturation of the core is avoided, and the number of turns in the secondary is minimum. Pick wire AWG 14, with cross sectional area equal to 2.08 mm, then $l = 0.00162737 \text{ m}$ (diameter of the cable). We want to compute the relative permeability μ_r to have an inductance of $3.5 \text{ } \mu\text{H}$, then from (3.15):

$$\mu_r = \frac{IL}{N^2 \mu_0 A} = 58.8646 \quad (4.2)$$

Use (4.2) to compute the number of turns, N , in the secondary to have $L_{\text{secondary}} = 0.1$ Henry inductance, so that voltage gain is considerable and the toroidal coil is not so big. In this case, the length of the coil is the perimeter of the toroidal core, $l = 0.09582 \text{ m}$ at same core cross sectional area A .

$$N = \left(\frac{IL}{\mu_0 \mu_r A} \right)^{\frac{1}{2}} = 1297.03 \approx 1297 \text{ turns} \quad (4.2)$$

To compute the capacitance values needed to set both sides of the transformer in resonance

$$\omega_0 = \left(\frac{1}{LC} \right)^{\frac{1}{2}} \quad (4.3)$$

The resultant circuit and its signals, Figures 47 and 48, works well for $f_0 = 13.56 \text{ MHz}$. However, the supply signal was set relatively large, $5 \text{ Sin}(\omega t)$, to force the circuit to deliver 1 mA . Note the expected size of the transformer to give here. Recall, that the sensor circuit, motive of this research, will be embedded in the body of a bridge and

should be kept to minimum size, so it does not perturb the physical structure of the bridge. To extend the distance between reader and sensor circuits, we need to consider the whole reader-sensor system of Figure 25, as is done in the next design.

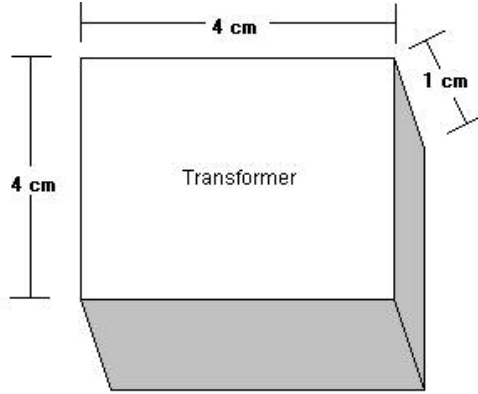


Figure 49. Size of the Up-Transformer

ii. Reader-Sensor system circuit with an up-transformer in resonance

From Figure 23, $M = k\sqrt{L_1L_2}$, (2.15) and considering $Z_2 = C_2 \parallel R_L$, it is possible to show that the output voltage in that sensor circuit is given by:

$$\begin{aligned}
 V_{out} = V_2 &= \frac{V_1 Z_2}{sL_2 + R_2 + Z_2} = \frac{V_1}{(sL_2 + R_2)(sC_2 + \frac{1}{R_L}) + 1} \quad (4.4) \\
 &= \frac{sk\sqrt{L_1L_2} I_1}{(sL_2 + R_2)(sC_2 + \frac{1}{R_L}) + 1}
 \end{aligned}$$

Note that C_2 may include the stray capacitances. If all parameters are fixed and the frequency is varied, a typical response of the circuit occurs, see Figure 50. As expected, there is a resonance frequency. As explained in chapter 2 and from (4.1) and Figure 50, it is a good idea to set the reader-sensor circuit in resonance to maximize V_{out} and consequently extending the reading distance. In the circuit of Figure 23 it is recommended to keep C_2 variable to get fine-tuning after the circuit is assembled, that is

equivalent to keep C_1 variable in Figure 51. The steps to design this circuit are the same as before, the circuit designed and its output signals are presented in Figures 51 and 52.

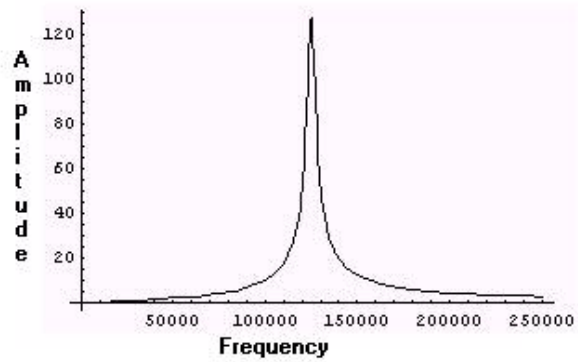


Figure 50. Frequency Response of (4.1)

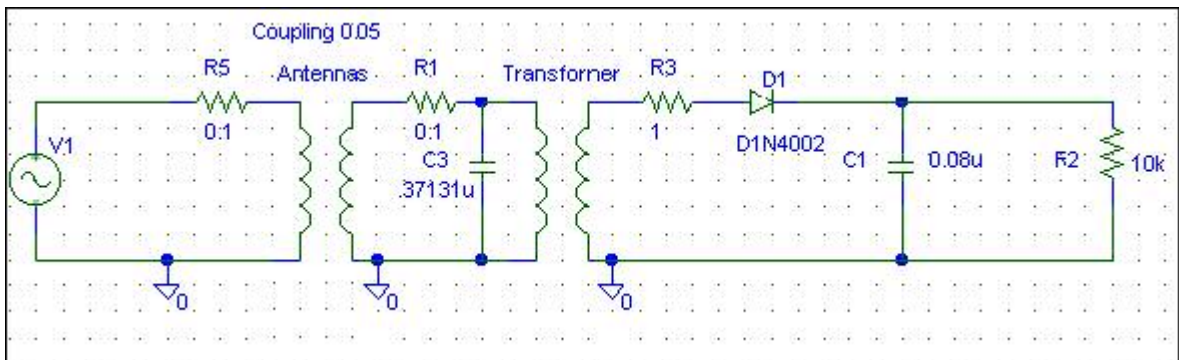


Figure 51. Reader-Sensor system circuit with an up-transformer in resonance

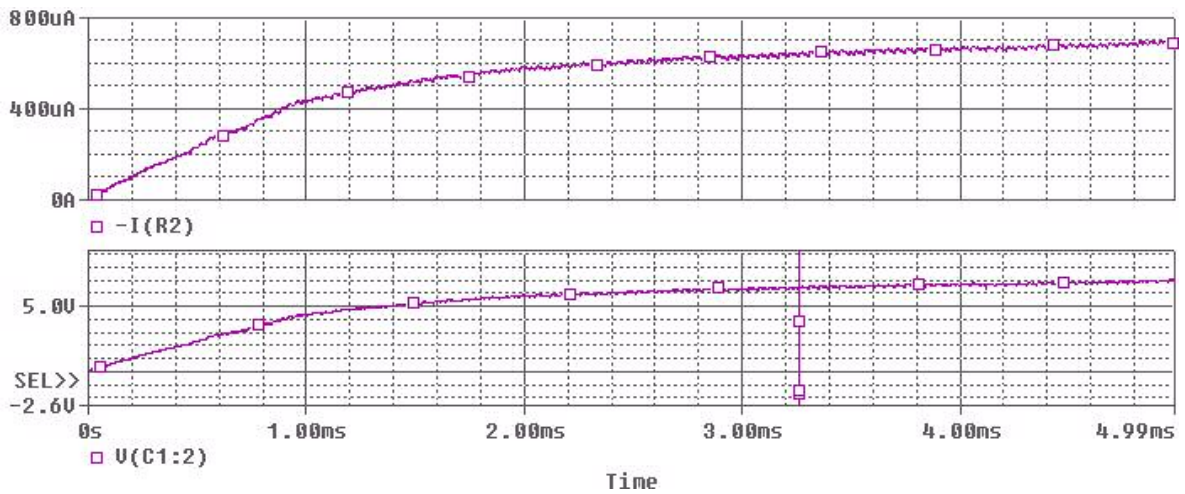


Figure 52. System Signals. From Top-to-Bottom: Load Current, Load Voltage

Note that the coupling factor $k = 0.05$, is very small and still the sensor circuit was able to deliver 7 volts with a load of 0.7 mA. The small load current the circuit is able to deliver put a pressure in the design of the rest of the sensor circuit, but at least the voltage is adequate. If the reading distance is incremented, the coupling factor k suffers an additional decrease, and at some point the circuit will not be able to deliver enough voltage, neither current, to the load.

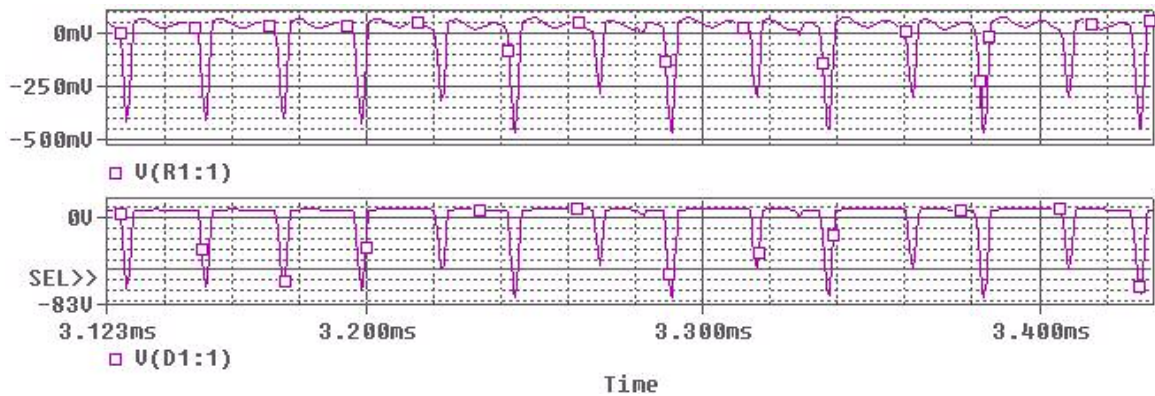


Figure 53. Reader-Sensor System Signals. From Top-to-Bottom: Voltage in Sensor Antenna, Voltage in Secondary of Transformer of Figure 51

Observe in Figure 53 that the display of the signals is when the DC output voltage is stable in Figure 52.

The top of Figure 53 shows how the antenna voltage at less than 0.5 V_{peak} is unable to overcome the silicon threshold voltage of the diode. The bottom plot shows the signal after the up-transformer, about 70 V_{peak} for a voltage gain of about 140. Resolution of the signals in PSpice is not good but still shows the important effect of the transformer.

The final DC voltage, 7 volts, is small because transformer works at constant power:

$$V_{primary} I_{primary} = V_{secondary} I_{secondary} \quad (4.5)$$

When the transformer amplifies the voltage signal, it must reduce the secondary current to keep the power at the same level.

Therefore, even though the transformer delivers a big amplitude voltage, at the same time, it is not able to provide more current to charge a bigger C_1 capacitor which could be used to feed a larger load. The size of the transformer is even now the same as in the basic sensor circuit with an up-transformer in resonance, Figure 49.

The next design step considers the use of a charge pump as a mean to increase the V_{DC} output level, or to keep the same V_{DC} level but requiring less turns in the transformer secondary, and consequently reducing the size of the transformer.

iii. Reader-Sensor system circuit with an up-transformer in resonance and output doubler charge pump

To investigate the use of a charge pump, there will be added a doubler to the circuit in Figure 51, as shown in Figure 54. The design steps are the same as for the previous two circuits with the addition of the doubler circuit; the circuit was fine-tuned to resonance again. The circuit delivers a smaller voltage than the previous circuit without the voltage doubler, but still is adequate to power the sensor circuit. However, observe that the load was significantly reduced from the previous design to force the circuit to deliver an adequate V_{DC} , and the load current is only 28.57% from that design. With the same load resistance as in Figure 51, the circuit cannot deliver more than one volt V_{DC} .

The problem seems to be that the addition of C_6 implies that the transformer must charge an additional capacitor, each capacitor at different semicycle, or equivalently $C_{equivalent}$ □

$C_1 + C_6$.

However, the low voltage effect persists even when C_1 and C_6 values are cut in half to compensate for the additional capacitance, and retuning. If additional voltage multiplier stages are added, the voltage drop and smaller driven load effects get worse.

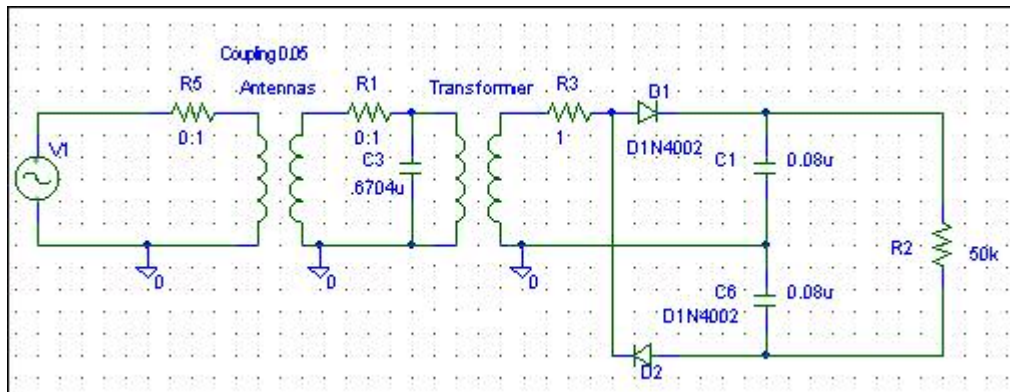


Figure 54. Reader-Sensor system circuit with an up-transformer in resonance and output doubler charge pump

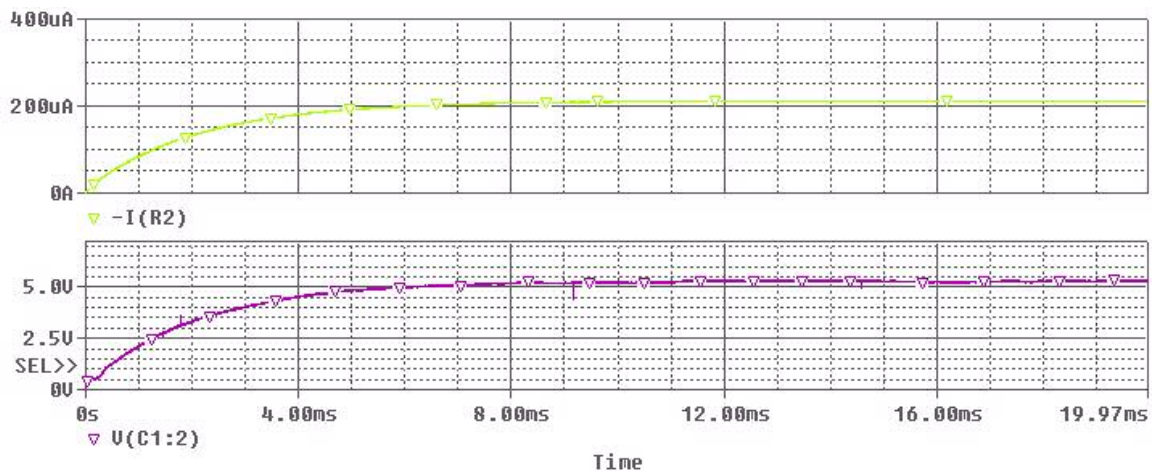


Figure 55. Circuit Signals. Bottom- Up:

Output Voltage, Load Current

We want to investigate why this severe voltage drop occurs when the charge pump circuit is added.

To start, let's modify (3.3) to include the effect of the transformer as $(N_{\text{secondary}}/N_{\text{primary}})$:

$$V_o = n \left(\frac{N_{secondary}}{N_{primary}} \right) V_{in} - V_{th} - \frac{n-1}{fC} I_{load} \quad (4.6)$$

A close analysis of (4.6) does not give any clue why the severe V_o drop, in fact, I_{load} is smaller than the previous design, $n = 2$, so, theoretically, from (4.6) we should expect a bigger output voltage than the previous circuit.

The reason of this severe drop was found in the combined effects of the transformer, the charge pump circuit and the resonance operation of the whole sensor circuit.

To explain how it happens a fast review of parallel and series resonance is necessary.

Resonance is the condition when the impedance effects of the reactive elements are cancelled, i.e.,

$$|Z_L| = |Z_C| = \omega_o L = \frac{1}{\omega_o C} \quad \text{then:} \quad \omega_o = \left(\frac{1}{LC} \right)^{\frac{1}{2}} \quad (4.7)$$

The (4.7) resonance occurs in both series and parallel LC circuits, see Figure 56.

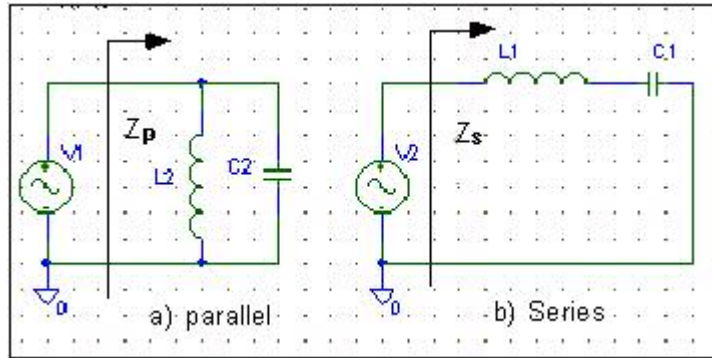


Figure 56. Parallel and Series LC Circuits

The impedance of the parallel LC circuit is given by

$$Z_p = Z_L \parallel Z_C = \frac{Z_L Z_C}{Z_L + Z_C} = \frac{j\omega L}{1 - \omega^2 LC} \underset{\omega = \left(\frac{1}{LC} \right)^{\frac{1}{2}}}{=} = \infty \quad (4.8)$$

(4.8) means that the LC parallel circuit at resonance behaves as an open circuit.

For the series LC circuit

$$Z_s = Z_L + Z_C = j\omega L + \frac{1}{j\omega C} \underset{\omega = \left(\frac{1}{LC}\right)^{\frac{1}{2}}}{\equiv} 0 \quad (4.9)$$

(4.9) indicates that the series LC circuit behaves as a short circuit at resonance.

More realistic LC circuits should include a resistor, Figure 57.

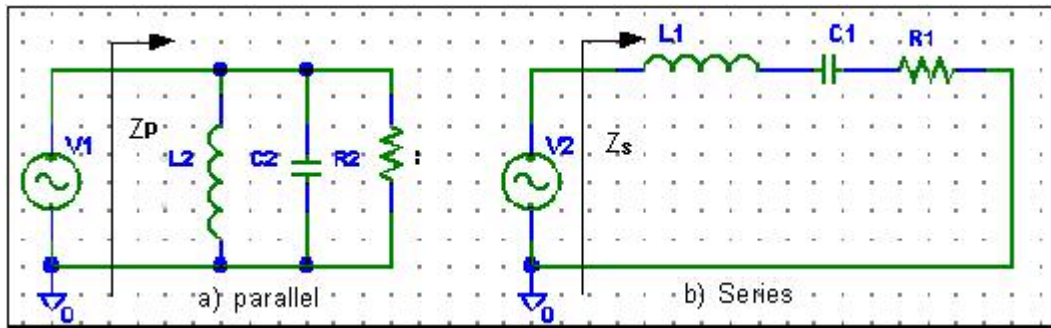


Figure 57. Parallel and Series LC Circuits with Resistance

The resonance frequencies are the same as described in (4.7). To compute the impedance in the parallel RLC circuit the Norton Transformation is used, then the admittance is computed and finally it is transformed to its equivalent impedance:

$$Y_p = Y_L + Y_C + G = j\omega C + \frac{1}{j\omega L} + G \underset{\omega = \left(\frac{1}{LC}\right)^{\frac{1}{2}}}{\equiv} G \quad \text{then} \quad Z_p = \frac{1}{Y_p} = R \quad (4.10)$$

For the series RLC circuit

$$Z_s = Z_L + Z_C + R = \left(j\omega L + \frac{1}{j\omega C} \right) + R \underset{\omega = \left(\frac{1}{LC}\right)^{\frac{1}{2}}}{\equiv} (0) + R = R \quad (4.11)$$

In both RLC circuits the equivalent impedance at resonance is just R.

Now we need to review the effect of the impedance on the ideal transformer model,

Figure 58. From the (4.9) circuit and the basic relations in a transformer model:

$$Z_{in} = \frac{V_1}{I_1}, \quad Z_L = \frac{V_2}{I_2}$$

$$V_2 = \frac{N_2}{N_1} V_1, \quad I_2 = \frac{N_1}{N_2} I_1 \quad \text{and} \quad a = \frac{N_1}{N_2} \quad (4.12)$$

then

$$Z_{in} = \frac{V_1}{I_1} = \frac{V_2}{a I_2} = \frac{I_2 Z_L}{a I_2} = \frac{Z_L}{a^2} \quad \text{or} \quad Z_{in} = \left(\frac{N_1}{N_2} \right)^2 Z_L \quad (4.13)$$

The impedance in the secondary is reflected to the primary side scaled by the factor a .

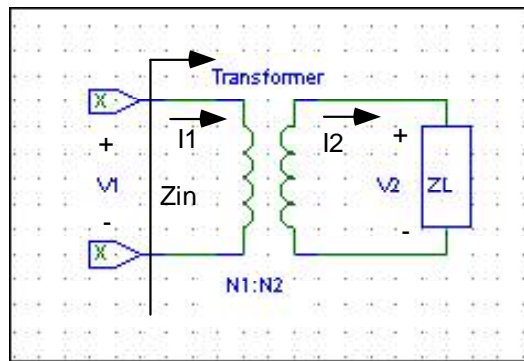


Figure 58. Ideal Transformer Model

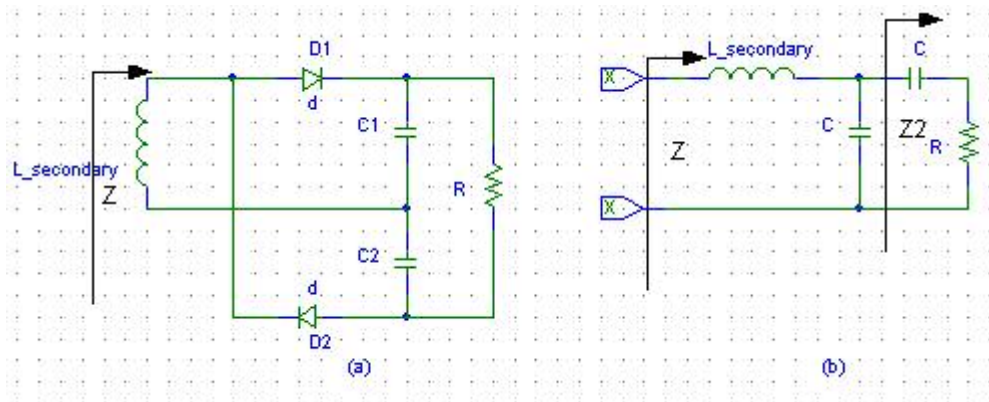


Figure 59. (a) Doubler Charge Pump. (b) Equivalent Circuit for Both Semicycles

We can use the last formulas to analyze the behavior of the doubler charge pump, from Figure 54, neglecting the inductor resistance, the equivalent circuit is described in Figure 59.a. The equivalent circuit for both semicycles, negative and positive, is shown in 4.10.b. Assuming both capacitors have same value, then

$$Z_2 = \frac{1}{j\omega C} + R$$

$$Z = j\omega L + \frac{X_c Z_2}{X_c + Z_2} = \frac{\omega^4 C^4 R^2 + 2\omega^2 C^2}{4 + \omega^4 C^2 R^2} + j \frac{\omega^3 C^3 R + \omega L(4 + \omega^4 C^2 R^2)}{4 + \omega^4 C^2 R^2} \quad (4.14)$$

At resonance the imaginary part goes to zero, and the solutions are:

$$\omega = 0, \frac{j2L^{\frac{1}{2}}}{(C^3 R + C^2 L R^2)^{\frac{1}{2}}} \quad (4.15)$$

Substituting (4.15) into the real part of (4.14) gives

$$Z = \frac{2L(LR - C)}{RC(LR + C)} \quad (4.16)$$

To observe the behavior of the impedance, first fix R and plot Z at resonance when L and C varies, then fix L and observe Z when C and R are varied, Figure 60. Note that the impedance in (4.16) is real.

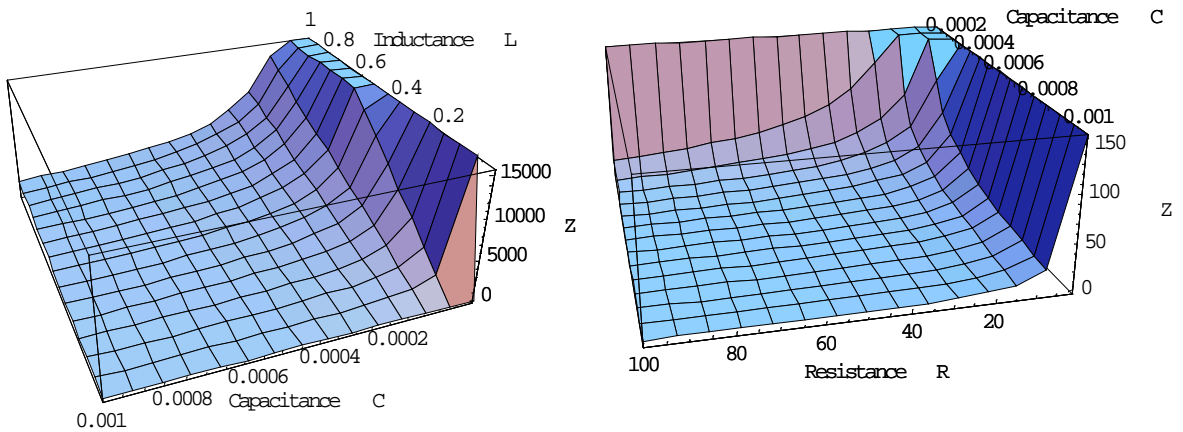


Figure 60. Impedance of the Charge Pump at Resonance

Note the scaled effect of the impedance. It was found that for $R > 500\ \Omega$ the effect of the charge pump circuit is to amplify the resistance, for $R < 500\ \Omega$ the impedance is attenuated, and for $R = 500\ \Omega$ the impedance stays constant.

At this point, two comments are important:

1. The intrinsic resistance of the diode in forward bias, Figures 23 and 59, was neglected because it is small compared to the load resistance. From [19, pp 247],

$$J_D = J_0 \left(e^{\frac{qV_a}{kT}} - 1 \right) \quad (4.17)$$

because the current is the charge crossing an area, then multiplying the current density J_0 by the area we get the ideal diode equation:

$$I_D = I_0 \left(e^{\frac{qV_a}{kT}} - 1 \right) \quad (4.18)$$

Plotting (4.18)

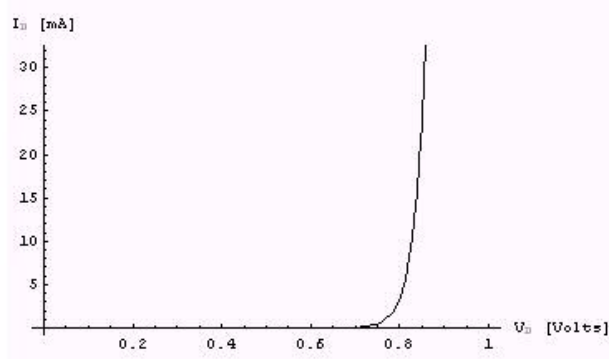


Figure 61. Diode Characteristic Curve at 25° C

From the Figure 61 diode curve, R_D varies with V_D , and as long as V_D is bigger than the diode threshold voltage, R_D goes to zero and therefore it can be neglected when compared to the load resistance R_L .

2. The capacitances of the diode in forward bias were not considered because they do not contribute to the voltage drop observed in the reader-sensor circuit with up-transformer and charge pump, as long as the circuit is tuned to resonance.

From (4.7), $\omega_0 = \sqrt{1/LC}$, a change in the capacitance, when the forward-bias diode capacitances are added, just results in a shift in the frequency of resonance, but it does not affect its amplitude at resonance. The effects of diode capacitance on inverse-bias will be reviewed later.

Now, from (4.16) and Figure 60 it is clear that the impedance is scaled up on the practical implementation of a reader-sensor system, motive of this research, where load resistances must be much bigger than 500Ω , given the scarce power available. A quick review of the quality factor Q for a series LC circuit combined with the impedance scale will give the reason of the voltage drop.

From [15, (3) and (15), pp 88 and 91], the quality factor Q for a series RLC circuit is defined as:

$$Q \equiv \omega \frac{\text{energy stored}}{\text{average power dissipated}} = \frac{\sqrt{\frac{L}{C}}}{R} \quad (4.19)$$

From (4.19) as R is increased Q decreases and the voltage in any of the reactive components decreases, Figure 62.

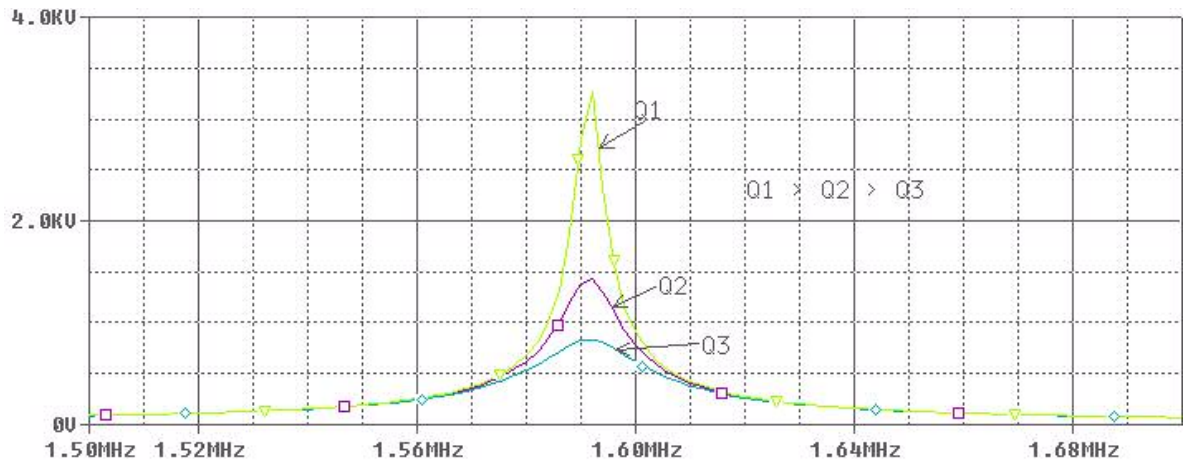


Figure 62. Resonance Curves $Q_1 > Q_2 > Q_3$

In the RLC circuit, series or parallel, the resistance causes a drop in the output voltage, more severe if it is taken between the two terminals of any of the two reactive components, because V_L or V_C is Q times the voltage between the terminals of the resistor. As Q is reduced, V_L or V_C reduces voltage in same proportion.

In the reader-sensor system with up-transformer and charge pump, the voltage drop is caused when the charge pump – up-transformer, working in resonance, multiplies the effect of the impedance in the secondary, (4.16), looking by the primary. The additional impedance in the primary reduces the flow of the current in the primary winding, producing less magnetic flux to reach the secondary circuit, and then generating less voltage in the secondary. The drop of voltage is severe because the multiplicative factor of the secondary impedance looking into the primary circuit can be in the order of thousands, Figure 60. A simplified model is described in Figure 63.

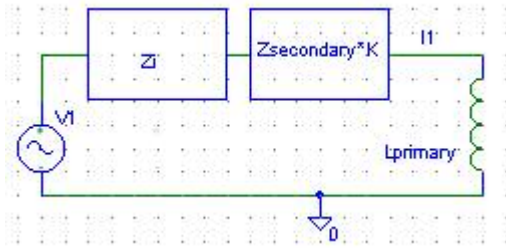


Figure 63. Model of the Primary Circuit with Charge Pump

Where K is the multiplicative effect of the secondary impedance when the charge pump is added in the secondary circuit, and Z_i and $Z_{secondary}$ are the original impedances.

Equation (4.6) is modified to include this effect:

$$V_o = n \left(\frac{N_{secondary}}{N_{primary}} \right) \left(\frac{X_{L_{primary}}}{X_{L_{primary}} + Z_i + K Z_{secondary}} \right) V_{in} - V_{th} - \frac{n-1}{fC} I_{load} \quad (4.20)$$

In general K should be calculated as

$$K = \frac{Z_{with\ charge\ pump}}{Z_{without\ charge\ pump}} \quad (4.21)$$

$Z_{with\ charge\ pump}$ is the impedance from the secondary looking into the primary circuit, like (4.16). The multiplicative effect occurs for three additional charge pump circuits that were analyzed, including the general implementation suggested in [17].

It is important to remark that all calculations, and the resulting formulas, are valid only at resonance or in its close vicinity.

From the previous discussion and simulations, it is evident that the circuit in Figure 51 with only the up-transformer in resonance is better suited to wirelessly power the sensor circuit.

Some people, [29, pp 15-23, 30, pp 28-31], are working in the fabrication of transformers on VLSI, however, the inductance of the transformer windings is still small,

less than 20 μH with Q in the order of 10. Therefore, the monolithic transformers are not still ready to be integrated in a chip, and the resultant sensor circuit will be relatively bulky as suggested in Figure 49.

The effect of the inverse-bias on a diode produces a leakage current [19, (4.3.8), pp190], as shown the plot of (4.22) in Figure 64. The effect becomes more evident as frequency increases.

$$|I_{leakage}| = \left| \frac{V}{Z_{capacitance}} \right| = V\omega \left(\frac{\epsilon_s}{2q \left(\frac{1}{N_a} + \frac{1}{N_d} \right) (\phi_i)} \right)^{\frac{1}{2}} \quad (4.22)$$

where N_a is the number of acceptors, N_d is the number of donors, ϵ_s is the permittivity of the silicon, ϕ_i is the built-in potential and q is the charge of the electron.

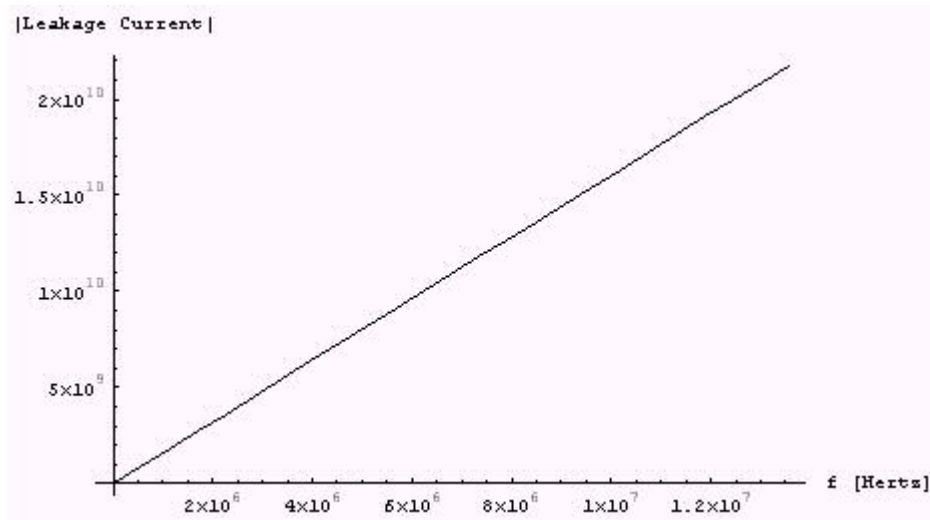


Figure 64. Leakage Current of an Inverse Biased Diode

Observe that time was fixed and the voltage is sinusoidal in Figure 64. The leakage diode current results in a partial capacitor discharge that contributes to the drop in voltage.

However, the voltage drop effect of the diode leakage-current is small when compared to other effects previously analyzed, and can be kept under control with well design diodes.

Next section will show the design of an all-MOSFET RF-to DC-Voltage circuit that avoids the PN junction threshold voltage, then faces the MOSFET channel threshold voltage and finally outcomes a free-threshold-voltage circuit.

b. Design of an RF-to-DC-Voltage Circuit for VLSI Implementation

The design of the radio frequency to DC voltage system to power a strain sensor is challenging because the current necessary to make work a commercial strain sensor: a minimum of about 1 mA at 3 volts with the present technology. However, as explained in next chapter, it could be possible to design a piezoelectric sensor that works with very small current and can be activated with currents in the μA range, in that case a MOSFET RF-to-DC-Voltage VLSI design is satisfactory.

First the design of the MOSFET rectifier is addressed, next the rectifier is extended to dual rectifiers with negative and positive output voltages. Finally a charge-pump circuit is cascade to form a complete RF-to-DC-Voltage. The circuit is suitable for MOSFET VLSI, and if fabricated under some characteristics it is possible to avoid the waste of any voltage to overcome threshold voltages.

In practice, it is not expected to get perfectly rid of the threshold voltage, but to reduce to a minimum threshold voltage close to zero.

i. MOSFET Antenna-Rectifier Circuit

Consider the class-B amplifier shown in Figure 65 [57, Figure 8.14, pp 449], this amplifier switch Q_1 ON and Q_2 OFF in the sinusoidal positive semicycle. Therefore, as long as the sinusoidal signal is positive it is amplified by Q_1 . In the negative semicycle Q_1 is turned OFF and Q_2 ON, and the signal is amplified by Q_2 . The drawback in this amplifier is the crossover distortion [57, pp 448-451].

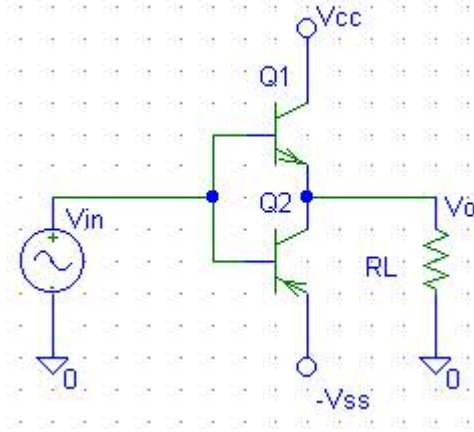


Figure 65. Class-B Amplifier

Now, let's extend the class-B amplifier idea to a rectifier implemented with MOSFET transistors. After some preliminary designs, the circuit in Figure 66 resulted.

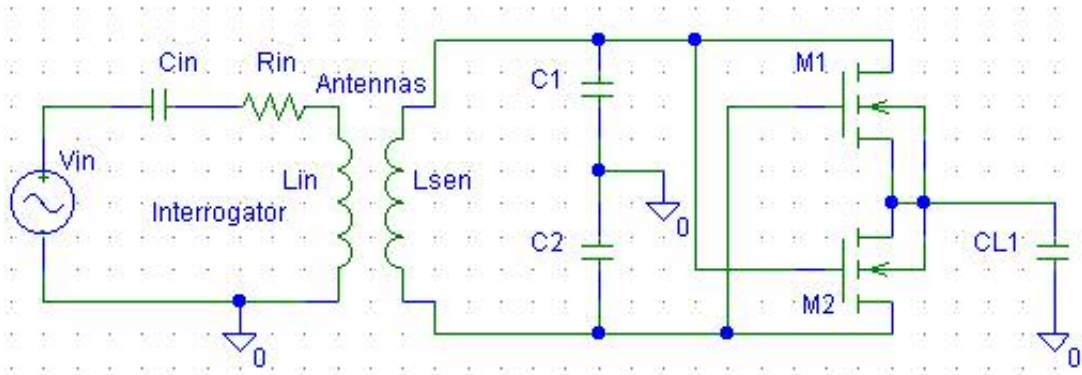


Figure 66. Proposed NMOS Rectifier

As in the class-B amplifier, in this circuit the positive semicycle turns M_1 ON and M_2 holds OFF and C_L is charged through M_1 . In the negative semicycle M_1 turns OFF and M_2 turns ON, now C_L is charged through M_2 . M_1 and M_2 are part of the rectifier and C_L is the filter, the output is a positive DC voltage. Note that the circuit still is working in resonance. The previous circuit worked with NMOS transistors, but the idea also works for PMOS transistors to get a negative DC voltage, see Figure 67.

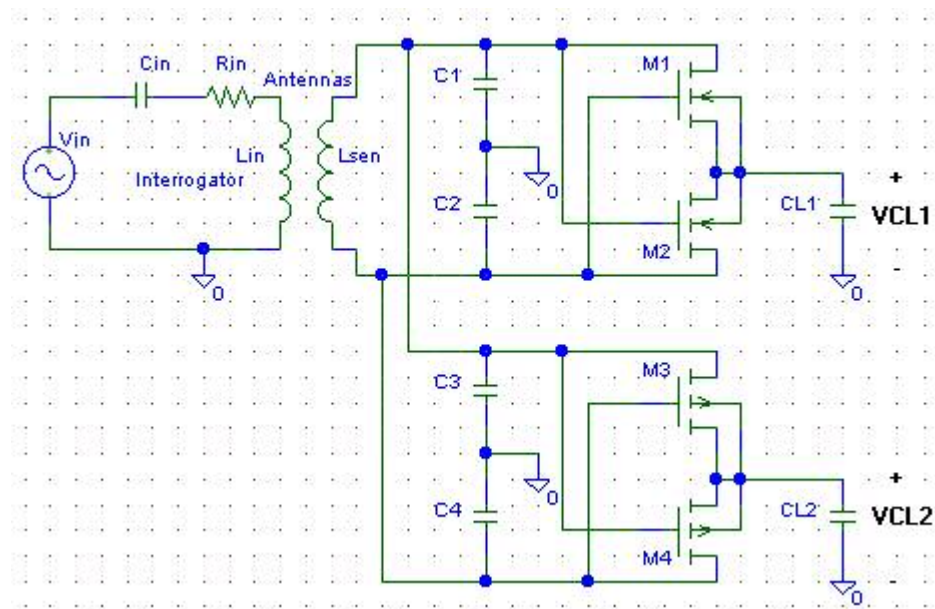


Figure 67. Dual MOSFET Rectifier

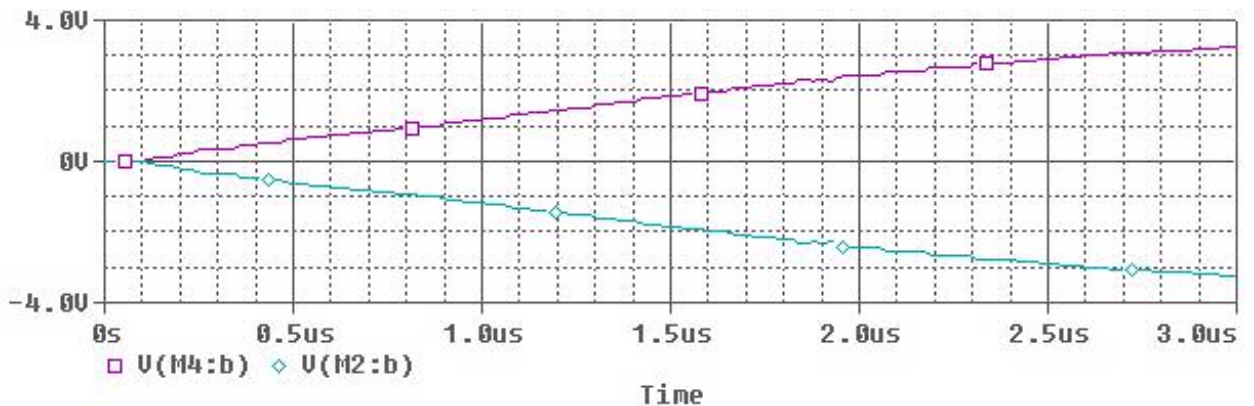


Figure 68. Dual MOSFET Rectifier Signals

V_{CL1} is a positive DC voltage and V_{CL2} is a negative DC voltage, both voltages are shown in Figure 68, the difference allows the generated voltage to be doubled, or to have negative and positive voltages to power the sensor circuit.

The problem, as in the diodes, is the threshold voltage V_{th} necessary to turn on the transistors. However, the threshold voltage of the MOSFET transistors is not to overcome a PN junction as to turn on the diodes but to open a channel between the drain and the source. To control the threshold voltage let us review the theory behind V_{th} of a MOSFET transistor. The depletion-region charge density per unit area, when the surface is inverted, is given by [19, equation (8.3.9), pp 396].

where N_a is the number of acceptors, N_d is the number of donors, ϕ_p and ϕ_n are the bulk

$$Q_d = \begin{cases} -\sqrt{2\epsilon_s qN_a (2|\phi_p| + V_S - V_B)} & PMOS Transistor \\ +\sqrt{2\epsilon_s qN_d (2|\phi_n| + V_B - V_S)} & NMOS Transistor \end{cases} \quad (4.23)$$

potentials, $q = 1.602 \times 10^{-19} C$ is the electronic charge, the permittivity of the silicon is

given by $\epsilon_s = \epsilon_0 \epsilon_r = (8.854 \times 10^{-14} F cm^{-1})(11.7)$, V_S is the source voltage and V_B is the

bulk voltage. Note $V_S = V_C$ as described in [19, Figure 8.9 pp 395].

In agreement with [19, equation (8.3.18), pp 398] the equations to compute V_{th} in the

MOSFET transistor are given by

$$V_{th} = \begin{cases} V_{FB} + V_S + 2|\phi_p| - \frac{Q_d}{C_{ox}} & PMOS \\ V_{FB} + V_S - 2|\phi_n| - \frac{Q_d}{C_{ox}} & NMOS \end{cases} \quad (4.24)$$

Where C_{ox} is the oxide capacitance, V_{FB} is the flat-band voltage [19, equation (8.1.1), pp 384] given by the difference in the work functions of the metal and silicon, typically negative for P and N channel MOSFET transistors

$$V_{FB} = \Phi_M - \Phi_S \equiv \Phi_{MS} \quad (4.25)$$

The potential at the neutral edge of the depletion-region in the P-and-N-type material [19, (4.2.9b), pp179] are

$$\begin{cases} \phi_p = \frac{-kT}{q} \ln \frac{N_a}{n_i} \\ \phi_n = \frac{+kT}{q} \ln \frac{N_d}{n_i} \end{cases} \quad (4.26)$$

where $k = 1.38 \times 10^{-23} JK^{-1}$ is the Boltzmann's constant, T is the absolute temperature in Kelvin degrees, $q = 1.602 \times 10^{-19} C$ and n_i is the intrinsic carrier density.

Equation (4.24) indicates how to control V_{th} in a MOSFET transistor. First, if the source-substrate reverse bias, V_{SB} , is increased then V_{th} is also increased. Therefore, we need to keep $V_S = V_B$, to cancel the body effect. And (4.24) becomes [19, (9.3.1) and (9.3.2), pp 443]

$$V_{th} = \begin{cases} V_{FB} - 2|\phi_n| - \frac{|Q_d|}{C_{ox}} & PMOS \\ V_{FB} + 2|\phi_n| + \frac{|Q_d|}{C_{ox}} & NMOS \end{cases} \quad (4.27)$$

Observe in (4.27) that V_{FB} is typically negative for both NMOS and PMOS transistors, and Q_d in a PMOS (when $V_S = V_B$) becomes

$$Q_d = \begin{cases} -\sqrt{2\epsilon_s qN_a (2|\phi_p|)} & PMOS Transistor \\ +\sqrt{2\epsilon_s qN_d (2|\phi_n|)} & NMOS Transistor \end{cases} \quad (4.28)$$

Clearly, from (4.27) to control V_{th} in a NMOS transistor we need

$$|V_{FB}| \approx 2|\phi_n| + \frac{|Q_d|}{C_{ox}} \quad (4.29)$$

with constraint

$$|V_{FB}| < 2|\phi_n| + \frac{|Q_d|}{C_{ox}} \quad (4.30)$$

Because we want V_{th} in our NMOS transistor to be positive but close to zero. This goal can be reached by control of N_d in Q_d on the fabrication process.

Similar analysis can be done for a PMOS transistor, and the control of V_{th} is reached by control N_a in Q_d . Note that in order to reduce V_{th} , N_a or N_d must be decreased for both MOSFETS, and is more difficult to reduce V_{th} in a PMOS transistor using this approach.

Another way to decrease V_{th} is by reducing the size of the MOSFET by a factor K . Table 1 shows how scaling affects the MOSFET parameters.

Scaling Rules for Constant Field Scaling	
	Scaling Factor
Surface Dimensions	1/K
Vertical Dimensions	K
Impurity Concentrations	1/K
Current, Voltages	K
Current Density	K
Capacitance per area	1
Transconductance	1/K
Circuit Delay Time	1/(K²)
Power Dissipation	1/K
Power Density	1
Power-Delay Product	1/(K³)

Table 1. Scaling Rules [19, Table 10.1, pp 497]

If the MOSFET becomes smaller, and $V_{SB} \gg 2|\phi_p|$, then V_{th} is also reduced as [19, (10.4.2), pp 497].

$$V_{th}' \approx \frac{V_{th}}{K} \quad (4.31)$$

where K is the scale factor when the area occupied by the MOSFET is reduced K times.

Observe that (4.31) is an approximation and even could be not valid in some cases.

Finally, ion implantation is commonly used to adjust V_{th} in the channel region without increase doping in the rest of the substrate, because the heavy doping worsen the performance of the MOSFET. The ion implantation is used to increases V_{th} by replace the original doping in the channel by $N_a' = N_{a(ion)} + N_a$ in the PMOS or $N_d' = N_{d(ion)} + N_d$ in the NMOS transistor in equation (4.23) and consequently in (4.24). If no ion-implant is executed at the fabrication process, then V_{th} is kept close to zero. Maybe the resultant MOSFETS will not be reliable for regular applications but they will be excellent in our rectifier-charge-pump circuits, Figures 66-70. The advantage of the channel-ion-implantation is so as to be selective, i.e., it is possible to execute ion implantation to all the MOSFETS of the VLSI circuit except the MOSFETS of the rectifier and charge-pump subcircuits.

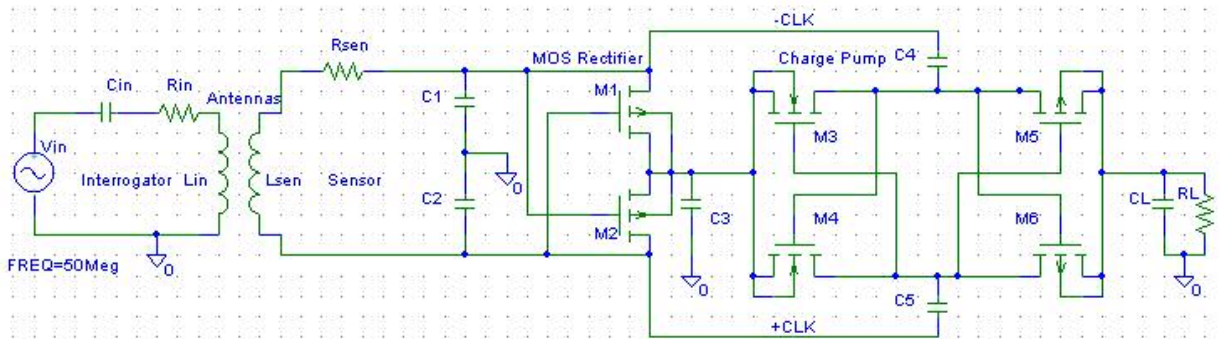
The short channel effects should also be considered to control V_{th} as well, refer to [19].

From the last discussion, we found that there is a collection of methods to reduce or keep close to zero the V_{th} in the fabrication of the MOSFET transistors used in the rectifier circuit and ,consequently, increases the interrogation distance in the interrogator-strain sensor system.

ii. MOSFET Antenna-Rectifier-Charge-Pump Circuit

Now let us increase the output voltage further through a charge pump as shown in Figure 69. The charge pump [55, pp 7] works well and delivered 3.5 volts at 50 MHz. To

further reduce the ripple noise of the output DC voltage the frequency of the incoming signal can be increased.



Part	Value	Part	Value
Vin	3.3V	C1	5p
Cin	2.5p	C2	5p
Rin	0.001	C3	10p
Antennas	L1 = L2 = 2u	CL	50p
Rsen	0.001	M1-M5	See Table 2

Figure 69. MOSFET Rectifier with Charge Pump

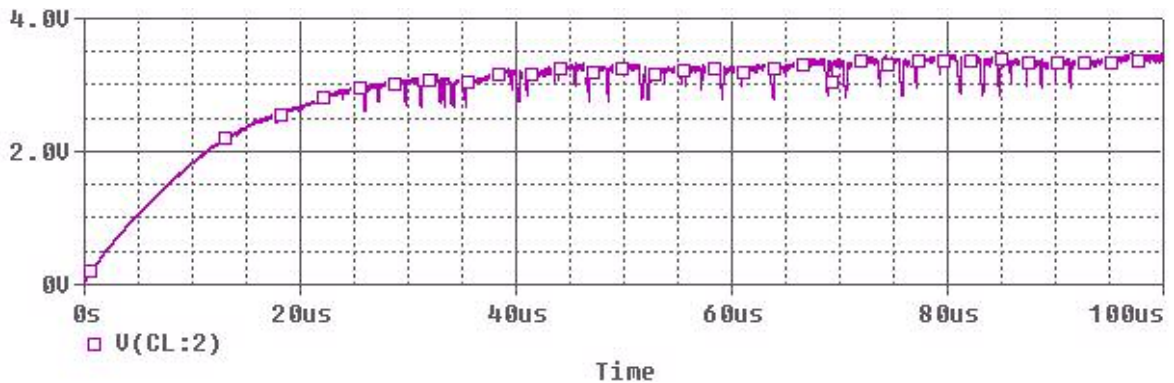


Figure 70. MOSFET Rectifier with Charge Pump Output DC Voltage

(2 μ MOSFET Transistor Form UMCP)

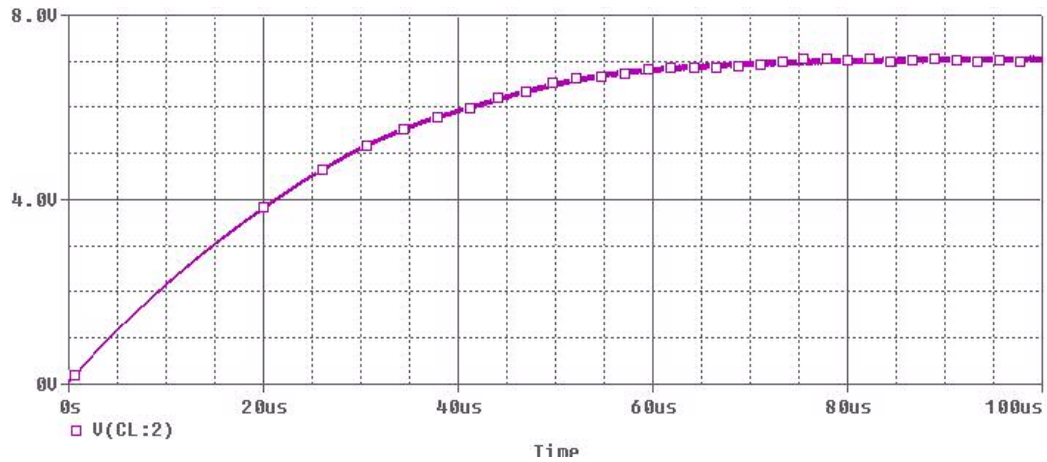


Figure 71. MOSFET Rectifier with Charge Pump Output DC Voltage
(0.5 μ MOSFET Transistor Form UMCP)

Technology [Micrometers]	MOSIS Transistor Run Name	MOSFET Transistors Names in the Circuit	Threshold Voltage Changed to [V]	Simulated Output Voltage in Figure	Simulated Maximum Output Current [MicroAmperes]
0.5, W=L=2.5	T13V	M1, M2, M5, M6	-0.01	71	59
0.5, W=L=2.5	T13V	M3,M4	0.01	71	59
2.0, W=L=10	N21H	M1, M2, M5, M6	-0.01	70	32
2.0, W=L=10	N21H	M3,M4	0.01	70	32

Table 2. Characteristics of the MOSFET Transistors Used in the Simulation and Output DC-Voltages and Currents in the Antenna-Rectifier-Charge- Pump Circuit [59]

Remarks:

- Note the increase of output voltage and maximum current of the circuit when the size of the MOSFET is reduced from width = length = 4 μ meters in the Bicmos12 family [59], to width = length = 3.15 μ meters in the Amcmos05 family.
- From Table 2 it is not possible to conclude that the most important factor in the grow of the output voltage and current is due to the threshold voltage

- The combination antenna-rectifier delivered: 45 μA , but with larger coupling coefficient than the antenna-rectifier-charge-pump circuits, i.e., smaller interrogator-sensor distance
- The charge pump of Figure 69 needs to operate at frequencies larger than 46 MHz, for smaller frequencies the output DC voltage drops sharply
- To improve the output current the threshold voltage should be reduced at fabrication phase. The RF to DC circuit of Figure 69 is adequate to power systems designed with MOSFET transistors, given the small currents that they need to operate.

c. Test results to the Commercial RFID MCRF355 Tag Chip

The MCRF355 is a commercial RFID chip used in tagging. The device operates at 13.56 MHz and can be reprogrammed with some code in its 154 bits memory. Figure 72 depicts the typical working ensemble.

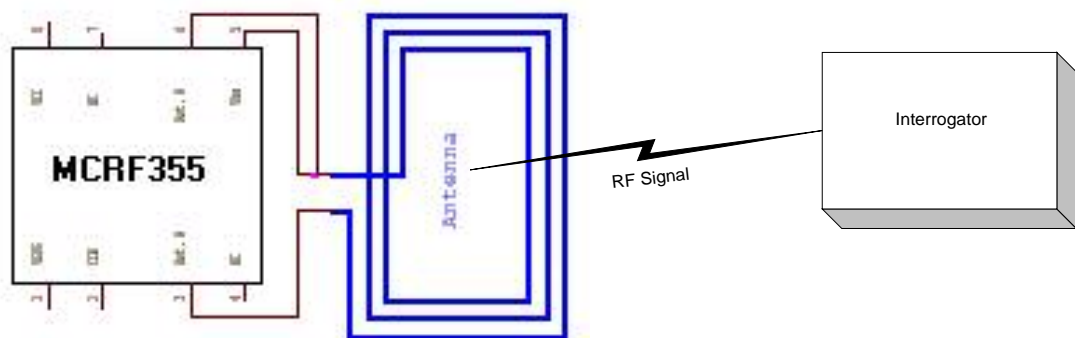


Figure 72. MCRF355 RFID Tag System

When the interrogator activates the MCRF355 through an RF signal, it responds by sending the word stored in its memory, and keeps sending this data as long there is sufficient power to keep it alive.

In the test, it was found that the MCRF355 chip is able to deliver power not just to its internal circuitry but to another circuit too. Between the pin 8, V_{DD} , and the pin 5, V_{SS} , is possible to get a positive voltage up to 3.2 volts when the distance between antennas is less than one centimeter and the incoming RF signal has a 20 MHz frequency. A summary of the tests is presented in Figure 73.

Figure 73.a shows the frequency response of the MCRF355, its behavior resembles a high pass filter. That test was run at 10 V_{peak} constant interrogator voltage. When the interrogator peak voltage is increased and the distance is keep constant the output DC voltage goes up accordingly, Figure 73.b. This test and next tests were run at 13.56 MHz.

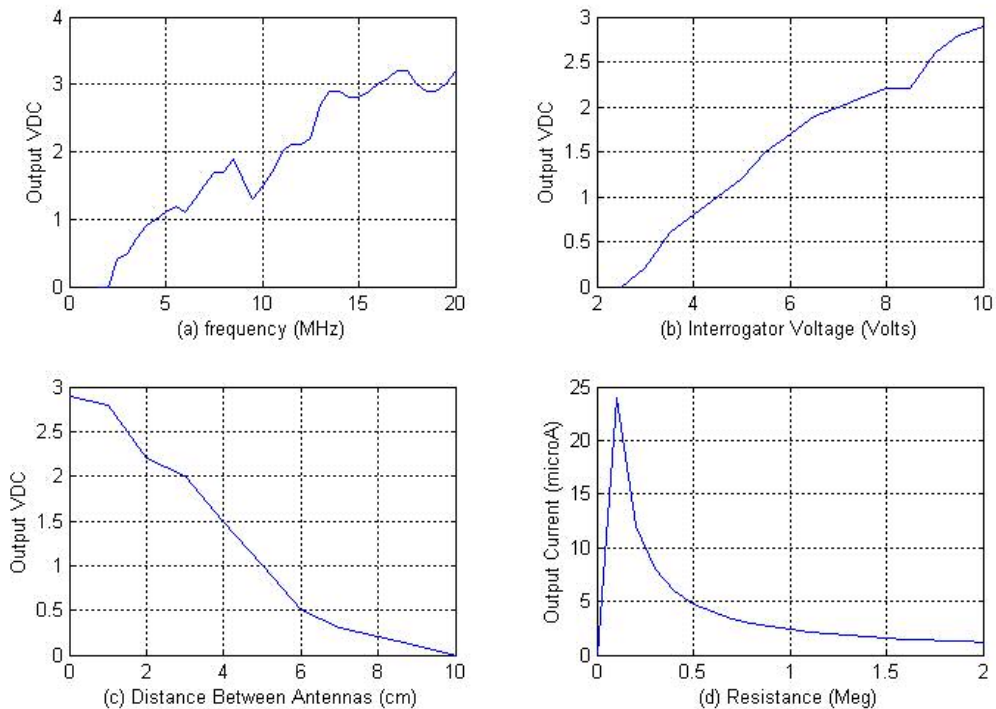


Figure 73. MCRF355 Output Signals

As expected, as the distance between interrogator and the MCRF355 antenna is increased, the output voltage decreases as described in Figure 73.c.

Figure 73.d describes the current the chip is able to deliver, up to $24 \mu\text{A}$ at a V_{DC} of 2.4 volts, i.e. a resistance of $100 \text{ K}\Omega$. If the resistance is slightly decreased from $100 \text{ K}\Omega$, the current and voltage drops to zero immediately.

The MCRF355 works well when the load demands no more than $24 \mu\text{A}$. Note that we do not know what is the voltage and current the MCRF355 can generate for its internal circuitry.

Figure 74 shows the signal of the MCRF355 chip, acquired with a logic analyzer. The important signal is number five, it shows the Manchester encoded signal send back by the MCRF355 to the interrogator circuit, when it is wirelessly powered through its antenna. Actually, this signal is sinusoidal, i.e., a binary Manchester encoded data modulated in amplitude. In order to freeze and record as TIFF file, an OPAM biased at five volts was used to fit the signal into the logic analyzer because the oscilloscope in the laboratory does not have recording capability.

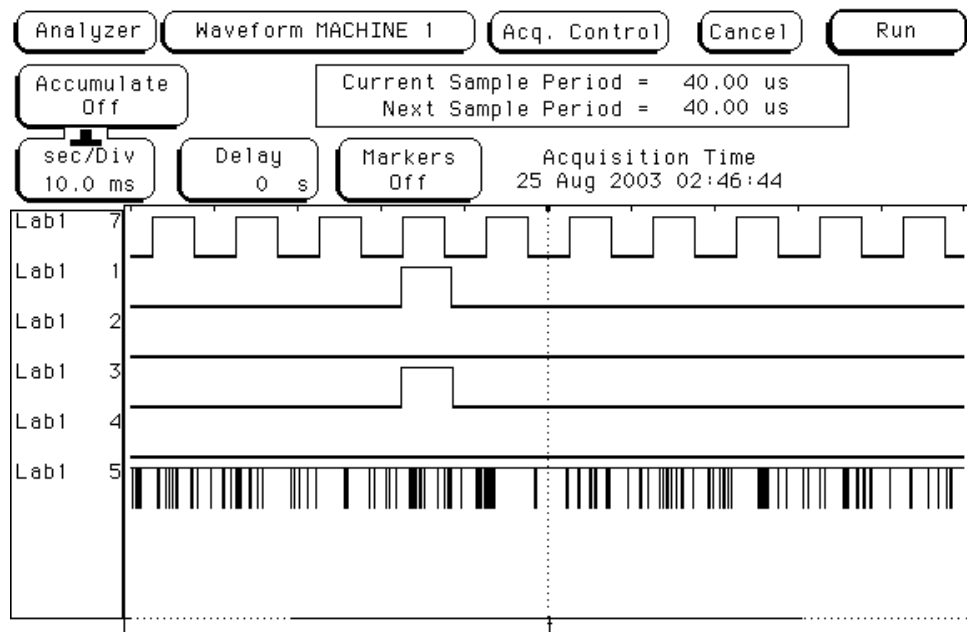


Figure 74. Recorded Signals on the Sensor Circuit

The signal in line five of Figure 74 shows that the MCRF355 is working, i.e., gets power from the RF signal and sends back the information data stored in its memory. Hence, the MCRF355 can be used in the design of a magnetic coupled strain sensor.

d. Construction Material Issues in the Design of Magnetic Coupled Circuits

As explained in the first chapter, the sensor circuit is expecting to be embedded in the body of a concrete bridge to measure the strain. The attenuation on the RF signal, introduced by the cement or other construction material, can make the sensor useless. From a basic test conducted in the Microelectronics laboratory, it seems that, at least for the brick used as the material of the bridge, the attenuation of the RF signal at 125 KHz introduced on average 0.16 volts. The effect is a slight reduction in the reading distance. The schematic setup for testing is described in Figure 75, the coil antennas are not shown. The rectifier-filter circuit was fully enclosed inside the brick. The cable of the oscilloscope is shielded by fabrication, so there was not way to pick up additional RF power via the cables.

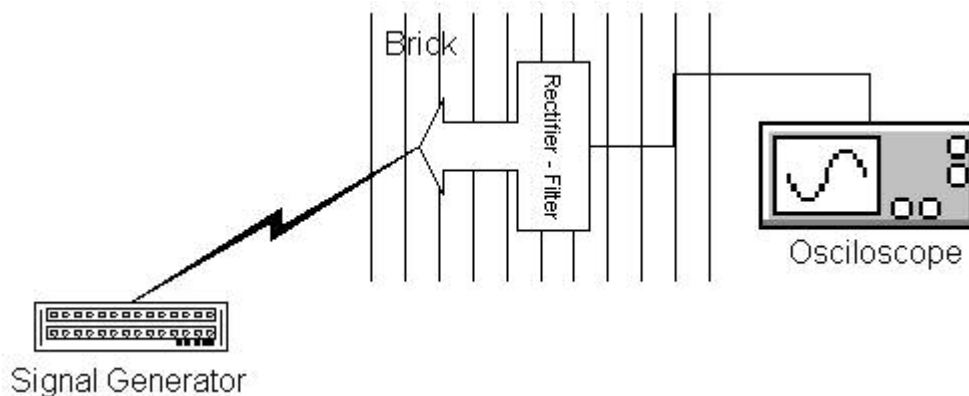


Figure 75. Construction Material Attenuation Test Setup

However, in real life every bridge is constructed with different materials and every material with different permeability μ . For that reason the sensor circuit must operate

at some frequency were the specific bridge construction material presents the lowest attenuation. In the worst case, when metallic-like materials are used in mix of the concrete used to build the bridge the RF signal will not be able to reach the sensor circuit because it will be practically shielded from the signal. The shielding effect could be also produced if after the end of the construction of the bridge, at some moment in its life, any metallic-like layer is applied to the surface of the bridge for protection or any other reason.

This shielding effect could be also produced in a natural way in the life span of the bridge when different materials deposit on the surface, creating a shield. Deposit speed could vary for different geographic areas, but deposit could be fastened on some industrial areas as pollution deposits on the surface of the bridge.

There has been some research on how concrete walls affect the electromagnetic signals used in cell telephony [32, pp 12-21]. The results on that research suggest us the use of shapes on the face concrete bridge as way to increase the absorption of the signal by the bridge, and consequently increase the power of the RF signal that could reach the strain sensor circuit.

Finally, changes in the best frequency to reach the strain sensor change with time. Through the life of the strain sensor its circuitry components get old, changing the resonance frequency, only slightly if good quality components are used. Besides, the concrete material used in the construction of the bridge are expected to change its permeability over time, hence changing the frequency that is better absorbed by the bridge to reach the strain sensor device. Moreover, that permeability change could be different for strain sensors embedded at different locations on the body of the bridge.

Previous discussion suggest us the addition of some features to the reader and the strain sensor circuits for improved performance:

1. The reader must transmit RF signals over an interval of frequencies, no just a frequency, to improve the chances to activate the strain sensor circuit. The price of this feature is a reduction on the reading distance, as the Q of the reader circuit is reduced. The reader can transmit all frequencies on that interval at the same time or sweep them over time, stopping in the frequency where the strain sensor is activated.
2. The strain sensor circuit must be able to adjust its resonance frequency, maybe on a limited range to avoid a significant reduction of the quality factor Q. Using this capability to search for the best frequency to receive power from the reader as soon as it is activated. The overhead on this feature is the additional power necessary to carry out the adjustment.

The auto-search for the best frequency in both, the reader and the sensor circuits, could also help to automatically overcome changes over time on the permeability of the concrete construction material and its resultant shift of the best frequency to transfer power. A limited solution is the addition of a feedback loop in the strain-sensor circuit, Figure 79.

Other, potential solutions and problems on the design and implementation of a wireless strain-sensor system will be given in the next chapter.

Chapter 5. CONCLUSIONS AND OPEN PROBLEMS

This work presented the feasibility of wireless techniques in the near field, to power a strain sensor circuit, possibly embedded in the body of a concrete bridge. The efficiency of the output power generated was enhanced by the use of voltage multipliers as charge pumps and transformers. Results of section 4.a showed that they operate better separately. The DC voltage drop when they worked jointly was analyzed. Theory and simulation shows the impedance multiplying effect on the primary circuit of the transformer results in a severe degradation of the DC output voltage when the charge pump is inserted in series.

The transformer working in resonance and followed by a rectifier-filter was the circuit with the best performance. The sinusoidal voltage generated in the terminals of the receiving antenna was as low as 20 mV, and yet capable to generating a DC voltage of about 6 volts for a multiplicative factor of 300, at 800 μ A. The output DC current is relatively small but sufficient to power a well-designed VLSI circuit. The drawback of this approach is the relatively big size of the transformer that potentially could disturb the strength of the bridge when embedded.

As shown in section 4.a.iii charge pumps showed poor results at low input voltages. The different charge pump circuits consistently suffered a DC voltage drop when the load was incremented. In the best case, at perfect resonance, one of them delivered up to 200 μ A.

The threshold voltage of the diodes, V_{th} , is a serious drawback on the use of charge pumps. When the peak voltage generated on the terminals of the antenna drop below V_{th} , 0.7 V for Si or 0.3 V for Ge, the output DC voltage and current were zero.

To overcome the threshold voltage the rectifier in Figure 66 was designed, the PN junction V_{th} was changed to a channel V_{th} . The discussion in chapter 4.b.i and 4.b.ii proved that the V_{th} of the channel can be done as small as desired at the MOSFET fabrication process. For practical purposes we can have a zero V_{th} rectifier. Note that the same fabrication principle can be applied to the charge pump in Figure 69, that makes the VLSI RF-to-DC-Voltage system practically threshold voltage free. That sounds great, but the VLSI RF-to-DC-Voltage system, even is able to generate 3.5 volts, it is not able to deliver the current necessary to power the less demanding commercial strain sensor, that is about 1 mA. For that reason, we propose the use of a surface acoustic wave as strain sensor, working in the topologies reported in Figures 77 and 78. In Figure 78 the VLSI RF-to-DC-Voltage system could be used to power the processing unit. The system in Figure 78 is restricted to frequencies in the 10 MHz to 2 GHz range, i.e., the response range of the SAW devices, and the SAW sensor must be fabricated in a separated chip of the rest of the circuit because it requires a piezoelectric material to operate. The MCRF355 can be used to implement a strain-sensor circuit based in commercial components as described in Figure 80. This prototype circuit could operate at 13.56 MHz.

Literature research on the effects of the bridge concrete suggested that they could be as small as to be neglected or as big as to make the system useless. If the concrete mix presents a shield effect, a magnetic coupling is impossible or very small and the sensor circuit becomes isolated from its activating RF signal. Tests in the laboratory showed that the RF signal to generate power suffered only a slight attenuation at 125KHz. However, some tests must be conducted on the concrete of every bridge, previous to the

design of the strain-sensor system, to look for the penetrating signal frequency that suffers less attenuation. Ideally, the penetrating frequency with the least attenuation should be used to design the system so maximizing the power that can reach the strain sensor antenna. Therefore, a designed system must be fit to every particular bridge.

a. Open Problems and Opportunities

The RF transfer of power explored in this research was done with the strain sensor system in mind. Interrogator devices should be portable and small as possible for easy use by technicians. And sensor circuits should be kept as small as possible so as not to disturb the bridge.

Given the results in this thesis still there are variables that must be analyzed to optimize the use of power. This work did not address any chip package model and its effects on the power consumption of the designed circuit. Neither considered the design of microstrip patch antennas as an alternative to the coil antennas or array of antennas.

Third, even in the most optimized design, the strain sensor is still dumb. Some intelligence should be added to allow the sensor to learn about its bridge environment in order to optimize its variables: strain accuracy, power consumption, frequency of communication, radiation pattern, etc. The problem in the last point is that the intelligence feature is power hungry, i.e., another open problem.

If the interrogator size constrain is relaxed then it is possible to use antenna arrays that can concentrate power to small areas, and increase the interrogation distance accordingly. The software of the interrogator could in a predetermined order switch on and off the antennas, and in the process sweep with the concentrated RF signal a big area. There are two main advantages in this approach: The reading distance is incremented, something

that is important in tall bridges where the distance between reader (interrogator) and the strain sensor embedded inside the concrete is relatively large. Secondly, because the RF power is concentrated in a smaller area the chances of collision, when more than one sensor are activated simultaneously, is minimized, see appendix A. The disadvantage is an increase of the size and complexity of the interrogator, mainly because of the antennas.

Another option is the use of ferromagnetic cores, with large permeability μ_r , inside the interrogator and sensor antennas. They could increase the efficiency of the transferred RF power. The area of the antennas could be reduced, but at the same time they could become bulky, i.e., wide and length are reduced but high is increased.

There are some other technologies that can potentially be used in the wirelessly interrogator-strain sensor system. Some of them will be visited in the rest of the chapter.

i. Surface Acoustic Wave Sensors

Because the existing commercial strain-sensors need to operate relatively large amounts of current, the design of a strain-sensor that consumes little current should be considered. By reducing the amount of power necessary to activate the sensor, the interrogation distance can be incremented or more power is available to operate the rest of the strain-sensor circuit. Surface Acoustic Wave devices (SAW devices) are heavily used in the telecommunication sector as filters. Nowadays, all the cell phones use the SAW devices to process signals. Since the 1980's there has been a strong interest in the application of the SAW devices as sensors because they can be interrogated wirelessly [33, pp 1281-1292].

SAW devices are constructed using piezoelectric crystals. When a RF signal sent by an interrogator device hits the antenna of the SAW device, the comb-like elements on the surface of the SAW device, called interdigital transducers (IDT), transform the RF signal into an acoustic surface wave that propagates on the crystal, see Figure 76.a.

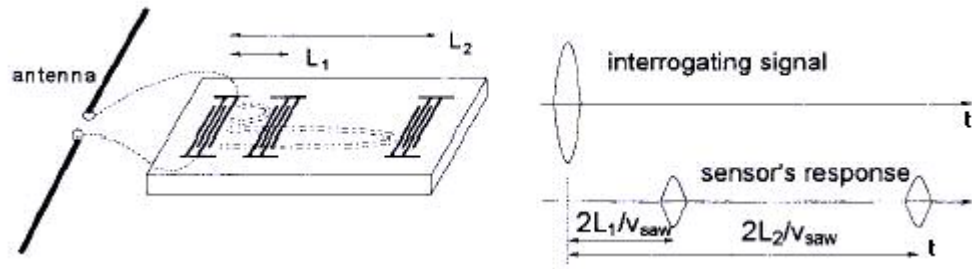


Figure 76. [34, pp 2208, fig.1] (a) Schematic Layout of the Passive SAW Sensor

(b) Signals

The propagated waves are reflected by other IDT arrays placed at distances L_1 and L_2 in the path of the acoustic waves. They propagate back to the IDT connected to the antenna. This IDT converts the sound signals back into electromagnetic signals and retransmits back to the interrogator device. The interrogator device processes the returning signals, Figure 76.b, to get the phase, delay and frequency information.

The delay, phase or frequency of the acoustic wave may change as a function of the variables that it is desired to sense. Different crystals are used to sense different variables like temperature, pressure, strain, etc. Some crystals are more sensitive than others to change the phase, delay or frequency of the acoustic wave as a function of the sensed variables.

Note that it is possible to place the IDT's at unique distances on the surface of the SAW device therefore the difference in delay between the returning signal bursts can be used as way to identify uniquely every SAW device [34, pp 2208].

According to [35, (13.20), pp 368], the phase of the returning signal burst can be used to sense the strain as:

$$\Delta\varphi \approx \omega_0 \varepsilon \tau_0 \quad (5.1)$$

where $\Delta\varphi = \Delta(\varphi_1 - \varphi_2)$ is the variation of the phase on the burst returning from the IDTS at distances L_1 and L_2 , $\varepsilon = \Delta(L_2 - L_1)/(L_2 - L_1)$ is the strain and τ_0 is the traveling time when the sensed strain is zero. Note that raising the operation frequency ω_0 can increase the sensitivity of this SAW sensor. SAW sensors can operate on frequencies from few hundred MHz to about 3 GHz, and readout distances up to 2.5 m with 10 mW peak power. There are advantages if SAW devices are used in the strain sensor researched in this thesis:

1. They do not need to operate in the near field, therefore theoretically they could be interrogated at bigger distances.
2. There is no need to receive power in the sensor to activate complex overhead circuitry, just the IDTS and the piezoelectric body of the sensor.
3. SAW devices are fabricated in stable single crystals that are nearly aging free.
4. As for the magnetic coupled system of this thesis, SAW sensors do not require a battery to operate.
5. They are small. Typically: 12 x 5 x 1 millimeters.

The disadvantages:

1. If the SAW sensors are embedded in the bridge concrete, and the concrete mix changes attenuation at the operating frequency, the SAW sensor could become useless.
2. The FCC (Federal Communications Commission) restricts the power of the electromagnetic signals radiated to a few milliwatts. This factor strongly limits the readout distance.
3. Addition of intelligence is limited, because digital processing could be power hungry

The first SAW sensor disadvantage can be overcome by placing groups of SAW sensors designed to operate at different frequencies, i.e., the expected window of frequencies with less attenuation where the concrete of the bridge will shift along its life span. Other ways to overcome the attenuation problem is by the use of magnetic coupling for the SAW sensor as described in Figure 77. The SAW sensor works as before, but the interrogator electrical signal is magnetic coupled.

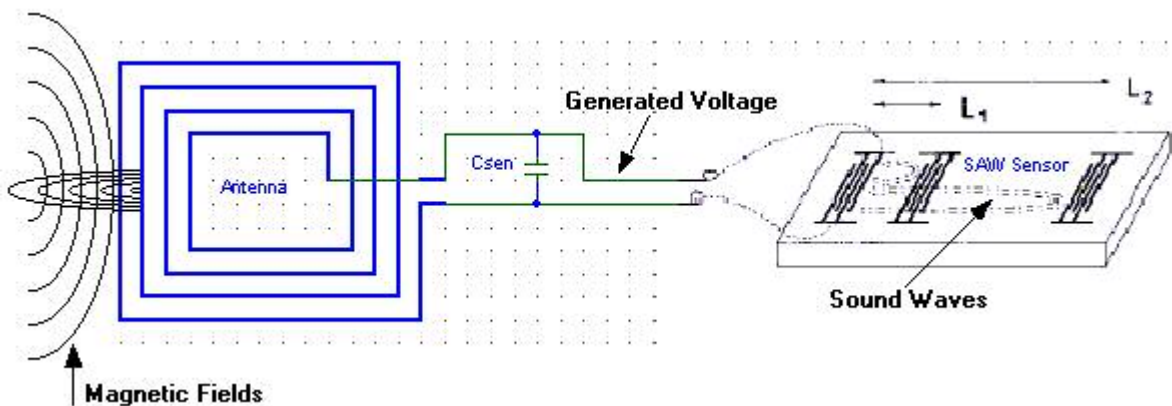


Figure 77. Strain SAW Sensor Operated with Magnetic Coupling

If it is desired to add extra features as security encoding and signal processing then the circuit in Figure 78 should be used.

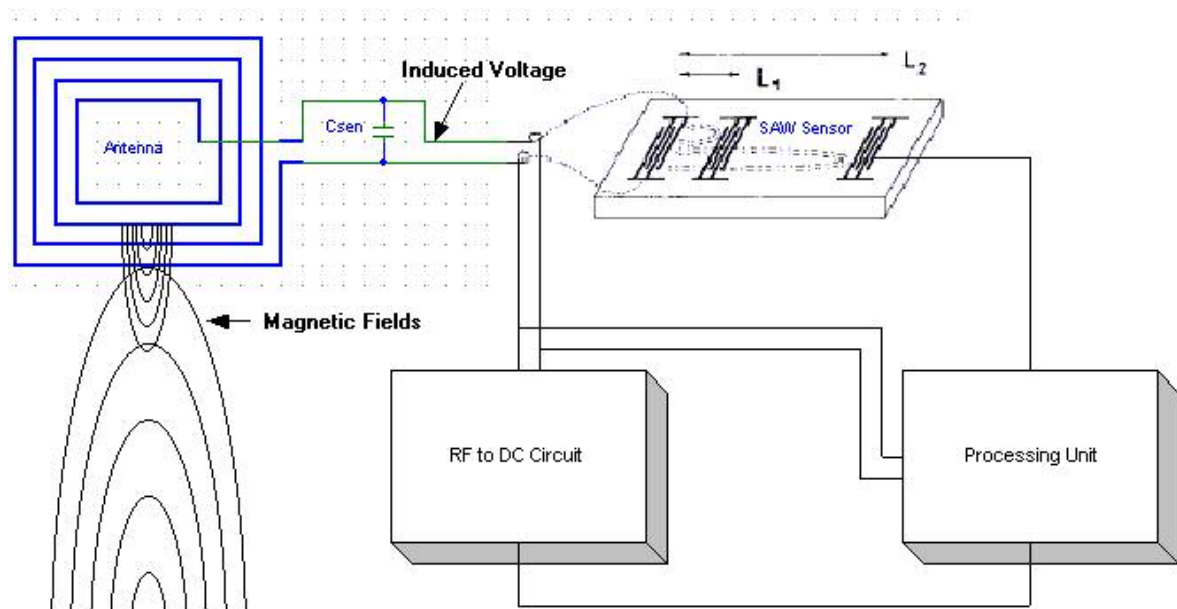


Figure 78. Strain SAW Sensor Operated with Magnetic Coupling and Processing Capacity

The second is a political but not technical limitation, so, presently there is no way to overcome this restriction in SAW sensors operating on plane waves. On the contrary, magnetic coupled systems have not that legal limitation.

The third constraint can be addressed with the arrangement of Figure 78. The processing unit could short-circuit some of the elements of the IDTS to change dynamically the characteristics of the SAW sensor, or maybe an array of sensors, as the environment changes.

ii. Out of the Box Reader-Sensor System Implementation

The circuit for a complete RF-to-DC-Voltage powered strain sensor can be implemented as shown in Figure 79. This circuit is an improved version of [54].

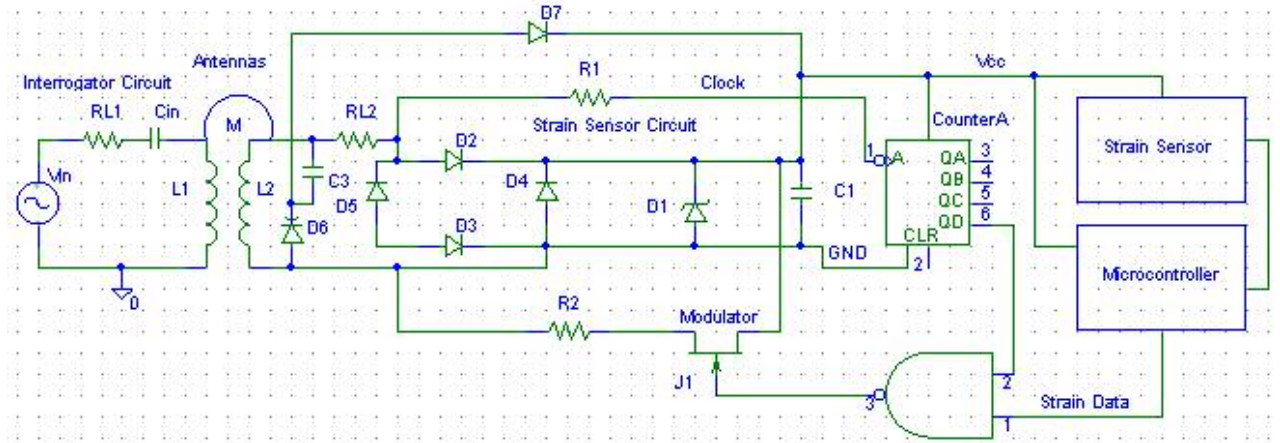


Figure 79. Basic Strain Sensor Circuit with Magnetic Coupling

The circuit works as follows:

1. The magnetic field is coupled between antennas.
2. The full-wave bridge of D₂, D₃, D₄ and D₅ rectifies the signal.
3. The capacitor C₁ filters the rectified signal, resulting in a DC voltage.
4. The Zener diode D₁ protects the rest of the circuit by clipping the output voltage to the chips operating voltage when the antennas are to close and generate a higher voltage than necessary.
5. When the strain sensor is supplied with sufficient power, it senses the strain and generated as output a voltage that is proportional to the strain.
6. The microcontroller converts the data from analog to digital, maybe encodes it, and sends it serially to the NAND gate.
7. The counter chip gets its clock signal from the RF signal, and counts in synchronization with the incoming RF signal.
8. The NAND gate turns on and off the FET modulator transistor in synchronization with the digitalized strain data.

9. The load “modulator”, FET, changes the load in concordance with the strain data, resulting in an amplitude-modulated signal. This load switch is sensed in the interrogator circuit through the magnetic coupling.
10. Diode D_7 and the varactor D_6 are used in a feedback loop to compensate for changes in the shift of the resonant frequency. When the output voltage drops the varactor changes its capacitance and shifts to the capacitance where the output voltage is maximum. This loop can be used to compensate for changes in aging components and surroundings.

The sensed signal is demodulated and decoded in the interrogator circuit. The decoded signal can be read by the operator or stored for future reference. The circuit is not optimized but is helpful for understanding the operation of a potential strain-sensor circuit.

The last circuit can be taken a step further. Based upon the results of tests of the MCRF355 it is possible to implement a strain-sensor circuit integrated with commercial chips as described in Figure 80.

The circuit works as follow. The strain sensor circuit generates a voltage that is proportional to the strain. The Microcontroller chip, PIC 16C71, performs a strain measurement, by sensing the voltage in pin 17, converts the measured voltage to its digital equivalent with its analog-to-digital converter, and saves its datum in its internal memory. After that, it transfers the information to the MCRF355 chip memory using 6-9 pines.

The MCRF355 is used to temporarily store the strain-measured data. Later, when the interrogator device is in its near field vicinity and transmits an adequate magnetic signal

to hit the MCRF355 antenna, it takes the power of the RF magnetic signal, and uses it to power its circuits. Then, the MCRF355 sends the information stored in its memory as long as it has enough power to do that. When the power of the received signal drops below some threshold the MCRF355 turn off, until another adequate RF signal is received. In the mean time, the microcontroller can transfer new strain information into the MCRF355 memory.

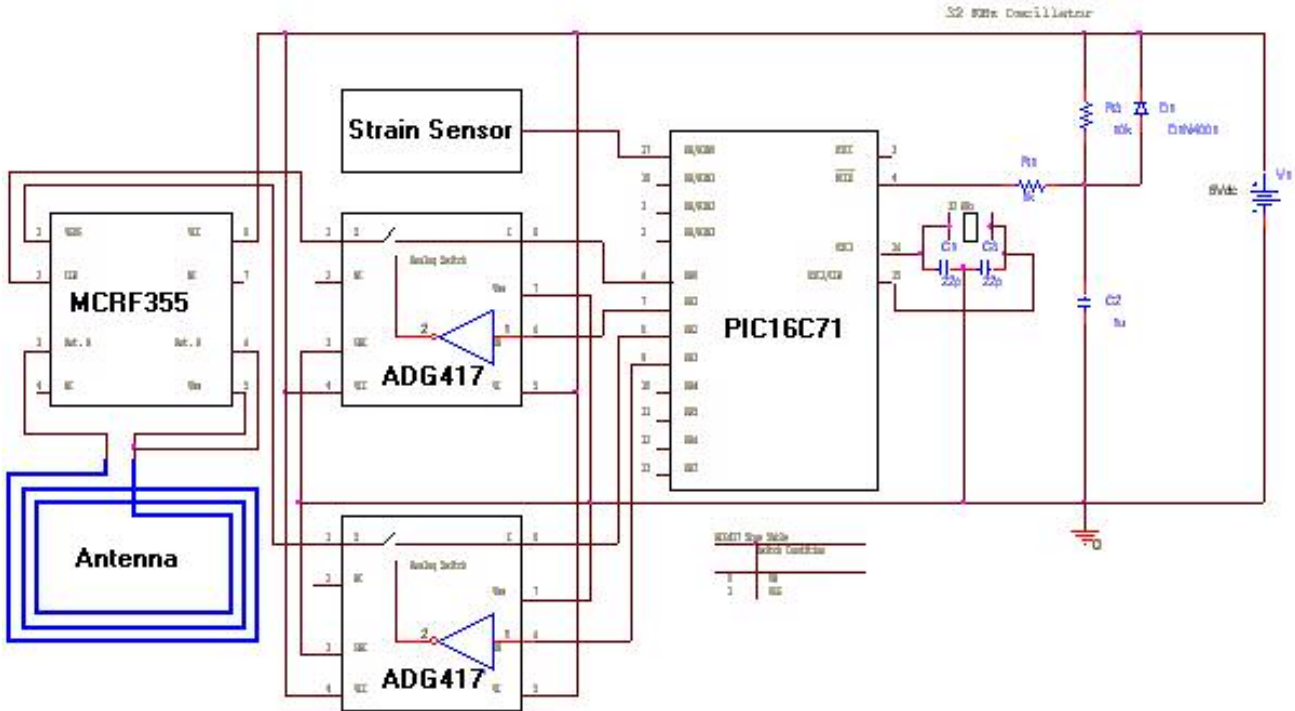


Figure 80. Strain-Sensor Circuit

The PIC16C71 is used in this circuit because of its low power consumption feature: 15 μ A, when working with a clock signal at 32 KHz, and less than 1 μ A on standby. The transfer of information between the microcontroller and the MCRF355 is performed in two handshake steps: first, a programming word is send and next the information data is transferred.

Note that the microcontroller, the ADG417 switches and the strain sensor are not powered by the RF signal. The RF signal send by the reader device is used just to power the MCRF355 and get the information stored in its memory.

In the prototype circuit of Figure 80, in the end, the microcontroller, switches and strain sensor must be powered by an external piezoelectric system that will be feeding power intermittently from the vibration and pressure generated by the cars circulating on the bridge.

Because that flow of power is not continuous, the microcontroller must transfer the last strain measurement data to the MCRF355 as soon as possible, before it loses power.

The microcontroller will take strain measurements and saving them into the MCRF355 memory as long as there is enough power available.

To read the data stored in the MCRF355 an interrogator circuit must be in the proximity of the sensor circuit. The interrogator circuit sends a constant 13.56 MHz sinusoidal signal, which arrives to the MCRF355 coil antenna. This signal is then rectified and filtered to generate a DC voltage, which powers the MCRF355 internal circuitry.

After activated, the MCRF355 modulates the load seen by the interrogator with the strain data stored in its memory; it looks like a signal modulated on AM for the interrogator device. The MCRF355 keeps sending the same information as long as there is enough RF signal to power its circuitry.

The maker of the MCRF355 indicates that when some data is recorded on the MCRF355, it is retained at a minimum of 200 minutes. This time allows the recover of the information on critical structures long time after no power is feed to the circuit.

Appendix A. RF Power Transfer in Free Space

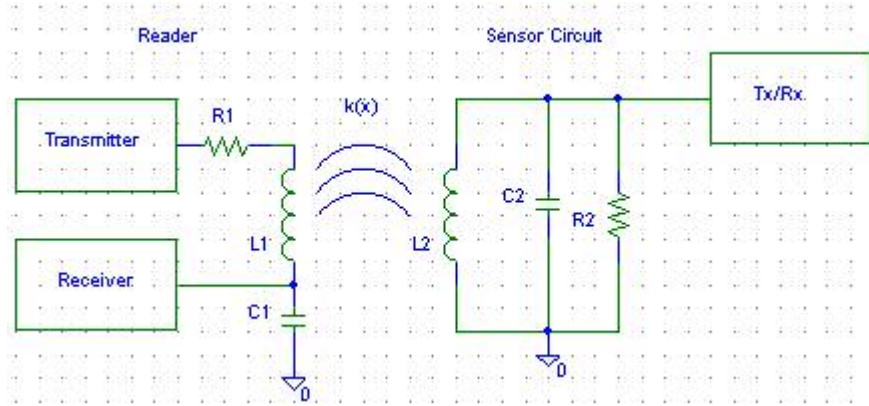


Figure 81. Interrogator-Strain Sensor Front-End

To analyze the transfer of power in the free space we start by computing the power density in the sensor circuit [38, (12.24), pp 673]:

$$PD = \frac{P_T G_A}{4\pi x^2} \quad (A.1)$$

where P_T is the transmitted power, G_A is the gain of the antenna and x is the distance between the reader (also called interrogator) and the sensor circuits. When this power arrives to the sensor circuit, it is used to energize the circuit, processing the signal and send back a signal with the strain measurement. This power process can be modeled as [38, (12.25), pp 674]:

$$P_s = kPD, \quad 0 \leq k \leq 1 \quad (A.2)$$

where k can be considered equivalent to the radar cross-section and is a measure of the amount of energy sends back to the reader. The actual value of k depends on the attenuation of the bridge material were the sensor circuit is embedded, angle between antennas, material of antennas and frequency.

To compute the power received back, we can use the effective absorption area of the reader antenna given by [37, pp 522]:

$$A_{eff} = \frac{\lambda^2 G_A}{4\pi} \quad (A.3)$$

Then the power received in the reader circuit will be [38, (12.27), pp 674]:

$$PD_{Rx} = \frac{P_T G_A A_{eff} k}{(4\pi)^2 x^4} \quad (A.4)$$

Or equivalently, by substituting A.3 into A.4:

$$PD_{Rx} = \frac{P_T G_A^2 \lambda^2 k}{(4\pi)^3 x^4} \quad (A.5)$$

From A.5, if we keep fixed all variables in this formula but want to double the readout distance, then the power to carry out the job must be increased by sixteen. Most of the power sent to the sensor circuit is lost on the free space.

Appendix B. Antenna Near Field Region

There is a still some debate regarding the use of formulas when working in the Fraunhofer region of the antenna, (far field region), the region where the propagated wave front from one antenna to the other antenna is essentially a plane wave, and the Fresnel region of the antenna (near field region), where the propagated wavefront is spherical. For some applications it can result in phase variation of the signal at the receiving antenna due to radiation of the signal from different parts of the transmitting antenna.

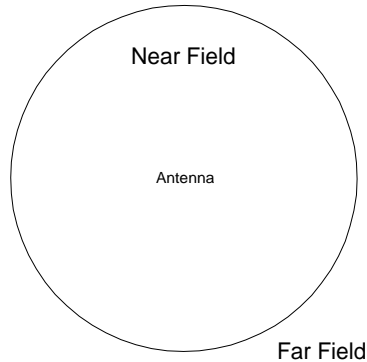


Figure 82. Near–Far Field Regions Boundary

The boundary line is rather diffuse, but it is customary to set it at $\lambda / 2\pi$, Figure 82. The characteristic impedance is given by [38, pp 17]: $Z = \sqrt{\mu_0 \epsilon_0} \approx 377\Omega$, and the typical behavior of the fields in both regions is described in Figure 83. Note that starting at $\lambda / 2\pi$ the electromagnetic wave impedance becomes independent of the distance from the antenna, or in other words: the electromagnetic wave has not effect on its generation antenna, and as a consequence there is no more inductive coupling, and the transformer model does not describe the system anymore. If there is not magnetic coupling, then there is not transfer of power. Therefore, for practical applications, the inductive coupling

must be carried out on the Fresnel field, and there is not way to extend this limit beyond $\lambda / 2\pi$.

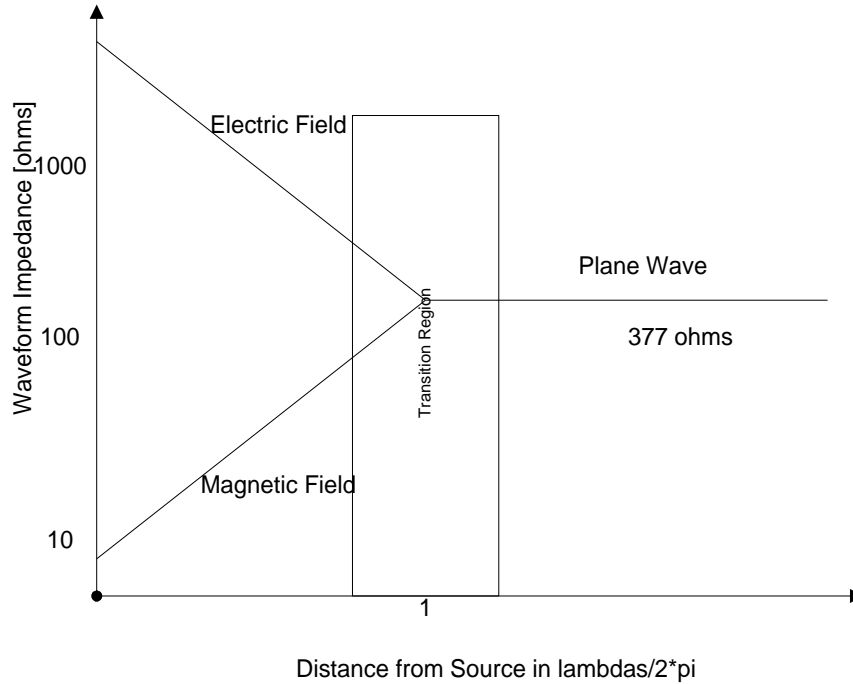


Figure 83. Transition Region Between Fields

Let's compute the free space loss for the system given in equation A.5. Knowing that the path loss is defined as [37, pp 522]: $P_L = P_T / P_D$, assuming $G_A = k = 1$ and $\lambda = c / f$ with $c = 3 \times 10^8$ m/s, then the path loss is:

$$P_L = \frac{P_T G_A^2 \lambda^2 k}{(4\pi)^3 x^4 P_T} \quad (B.1)$$

and becomes

$$P_L [dB] = -147.56 + 2(20)\log(x) + 20\log(f) \quad (B.2)$$

Note that in B.2 that the second term represents the loss of power of the RF signal when it propagates in free space from the interrogator to the sensor circuit and vice versa [40,

pp 49]. Plot of B.2 results in a signal attenuation of 20 dB by decade, which is true for the far field, Figure 84.

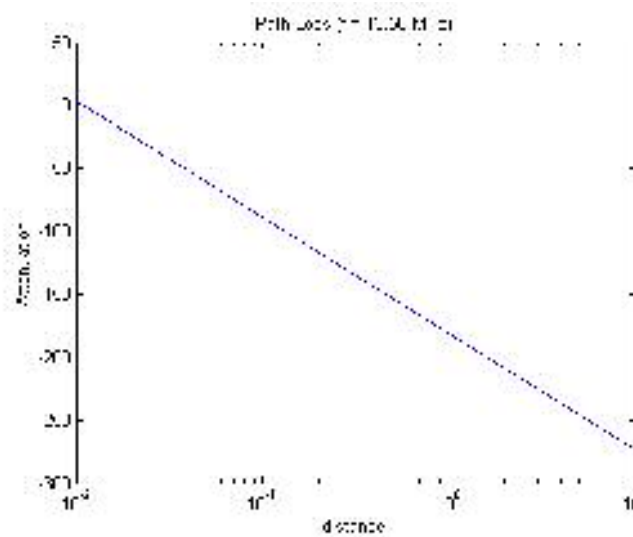


Figure 84. Free Space Loss in a Sensor–Interrogator System

However, in the near field the magnetic field, H falls off at rate $1/x^3$ or 60 dB per decade, and there is a transition distance in the vicinity of $\lambda/2\pi$ as indicated in Figure 83.

Observe how at 40MHz the border of the near field is roughly one meter, i.e., this is the maximum readout distance in an interrogator-strain sensor system based on magnetic coupling. Of course, it is possible to overcome this limit by:

1. Grow the size of the interrogator and sensor antennas.
2. Increase considerably the power delivered by the reader circuit.
3. Decrease the frequency of the system.

Though, those are not practical solutions for some applications given the increase in cost and size of the system.

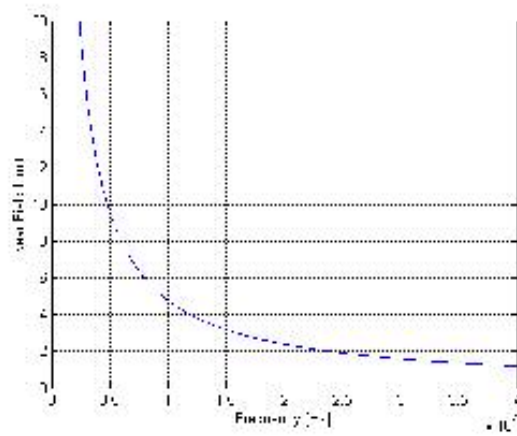


Figure 85. Near Field Boundary Distance From Antenna

Appendix C. Interrogator–Sensor Communication Issues

Chapter 4 described the implementation of a sensor circuit based on commercial components. One of the chips used is the MCRF355, this chip gets its power from the RF signal, and sends the strain information stored in its memory to the interrogator circuit through the same receiving antenna. This appendix was written to explain how the strain data is encoded and modulated by the sensor system.

a. Modulation

Communication of the measurement data in the system becomes more complex when there is more than one sensor circuit. A model of a communication network better fits this expanded scheme. A useful communication model depicted through encoding – decoding and modulation – demodulation blocks is shown in Figure 86.

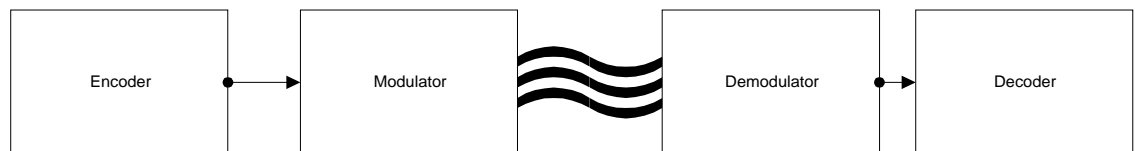


Figure 86. Communications Scheme of the Interrogator–Sensor System

The encoder–decoder takes care of security and error–correction of the measured data and the modulator–demodulator blocks care to send and receive the information wirelessly. Collision is the event when two or more devices transmit simultaneously.

There are three basic digital modulations: amplitude shift keying (ASK), frequency shift keying (FSK) and phase shift keying (PSK). ASK is important when dealing with collision on a low power passive circuits, and is used in some of the commercial implementations for RFID tag circuits like the MCRF355.

An ASK signal is described by [41, pp 333-336]

$$x(t) = Am(t) \cos(\omega_c t) \quad (C.1)$$

with envelope $y(t) = Am(t)$. If we assume NRZ unipolar with two equally likely values A and 0. Then the power spectrum density will be [41]:

$$P_y(f) = \frac{A^2}{2} \left[\delta(f) + T_b \left(\frac{\text{Sin}(\pi f T_b)}{\pi f T_b} \right)^2 \right] \quad (C.2)$$

With average normalized power $A^2 / 2$ for $x(t)$ peak value $\sqrt{2}$. An example of the baseband and ASK signals for bipolar NRZ are shown in Figure 87.

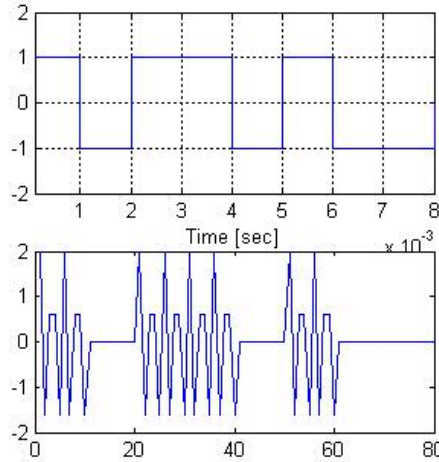


Figure 87. ASK Signal

b. Encoding – Decoding

In an interrogator-to-one – strain sensor system operating in the near field, the communication is smooth. However, when the system grows to include more than one sensor in the proximity of each other there is a chance that two or more circuit sensors try to send information to reader at the same time, this condition results in collision. The standard approach is, after detecting collision, to wait some random time before try to

establish communication again. This approach was first used by the University of Hawaii in 1971 and has been widely studied.

If the data words (packets) sent by all sensors are defined as traffic, then there will be some reasonable expectation that some of the packets will collide as illustrated in Figure 88.

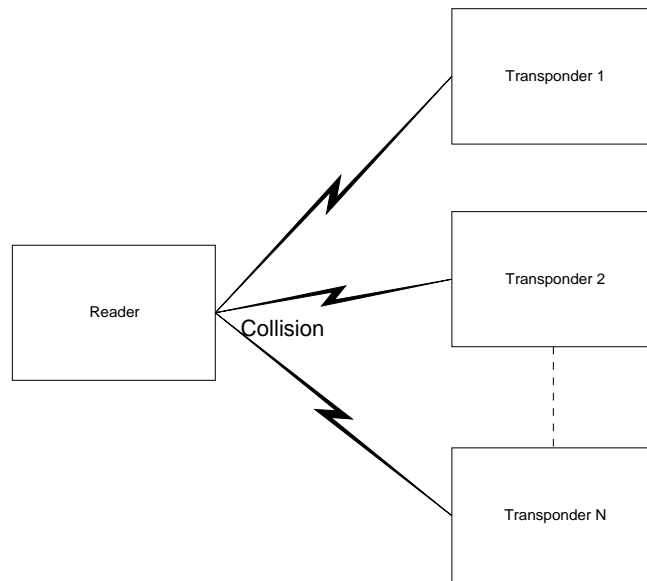


Figure 88. Signal Collision on the Interrogator-Multisensor System
in Near Field Region

From traffic theory, let λ be the total traffic arriving to the reader, then it can be decomposed in traffic accepted λ_a and unsuccessful traffic λ_r , then [42, (11.16), pp 679]:

$$\lambda = \lambda_a + \lambda_r \quad (C.3)$$

If the length of every message is b , the average accepted traffic would be $\rho' = b\lambda_a$. If the channel capacity is defined in R bits per second, then the normalized average accepted traffic, or throughput, becomes [42, (11.19), pp 680]:

$$\rho = \frac{b\lambda_a}{R} \quad (C.4)$$

and the total normalized total traffic

$$G = \frac{b\lambda}{R} \quad (C.5)$$

The time every packet will take to be transmitted is [42, (11.21), pp 680]:

$$\tau = \frac{b}{R} \quad (C.6)$$

Let's (C.4) and (C.5) to be rewritten as

$$G = \lambda\tau \quad (C.7)$$

$$\rho = \lambda_a\tau \quad (C.8)$$

When some sensor transmit it will take τ seconds to successfully send its information. However, if any of the other sensors inside the near field region try to send information before the previous sensor finish then collision will occur. If it is assumed that packets are independent, then traffic can be modeled as Poisson Process, with distribution [42, (11.24), pp 680]

$$P(x = k) = \frac{(\lambda\tau)^k e^{-\lambda\tau}}{k!} \quad (C.9)$$

To avoid collision is necessary that only one packet is sent in one 2τ interval, therefore (C.9) becomes

$$P(x = 0) = \frac{(2\lambda\tau)^0 e^{-2\lambda\tau}}{0!} = e^{-2\lambda\tau} \quad (C.10)$$

By definition, the probability to have a packet successfully transmitted is

$$P(x = 0) = \frac{\lambda_a}{\lambda} \quad (C.11)$$

From (C.10) and (C.11) we get:

$$\lambda_a = \lambda e^{-2\tau\lambda} \quad (C.12)$$

If (C.12), (C.7) and (C.8) are combined

$$\rho = G e^{-2G} \quad (C.13)$$

Where (C.13) represents the normalized successful traffic as function of the total traffic. Figure 89 shows the graph of this function. Note how successful traffic increases as traffic increases up to half of the communication channel capacity, after reaching that point, the traffic produces numerous collisions and as a result successful traffic decreases becoming almost zero when traffic is four times the capacity of the channel.

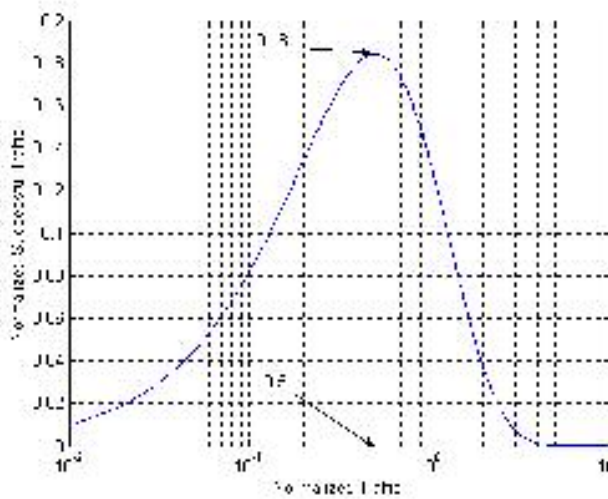


Figure 89. Normalized successful Traffic Versus Normalized Total Traffic

From this graph, the maximum normalized successful traffic is $1/4$ or 0.25, i.e., the maximum successful traffic is 25% of the channel capacity. That means that collisions occur regularly in a digital communication system. Fortunately, the interrogator–sensor system generates traffic well below this value in the readout range.

c. Bandwidth, DC Component and Collision Detection

Encoding the measured data has many objectives, but one of the most important, in passive magnetic coupling, is to cancel the DC component of the signal send from the sensor to the interrogator. The energy in the DC component is wasted because magnetic couplings have not sensitivity to DC or even to low frequency signals. Therefore, the encoding process must allocate all the energy on higher frequencies. However, there is tradeoff between the power saved by not encoding the DC component and the additional power used to encode the measured data.

From chapter two, it is known that the antennas in the interrogator and sensor circuits work in resonance and therefore they can be modeled as band-pass filters. A higher Q is desirable to increase the reader distance, however there is a tradeoff, because of the affect of a narrow bandwidth on the encoded signal as shown in Figure 90.a.

Note that, as the system bandwidth becomes smaller, the recovered signal suffers higher delay and distortion when compared with the original data, in the last row of plots it is not possible to differentiate between the ones and zeros. This problem is exacerbated if there is an important amount of noise as seen in Figure 90.b. To observe the effect of both variables, bandwidth and noise, it is customary to use the eye diagram. An open and clean eye diagram is desirable, the closer and smaller eye imply difficulty on estimation and detection of the incoming data by the interrogator circuit.

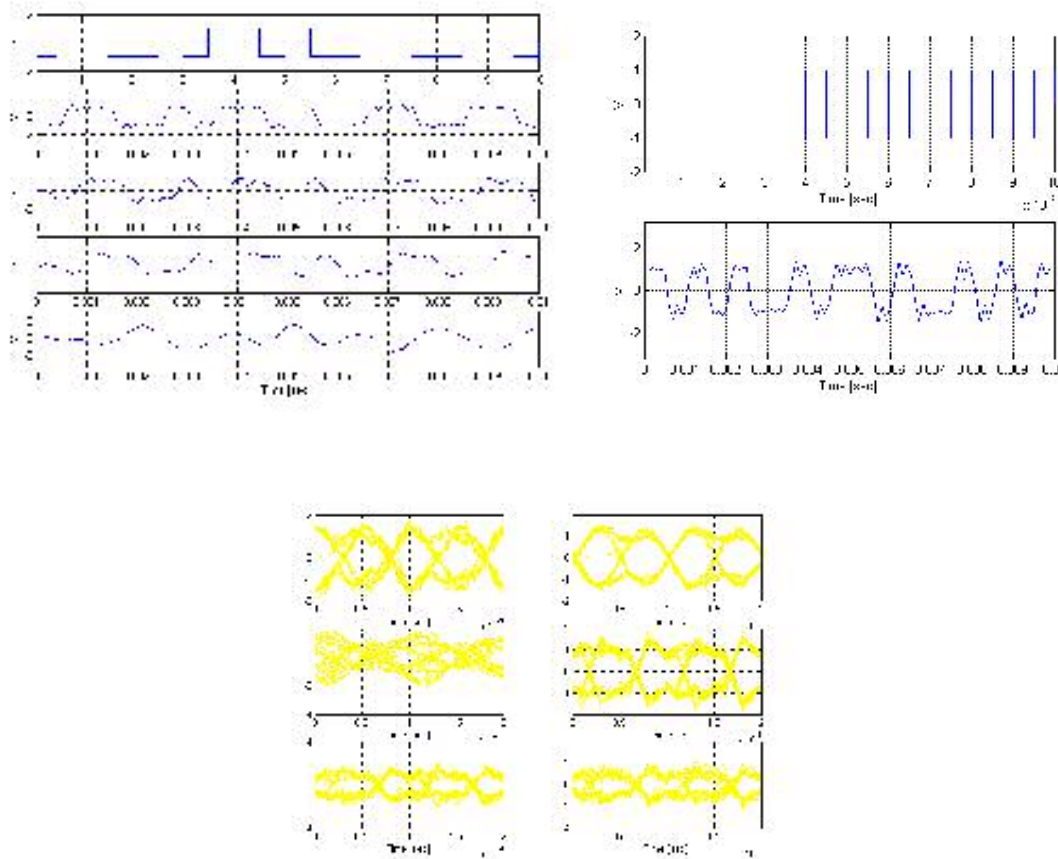


Figure 90. (a) Effect of decreasing Bandwidth on a Digital Signal (5000,3000, 2000, 1000 and 500 Hz of Bandwidth). (b) Encoded Signal Plus Noise (c) Eye diagram (see paragraph for an explanation)

In the first column of plots, the noise power is kept to 0.01 watts but bandwidth is decreased from 3KHz to 2KHz and to 1KHz. On the second column of plots, the bandwidth is constant at 4KHz, but the power noise is incremented from 0.02W to 0.08W and to 0.10W. In both cases, the bandwidth of the incoming signal is 1KHz.

From discussion in chapter 4, a higher Q is desirable to increase the readout distance, however, Q must be kept to an adequate value to allow the system to transfer

data without appreciable distortion. There is a relation between Q and the bandwidth of the communication system given by [9, (12), pp 90]:

$$\frac{BW}{\omega_0} = \frac{1}{Q} \quad (C.14)$$

Where BW is the bandwidth of the communication system, and ω_0 is the resonance frequency. Addition of an error correcting coding algorithm in the interrogator circuit can mitigate the problem, but again, it will also add on overhead, cost and complexity on the strain sensor circuits.

The Detection of collision can be done by encoding the measured data before modulate. Figure 91 shows three popular line encoding methods and their power spectrums: NRZ, RZ and Manchester. Note how RZ and Manchester requires twice the bandwidth of NRZ. However, RZ and Manchester have inherent synchronizing features that allow them to recover the clock from the incoming data signal, with a relatively low complexity PLL circuit.

Also, observe that the DC component presents important magnitudes in RZ and NRZ, but that component is almost inexistent for Manchester. That is an important saving on power for passive sensors.

There are many ways to implement error-correcting codes, some more energy efficient than others. But in a magnetic coupled sensor system, with more than one strain sensor circuit, the most important source of errors is not the environment noise but collisions. Therefore, collision detection is very important. The most important advantage of Manchester Encoding is its ability to generate a clear error when a collision occurs.

Figure 92.a shows when two sensors, first row of plots, transmit at the same time. The second row shows the ASK encoded signals, and the last row, first column shows the received signal in the reader after a collision occurs. Finally, in the very last graph the NRZ decoded signal is displayed. Observe that not error is generated in the decoded signal when collision occurs, and therefore the collision is not detected.

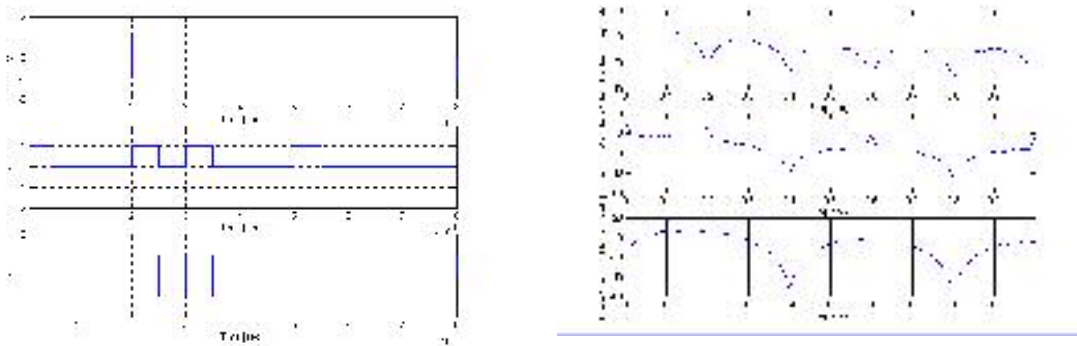


Figure 91. (a) Line Encoding. (b) Spectrums for NRZ, RZ and Manchester

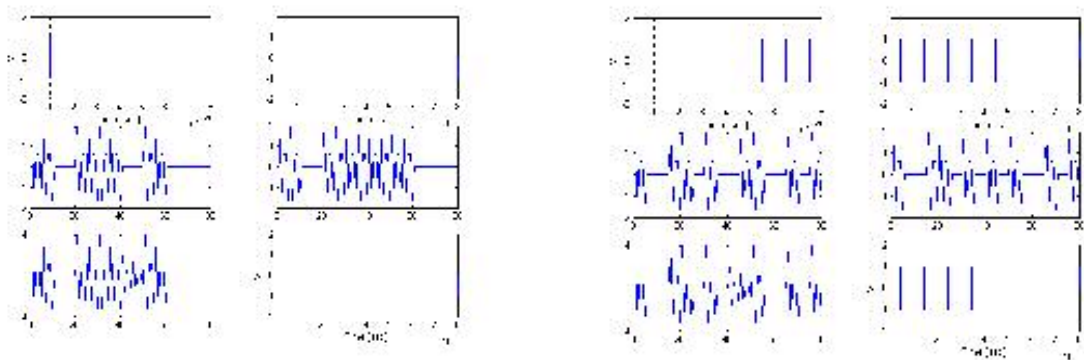


Figure 92. (a) Collision on NRZ Encoded Sensor Signals

(b) Collision in Manchester (See text for explanation)

Figure 92.b shows same situation when two sensor signals are transmitted at the same time, but now the signals are encoded in Manchester. The first and second rows of

plots show the Manchester encoded sensor signals and their ASK modulated representation. The last row, first column, shows the ASK signal received in the reader and the very last plot shows the decoded signal.

Observe that the wider pulse is not possible in a well Manchester encoded signal, and therefore an error is detected and that packet of information is discarded. See [42] on page 87 for an explanation on Manchester coding.

d. Error Correcting Codes and Security

In regular use, an error correcting encoding take cares of the detection and correction of the errors generated in the transmission of information. A well-designed error correcting coding should save power because; even it adds redundant bits, on the average, it avoids retransmission of packets of data that use additional power, therefore, on the average the bit per symbol is decreased.

In the interrogator–sensor system the error correction system is not necessary because the collision already generates a sequence that is not allowed in Manchester encoding. This condition indicates to the interrogator that there is an error in the received data, and consequently the data is discarded. Then, the interrogator waits to receive the data again. The sensor circuits transmit their ID and data at random time intervals as long as they get adequately power from the RF reader signal. Therefore, the interrogator gets the same data more than once, given it the opportunity to correct or update its database.

From chapter two we know that all magnetic-coupling communications must occur inside the near field, which limit is calculated as $\lambda / 2\pi$. For a 13.56 MHz communication, the limit would be a radius of 3.521 meters.

However, as depicted in Figure 93, an eavesdropper could potentially get the signal send by the sensor circuit outside the limit of the near field. If there is need to protect the sensor data from eavesdroppers then an encryption algorithm must be added to the measured data before the transmission.

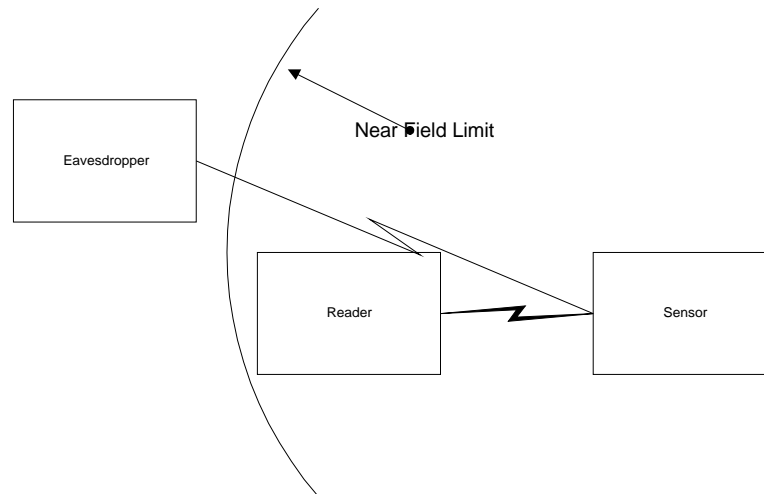


Figure 93. Eavesdroppers in an Interrogator-Sensor System

The encryption algorithms use a key word, which is known by both parties but not by the eavesdropper to encode the data before sending to the communication channel.

To encode the key word and data, an XOR digital gate takes, one-by-one, a bit from the key and another bit from the data words. The output word is send to the channel. In the receiver, the incoming word is XOR gating again with the same key word and the original data is recovered. For additional information on encryption algorithms see [44, pp 12-49].

Appendix D. Wiring and Matching in the Strain-Sensor System Design

There are common improvements, in addition working at resonance for both the reader, also known as interrogator, and the sensor circuit, with the purpose of maximize the amount of power transfer to the sensor circuit.

First, the length of the cable from the circuit to the antenna must be on the vicinity of zero or multiples of $\lambda/4$. This fact is based on the assumption that perfect match between the circuits and their antennas is not perfect and therefore by controlling the length of the cable between the circuit and the antenna we can control the reflected signals to the minimum.

Let us elaborate on this assumption. It is known [9, (55), pp127] that the quotient Z_L/Z_{in} of the load and input impedances of a transmission line is given by:

$$\frac{Z(z)}{Z_{in}} = \frac{Z_L \cos(\beta z) - jZ_{in} \sin(\beta z)}{Z_{in} \cos(\beta z) - jZ_L \sin(\beta z)} \quad (D.1)$$

Figure 94 shows (D.1) plot. Observe that only when there is perfect match the quotient is constant and equal to one, all other cases are periodic.

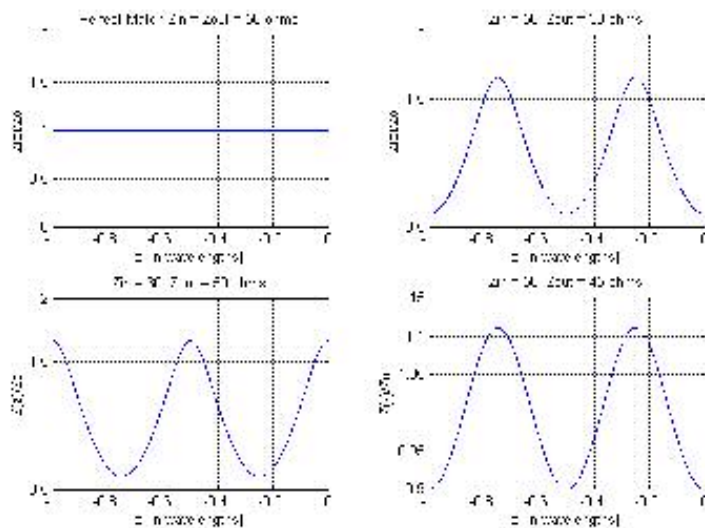


Figure 94. Impedance Behaviors Along a Transmission Line

Recall, the reflection coefficient is given by [9, (47) and (48), pp 126]:

$$\Gamma = \frac{\frac{Z_L}{Z_{in}} - 1}{\frac{Z_L}{Z_{in}} + 1} \approx \frac{\frac{Z(z)}{Z_{in}} - 1}{\frac{Z(z)}{Z_{in}} + 1} \quad (D.2)$$

In the second part of the equation, the reflection coefficient was modified to observe its behavior along a transmission line. Clearly from (D.2) and Figure 94, the only lengths of the transmission line that result in a reflection coefficient equal to one are multiples of $\lambda/4$, all other lengths result in reflected signals, and therefore in lost power. The reflected power results in a decreased reading distance. In Figure 94, the second and third plots show cases for $Z_{in} = 50\Omega$, $Z_L = 30\Omega$ and $Z_{in} = 30\Omega$, $Z_L = 50\Omega$, i.e., a strong mismatch between the impedances of the circuit and the antennas. Note, that the swing of the impedance quotient, equation (D.1), has a shift phase of 180° , but still presents perfect match at multiples of $\lambda/4$.

As an example, for a reader-sensor system working a 2.4 GHz $\lambda/4 = 3.125$ cm, and the length of the cable feeding the antenna must be close to zero, ideally zero, or multiple of 3.125 cm.

If the design frequency of the sensor circuit is 13.56 MHz, i.e., $\lambda/4 = 5.531$ m, the length of the wires is not an issue in the optimization of the interrogation distance because all the expected cable lengths are less than 20 cm length. However, as frequency increases, the length of the feeding cable must be carefully restricted to multiples of $\lambda/4$.

Second, the design of a match circuit must be considered. Perfect match is very difficult to get in practice; most of the time, after the design is completed some of the reactive components must be keep variable so that a tune up is available to maximize

interrogation distance. Tune up should be done in conditions close to the final environment where the circuits will be operating, in order to consider the parasitic capacitances of the surrounding materials and operators.

However, after the circuit is finished and placed in its final location, components get older, capacitors dry off and change their values, and the sensor circuit loses its matching effect, conveying a decrease in the interrogation distance.

The design of the matching circuit starts by considering the transformation from a series to a parallel circuit, as a helping tool to design. It is described in Figure 95.

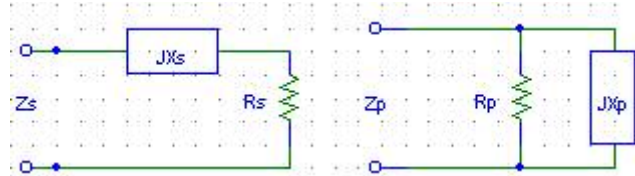


Figure 95. Series and Parallel Complex Circuits

It is wanted $Z_s = Z_p$, index s stand for series and p by parallel, or

$$R_s + jX_s = \frac{R_p jX_p}{R_p + jX_p} \quad (D.3)$$

After some algebra

$$R_s = \frac{R_p X_p^2}{R_p^2 + X_p^2} \quad \text{and} \quad X_s = \frac{X_p R_p^2}{R_p^2 + X_p^2} \quad (D.4)$$

If we have a parallel circuit, with some Z_p , the R_s and X_s values necessary to keep $Z_s = Z_p$ but implemented as series circuit are given by (D.4).

In the same way, it is wanted $1/Z_s = 1/Z_p$, and the algebra yields

$$R_p = \frac{R_s^2 + X_s^2}{R_s} \quad \text{and} \quad X_p = \frac{R_s^2 + X_s^2}{X_s} \quad (D.5)$$

Now, If we have a series circuit with some Z_S , the R_P and X_P values necessary to keep $Z_S = Z_P$ implemented as series circuit are given by (D.5).

As an example of design, consider the match of a voltage source in series with a 50Ω resistance, to an impedance given by: $10+j20$. From (D.5)

$$X_p = \frac{R_s^2 + X_s^2}{X_s} = \frac{10^2 + 20^2}{20} = 25 \quad (D.6)$$

Because the original reactive component $j20$ is positive then the reactive component given by (D.6) must be negative, i.e., a capacitor. The capacitor must be placed in parallel as described in Figure 96.

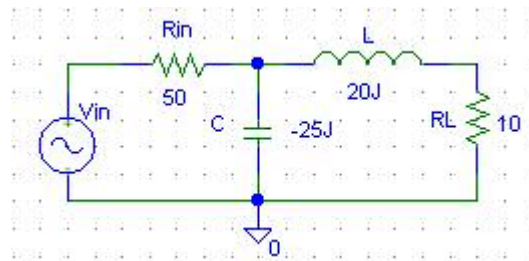


Figure 96. Matched Circuit

To check that the circuit was matched the equivalent impedance is calculated in (D.7)

$$Z_{equivalent} = \frac{(10 + 20J)(-25J)}{10 + 20J - 25J} = \frac{50(10 - 5J)}{10 - 5J} = 50\Omega \quad (D.7)$$

Because $Z_{equivalent}$ is the same as R_{in} the circuit has been matched. In the strain-sensor system, matching is more elaborated because resonance must be preserved. Therefore, the capacitors of the matching circuit should be variable for fine-tuning.

Appendix E. Standards

Standards		
<i>Standard</i>	<i>Frequency</i>	<i>Power (depending on class)</i>
		437.7 dB μ A/m at 10m (at 135 kHz, descending 3 dB/octave from 135 kHz to 1 MHz)
EN 300 330 - 1 V1.3.1	9 kHz-30 MHz	
EN 300 220-2 V1.3..1	25 - 1000 Meg	up to 500mW
EN 300 328 - 1: V 1.2.2	2.4-2.4835 GHz	up to 100mW
ISO 18000- 3 (FCC)	13.553-13.567MHz	max 10mV/m at 30 meters
ISO 15240	425-435 MHz	max 11mV/m at 3 meters
ISO 18000- 6B (FCC)	900 MHz	4 W

ISO International Organization for Standardization

EN European Telecommunications Standards Institute (ETSI)

Table 3. Standards [60, 61, 62]

REFERENCES

1. E – Zpass New Jersey Costumer Service.
<http://www.ezpass.com/static/info/howit.shtml>
2. Maryniak, G.E., “Status of International Experimentation in wireless power transmission”, Solar Energy, Vol. 56, No. 1, pp 87-89, January 1996.
3. Sato, H., Domae, H., Takahashi, M., Abe, M., “Reflection and Transmission Control of Electromagnetic Wave for Concrete Walls”, Electronics and Communications in Japan, Part 2, vol. 83, No. 11, pp 674–682, 2000.
4. Tsukamoto, H., “Hermetically Sealed Lithium Rechargeable Batteries for High Reliability Applications: Medical, Aerospace and Other Specialties”, Proceedings of the 17th Annual Battery Conference on Application and Advances, Long Beach, pp 129-134, January 2002.
5. Brown, C.B., “The History of Power Transmission by Radio Waves”, IEEE Transactions on Microwave Theory and Techniques”, Vol. MIT-32, No. 9, pp 1230-1242, September 1984.
6. Palmer, C. R., “The Bar Code Book”, Helmers Publishing, Inc., Peterborough, New Hampshire, 3rd edition, pp 123 – 127, November 1995.
7. Daugman, J., “How Iris Recognition Works”, The Computer Laboratory, Cambridge, UK, pp 1-3, <http://www.CL.cam.ac.uk/users/jgd1000>
8. Cohen, J., “Automatic Identification and Data Collection Systems”, McGraw Hill, New York, November 1994.
9. Lee, T.H., “The Design of CMOS Radio – Frequency Integrated Circuits”, Cambridge University Press, New York, 1998.

10. Austin, B. A., "Electromagnetic Propagation Underground with Special Reference to Mining", Trans. SAIEE (The South African Institute of Electrical Engineers), Vol. 76, No. 1, pp 1-5, January 1985.
11. Winch, R. P., "Electricity and Magnetism", Second Edition, Prentice-Hall, Englewood Cliffs, N.J., 1963.
12. Vasudeva, D.N., "Fundamentals of Magnetism and Electricity", S. Chand & Co., Delhi, 1966.
13. Baker, R.J., Li, H. W., Boyce, D.E., "CMOS Circuit Design, Layout, and Simulation", Wiley InterScience, New York, 1998.
14. Pylarinos, L. and Roger, E. "Charge Pumps: An Overview", Department of Electrical and Computer Engineering, University of Toronto, pp 2 – 3, <http://www.eecg.toronto.edu/~kphang/ece1371/chargepumps.pdf>
15. Okamura, H., Atsumo, T., Takeda, K., Takada, M., Imai, K., Kinoshita, Y., Yamazaki, T., "A Sub-2.0 BiCMOS Logic Circuit with a BiCMOS Charge Pump", IEEE Journal of Solid-State Circuits, Vol. 31, Issue 1, pp 84-90, January 1996.
16. Stremmler, F.G., "Introduction to Communication Systems", 3rd Edition, Addison-Wesley, New York, pp 372-413, 1990.
17. Lin, P.M., "Topological Generation and Analysis of Voltage Multiplier Circuits", IEEE Transactions on Circuits and Systems, Vol. CAS-24, No. 10, p 528, October 1977.
18. Peikari, B., "Fundamentals of Network Analysis and Synthesis", First Edition, Robert E. Krieger Publishing Company, Malabar, Florida, 1981.

19. Muller, R. S. and Kamins, T.I, "Device Electronics for Integrated Circuits",
Second Edition, John Wiley & Sons, New York, 1986.
20. Dickson, J.F., "On-Chip High-Voltage Generation in MNOS Integrated
Circuits Using an Improved Voltage Multiplier Technique", IEEE Journal of
Solid-State Circuits Vol. SC-11, No. 3, pp 374-378, June 1976.
21. Di Cataldo, G., Palumbo, G., "Optimized design of 4 stage Dickson voltage
multiplier", IEEE International Symposium on Circuits and Systems,
London, UK, Vol. 5, pp 693-696, June 1994.
22. Di Cataldo, G., Palumbo, G., "Dynamic analysis of 3 stage Dickson voltage
multiplier for an optimized design", Proceedings of the Electrotechnical
Conference, 7th Mediterranean, Antalya, Turkey, Vol.2, pp 633-636, 12-14
April 1994.
23. Starzyk, J.A., Jan, Y., Qiu, F., "A DC-DC charge pump design based on
voltage doublers", IEEE Transactions on Circuits and Systems I:
Fundamental Theory and Applications, Vol.48, Issue 3, pp 350-359, March
2001.
24. Kip, A. F., "Electricity and Magnetism", McGraw-Hill, New York, 1962
25. Baker, R.J., Li, H. W., Boyce, D.E., "CMOS Circuit Design, Layout, and
Simulation", Wiley InterScience, New York, pp 33 – 41, 1998.
26. Pylarinos, L., Phang, K., "Analysis of output ripple in multi-phase clocked
charge pumps", Proceedings of the 2003 International Symposium on
Circuits and Systems, ISCAS '03, Vol.5, pp 25-28 May 2003.

27. Ioth, K., Fridi, A.R., Bellaouar, A. and Elmasry, M.I., "A Deep Sub-V Single Power supply SRAM Cell with Multi-VT Boosted Storage Node and Dynamic Load", 1996 Symposium on VLSI Circuits, Digest of Technical Papers, Honolulu, HI, pp 132-133, June 1996.
28. Choi, K., Park, J., Kim, J., Jung, T. and Suh, K., "Floating-well Charge Pump Circuits for Sub-2.0V Single Power Supply Flash Memories" 1997 Symposium on VLSI Circuits, Digest of Technical Papers, pp 61-62, June 1997.
29. Allstot, D.J., Park, J., Choi, K., "Parasitic-Aware Optimization of CMOS RF Circuits", Kluwer Academic Publishers, Boston, Massachusetts, 2003.
30. Niknejad, A.M. and Meyer, R.G., "Inductors and Transformers for Si RF ICs", Kluwer Academic Publishers, Boston, Massachusetts, 2000.
31. MCRF355/360 Datasheet, Microchip Co., pp 7, <http://www.microchip.com>
32. Sato, H., "Reflection and Transmission Control of Electromagnetic Wave for Concrete Walls", Electronics and Communications in Japan, Part 2, Vol. 83, No. 11, pp 12-21, 2000.
33. Reindl, L., Scholl, G., Ostertag, T., Scherr, H., Wolff, U., Schmidt, F., "Theory and Application of Passive SAW Radio Transponders as Sensors", IEEE Transactions on Ultrasonics, Ferroelectrics, and Frequency Control, Vol. 45, No. 5, pp 1281-1292, September 1999.
34. Pohl, A., Seifert, F., "New Applications of Wirelessly Interrogable Passive SAW Sensors", IEEE Transactions on Microwave Theory and Techniques, Vol. 46, No. 12, pp 2208-2211, December 1998.

35. Gardner, J.W., "Microsensors MEMS and Smart Devices", John Wiley & Sons, New York, 2001.
36. Schmidt, F., Sczesny, O., Ruppel, C., Magori, V., "Wireless Interrogator System for SAW-Identification-Marks and SAW-Sensor Components", Proceedings of the 1996 IEEE International Frequency Control Symposium, Honolulu, HI, pp 208-215, June 1996.
37. Haykin, S., "Communication Systems", 4th edition, John Wiley & Sons, New York, 2000.
38. Pozar, D., "Microwave Engineering", Wiley, New York, 1998
39. Saunders, S., "Antennas and Propagation for Wireless Communication Systems", Wiley, New York, 1999.
40. G. Kohn, "Theoretische Elektrotechnik und Elektronik", Springer Verlag, Wien, Austria, 14th Edition, 1993.
41. Couch, L.W., "Digital and Analog Communication Systems", Prentice Hall, Englewood Cliffs, New Jersey, 1997.
42. Sklar, B., "Digital Communications. Fundamentals and Applications", Second Edition, Prentice Hall, Englewood Cliffs, New Jersey, 2000.
43. Wicker, S.B., "Error Control Systems for Digital Communication and Storage", Prentice Hall, Englewood Cliffs, New Jersey, 1995.
44. Trappe, W. and Washington, L., "Introduction to Cryptography with Coding Theory", Prentice Hall, Englewood Cliffs, New Jersey, 2002.
45. Warneke, B., Awood, B., Pister, K.S.J., "Smart Dust Mote Forerunners", Proceedings of The 14th IEEE International Conference on Micro Electro

- Mechanical Systems, 2001. MEMS 2001, Interlaken, Switzerland, pp 357-360, January 2001.
46. Raza, N., Bradshaw, V., "Applications of RFID Technology", Proceedings of The IEE Colloquium on RFID Technology, Savoy Place, London, pp 1-5, October 1999.
47. Rotter, M., Ruile, W., Bernklau, D., Riechert, H., Wixforth, A., "Significantly Enhanced SAW Transmission in Voltage Tunable GaAs/LiNbO₃ Hybrid Devices", Proceedings of The IEEE Ultrasonic Symposium, Sendai, Japan, Vol. 1, pp 69-72, October 1998.
48. Schmidt, V.H., "Piezoelectric Energy Conversion in Windmills", IEEE Proceedings of Ultrasonic Symposium, Tucson, AZ, Vol. 2, pp 897-904, October 1992.
49. Smith, G.A., Barnes, S.A., "Electrical Power Generation from Heat Engines", IEE Colloquium on Power Electronics for Renewable Energy, Digest N. 1997/170, London, UK, pp 5/1-5/6, June 1997.
50. Hamakawa, Y., "Recent Progress of Amorphous Silicon Cell Technology in Japan", IEEE Conference Record of the Twenty Second, Las Vegas, NV, Vol. 2, pp 1199-1206, October 1991.
51. Doig, A., "Off-grid Electricity for Developing Countries", IEE Review, Vol. 45, Issue 1, pp 25-28, January 1999.
52. Chaudhuri, S.K. and Lovley, D., "Electricity Generation by Direct Oxidation of Glucose in Mediatorless Microbial Fuel Cells", Nature Biotechnology, Vol. 21, No. 10, pp 1229-1232, October 2003.

53. Van, J. W., "Biotechnology and the Utilization of Biowaste as a Resource for Bioproduct Development", Trends in Biotechnology, Vol.19, Issue 5, pp 172-177, 2001.
54. Shenck, N.S., "Piezoelectric shoe power: two approaches " IEEE Computer Society, Internet Page Article, 2002.
http://www.computer.org/micro/homepage/may_june/shenck/01a.htm
55. Pelliconi, R., "Power Efficient Charge Pump in Deep Submicron Standard CMOS Technology", Proceedings of The 27th European Solid- State Circuits Conference, Session 1.4 Voltage Regulators, Villach Austria, p 7, September 18th 2001.
56. Richalot, E., Bonilla, M., Wong, M., Fouad-Hanna, V., Baudrand, H., Wiart, J., "Electromagnetic Propagation into Reinforced-Concrete Walls", IEEE Transactions on Microwave Theory and Techniques, Vol. 48, No. 3, pp 357-366, March 2000.
57. Boylestad, R., Nashelsky L., "Electronic Devices and Circuit Theory", Prentice Hall, Englewood Cliffs, New Jersey, 1972.
58. Assaderaghi, F., Parke, S., Sinitsky, D., Bokor J., Ko, P.K., "A Dynamic Threshold Voltage MOSFET (DTMOS) for Very Low Voltage Operation", IEEE Electron Device Letters, Vol. 15, No. 12, pp 510-512, December 1994.
59. Newcomb, R.W., "Microsystems Laboratory VLSI Page",
<http://www.ee.umd.edu/newcomb/mslab-vlsi.html>
60. Federal Communications Commission, <http://www.fcc.gov/>

61. International Organization for Standardization,

<http://www.iso.ch/iso/en/ISOOnline.frontpage>

62. The association for automatic identification and Data Capture Technologies,

<http://www.aimglobal.org/standards/rfidstds/RFIDStandard.htm>